Adsorption of Arsenate and Phosphate on Gibbsite from Artificial Seawater

Alexander John Fitzpatrick
Department of Earth and Planetary Sciences
McGill University, Montreal
December 1998

A thesis submitted to the faculty of Graduate Studies and Research in partial fulfillment of the requirements of the degree of Master of Science.

Abstract

Anomalously high concentrations of arsenic and phosphate are found in the sediments of the Saguenay Fjord in comparison to those of the Gulf and St. Lawrence Estuary. The source of the phosphate appears to be anthropogenic (i.e., from regional human and industrial activities) but the source of arsenic is unclear. The latter could be supplied to the Fjord by the marine waters which enter from the St. Lawrence Estuary or may have accumulated as a result of historically high levels of effluent input.

In estuarine environments, adsorption to suspended particulate matter is commonly cited as an important vector of trace metals to sediments. In the case of arsenic and phosphate, this is especially true when particles are made up of iron oxyhydroxides. Nevertheless, manganese and aluminum oxides are also known to be strong adsorbants of these elements. The waters of the Saguenay Fjord are also characterized by anomalously high particulate aluminum concentrations (i.e., $[Al]_{tot}/[Al]_{diss} > 1$), introduced as a result of the aluminum refining activity along the shores of its tributaries. Gibbsite ($Al(OH)_3$), a by–product of this activity, is known to strongly adsorb phosphate and arsenate from low ionic strength aqueous solutions, and may act as a vector for these two elements to sediments of the Saguenay Fjord.

Experiments conducted in artificial seawater have shown that adsorption of arsenate and phosphate to gibbsite from seawater is at least two orders of magnitude less than in dilute solutions. The limited adsorption is ascribed to the competition for adsorption sites by the major seawater ionic constituents. The competition is a reflection of both the specific adsorption affinity of the ions and their relative abundance in seawater. The affinity of fluoride ions for gibbsite is probably the major cause of the diminished adsorption. The kinetics of phosphate adsorption are made more complicated by this competitive adsorption. The influence of artifcial seawater appears to be limited to competition for adsorption sites and does not influence adsorption in regards to ionic strength or other factors.

The small amount of arsenate and phosphate adsorbed onto gibbsite from seawater indicates that their adsorption to particulate aluminum in the water column cannot account for the elevated levels of arsenic and phosphate in the sediments of the Saguenay Fjord.

Résumé

Des concentrations anormalement élevées d'arsenic et de phosphate ont été observées dans les sédiments du Fjord du Saguenay. Le phosphate provient vraisemblablement de sources anthropiques (activités humaines et industrielles régionales) tandis que la source de l'arsenic est incertaine. Ce dernier pourrait provenir des eaux marines qui se déversent dans le Fjord à partir de l'Estuaire du St.-Laurent ou aurait pu s'accumuler suite à des déversements passés riches en arsenic.

Dans les environnements estuariens, l'adsorption sur la matière particulaire en suspension est souvent cité comme le vecteur principal de métaux traces vers les sédiments. Dans le cas de l'arsenic et du phoshore, ce processus s'avère tout particulièrement efficace lorsque les particules se composent d'oxihydroxides de fer. Néammoins, les oxides de manganèse et d'aluminium sont aussi de très bons adsorbants de ces deux éléments. Les eaux du Fjord du Saguenay contiennent des fortes concentrations d'aluminium particulaire ($[Al]_{tot}/[Al]_{diss} > 1$) dont la provenance est associée aux activités d'affinement de l'aluminium sur les rives de ses tributaires. La gibbsite ($Al(OH)_3$), un produit intermédiaire du processus d'affinage et dont l'affinité pour les ions arsenate et phosphate est bien documentée dans des solutions de faible force ionique, pourrait être un vecteur important de ces deux éléments vers les sédiments du Fjord.

Des mesures en laboratoire ont démontré que l'adsorption des ions arsenate et phosphate sur la gibbsite à partir d'une solution d'eau de mer est plus de cent fois plus faible que dans une solution de faible force ionique. L'adsorption réduite est expliquée par une compétition pour les sites d'adsorption par les ions majeurs de l'eau de mer. La compétition reflète une combinaison de l'affinité spécifique des ions et de leur abondance relative en eau de mer. L'affinité de l'ion fluorure pour la surface de la gibbsite est probablement responsable de la faible adsorption des ions arsenate et phosphate. La cinétique d'adsorption du phosphate semble aussi fortement affectée par cette compétition.

Les faibles quantités d'arsenate et phosphate adsorbées à la surface de la gibbsite à partir de l'eau de mer nous permettent de conclure que l'adsorption sur l'aluminum l'aluminium particulaire dans la colonne d'eau du Fjord ne contribuent pas de façon significative à la concentration de ces deux éléments dans les sédiments du Fjord du Saguenay.

Acknowledgements

This thesis while written under one name benefited greatly from the direct and indirect assistance of many. The largest share of the credit goes to Dr. Alfonso Mucci. His able supervision helped organize a jumble of confused thoughts into a coherent sequence. He was also always ready with a word of encouragement when it was most needed. His willingness to critically read the manuscript multiple times is also appreciated.

The assistance of Alcan, especially Mr. Jacques Labrie, is acknowledged. Alcan provided the gibbsite and allowed access to their facilities in the Saguenay region.

The patience and assistance of Constance Guignard in analytical matters is appreciated. Sandra Lalli and Glenna Keating provided more than able advice and technical support for the operation atomic adsorption spectrophotometer. They also put up gracefully with incessant question about when the AAS would be back on line.

Sam Alpay, Yan Gao and Gela Crane all provided useful criticisms of the thesis in its various stages. The process helped clarify some muddled conclusions. Chris Daughney, through his teaching of Aqueous Geochemistry, first raised my interest in adsorption and providing valuable input in the early stages of the study.

The project was supported financially by the NSERC research grant of Dr. Alfonso Mucci. Additional financial support was given in the form of a scholarship from GEOTOP, UQAM as well as teaching assistantships in the Department of Earth and Planetary Sciences McGill University.

Finally, I would like to thank my parents Gordon and Caroline Fitzpatrick who have always encouraged me in whatever I wished to do.

Table of Contents

List of Figures

List of Tables

Chapter 1 Introduction

In recent years the waters and sediments of the Saguenay Fjord have been the object of intense research activity. Part of the activity has been directed towards developing a geochemical model for the behaviour of chemical species that transit through the Fjord. This effort has included the analyses of both water and sediments. These analysis have revealed peculiar geochemical anomalies (Mucci & Edenborn, 1992; Gagnon et al., 1995; Richard, 1997; Alpay et al., 1998).

Amongst these anomalies are the elevated levels of arsenic in sediments of the Fjord compared to the Gulf and St. Lawrence Estuary. Elevated levels of arsenic have also been found in other estuarine environments (Peterson & Carpenter, 1986; Farmer & Lovell, 1986). These anomalies are obviously related to local conditions such as the geology of the drainage basin as well as local industrial and urban inputs. Anthropogenic sources (Peterson & Carpenter, 1986) as well as natural enrichment induced by post-depositional diagenetic remobilization (Farmer & Lovell, 1986) have been cited as causes. Arsenic is strongly associated with iron oxyhydroxide in lacustrine (Belzile, 1988; Belzile & Tessier, 1990; De Vitre et al., 1991; Widerlund & Ingri, 1996), marine (Sullivan & Aller, 1996) and estuarine sediments (Maher, 1984). Sediment arsenic is reported to be strongly associated with manganese oxides in coastal sediments and intermittently anoxic Fjords (Peterson & Carpenter, 1986). Extremely high arsenic levels without associated increases in manganese or iron found in Puget Sound were attributed to a high anthropogenic input (Peterson & Carpenter, 1986). Arsenic in the sediments of Lake Washington was found to be strongly associated with iron, manganese and aluminum compounds (Crecelius, 1975). Although it seems clear that arsenic is scavenged from the waters of the Fjord by settling particles; the precise scavenging agent or agents are unknown. There are also questions regarding the source of the arsenic. Elevated levels of phosphorus, in the form of phosphate are also found (Richard, 1997). The source of the phosphorous is more clearly defined as anthropogenic, primarily from

agricultural use of fertilizers and domestic waste water. The chemical similarity of phosphorous and arsenic suggests a similar scavenging process.

The adsorption of arsenic and phosphate to various geological materials is well established. As both of these elements have considerable importance to agriculture (phosphorus as a biolimiting nutrient and arsenic as a pesticide) the majority of the research was conducted on soil waters (i.e. low ionic strengths) and results have appeared in the soil science literature. Phosphate adsorption by soils has been correlated to their aluminum and iron oxide content by many authors (e.g. McLaughlan et al., 1981). The earliest work dealing with arsenic correlated its toxicity to plants in various soil types; arsenic toxicity in plants was found to decrease with increasing clay and iron oxide content and was ascribed to the immobilization of arsenic by iron oxides (Albert, 1932; Cooper et al., 1932; Giles, 1936).

The Saguenay Fjord is distinguished by high particulate aluminum anomalies; total amount of aluminum present is greater that the dissolved aluminum. The anomalies are introduced by the presence of extensive aluminum production facilities within the region. The nature of the production process and chemical considerations make it likely that gibbsite ($Al(OH)_3$) is the phase of the particulate aluminum. Aluminum oxides have been identified in the waters of the Fjord from microscopic examination of particulate matter recovered on filters of various pore sizes (S. Alpay, pers. comm.). This observation and the established affinity of arsenate for Al-oxides lead us to the hypothesis that adsorption onto gibbsite may be the cause for the arsenic and phosphate enrichment in the sediments of the Saguenay Fjord.

1.1 Objectives

The existence of both particulate aluminum and sediment arsenic anomalies in the Saguenay Fjord suggests a causal link. The known adsorption affinity of arsenate to gibbsite suggests adsorption as the active process of the link. The same process may also

be responsible for elevated phosphate levels. Therefore, the objective of this study is to establish the effectiveness of gibbsite as a vector for arsenic and phosphate to the sediments of the Saguenay Fjord.

The importance of this mechanism can be determined by measuring the adsorption of arsenate and phosphate to gibbsite from seawater solutions. The influences of temperature and the kinetics of the adsorption reaction will also be investigated to better constrain the role of adsorption in scavenging these ions in the water column of the Fjord. The adsorption will be described by the use of isotherms.

1.2 Structure of the Thesis

The thesis is presented in five chapters. The first chapter is an introduction setting out the rationale and objectives of the thesis.

Necessary background to the experimental work is presented in chapter two. This includes a description of the relevant physical and chemical characteristics of the Saguenay Fjord, the main anthropogenic sources to the Fjord. A summary of adsorption theory, and a description of the three major components of the experimental system. Details of previous adsorption studies are presented. The data are used to predict the influence of artifical seawater on the adsorption of phosphate and arsenate on gibbsite.

Chapter 3 presents the methods that were used in the experimental study. Chapter 4 contains the results and corresponding discussion of the experiments. Adsorption is described by isotherms and comparisons between results of the adsorption studies are made. This includes an attempt to derive a specific surface area. Based on the results, adsorption equilibria are proposed. There follows a discussion concerning the adsorption behaviour of sea salts, including fluoride. Results of the kinetic, temperature effects, and solid solution dependence experiments follow. Interpretations of the adsorption behaviour in the artificial seawater are proposed and a calculation is made to estimate the significance of adsorption to gibbsite on the enrichment of arsenic and phosphorus in the

Saguenay Fjord sediments. The last part of this chapter is a discussion of other potential causes for the enrichment of the sediments.

Conclusions are drawn in chapter five. In addition suggestions for future research are made. The reference list follows.

Chapter 2 Background

In recent years the waters and sediments of the Saguenay Fjord have been the object of intense research activity. Part of the activity has been directed towards developing a geochemical model for the behaviour of chemical species that transit through the Fjord. This effort has included the analyses of both water and sediments. These analysis have revealed peculiar geochemical anomalies (Mucci & Edenborn, 1992; Gagnon et al., 1995; Richard, 1997; Alpay et al., 1998).

Amongst these anomalies are the elevated levels of arsenic in sediments of the Fjord compared to the Gulf and St. Lawrence Estuary. Elevated levels of arsenic have also been found in other estuarine environments (Peterson & Carpenter, 1986; Farmer & Lovell, 1986). These anomalies are obviously related to local conditions such as the geology of the drainage basin as well as local industrial and urban inputs. Anthropogenic sources (Peterson & Carpenter, 1986) as well as natural enrichment induced by post-depositional diagenetic remobilization (Farmer & Lovell, 1986) have been cited as causes. Arsenic is strongly associated with iron oxyhydroxide in lacustrine (Belzile, 1988; Belzile & Tessier, 1990; De Vitre et al., 1991; Widerlund & Ingri, 1996), marine (Sullivan & Aller, 1996) and estuarine sediments (Maher, 1984). Sediment arsenic is reported to be strongly associated with manganese oxides in coastal sediments and intermittently anoxic Fjords (Peterson & Carpenter, 1986). Extremely high arsenic levels without associated increases in manganese or iron found in Puget Sound were attributed to a high anthropogenic input (Peterson & Carpenter, 1986). Arsenic in the sediments of Lake Washington was found to be strongly associated with iron, manganese and aluminum compounds (Crecelius, 1975). Although it seems clear that arsenic is scavenged from the waters of the Fjord by settling particles; the precise scavenging agent or agents are unknown. There are also questions regarding the source of the arsenic. Elevated levels of phosphorus, in the form of phosphate are also found (Richard, 1997). The source of the phosphorous is more clearly defined as anthropogenic, primarily from

agricultural use of fertilizers and domestic waste water. The chemical similarity of phosphorous and arsenic suggests a similar scavenging process.

The adsorption of arsenic and phosphate to various geological materials is well established. As both of these elements have considerable importance to agriculture (phosphorus as a biolimiting nutrient and arsenic as a pesticide) the majority of the research was conducted on soil waters (i.e. low ionic strengths) and results have appeared in the soil science literature. Phosphate adsorption by soils has been correlated to their aluminum and iron oxide content by many authors (e.g. McLaughlan et al., 1981). The earliest work dealing with arsenic corelated its toxicity to plants in various soil types; arsenic toxicity in plants was found to decrease with increasing clay and iron oxide content and was ascribed to the immobilization of arsenic by iron oxides (Albert, 1932; Cooper et al., 1932; Giles, 1936).

The Saguenay Fjord is distinguished by high particulate aluminum anomalies; total amount of aluminum present is greater that the dissolved aluminum. The anomalies are introduced by the presence of extensive aluminum production facilities within the region. The nature of the production process and chemical considerations make it likely that gibbsite ($Al(OH)_3$) is the phase of the particulate aluminum. Aluminum oxides have been identified in the waters of the Fjord from microscopic examination of particulate matter recovered on filters of various pore sizes (S. Alpay, pers. comm.). This observation and the established affinity of arsenate for Al-oxides lead us to the hypothesis that adsorption onto gibbsite may be the cause for the arsenic and phosphate enrichment in the sediments of the Saguenay Fjord.

2.1 The Saguenay Fjord

The Saguenay Fjord is a long and narrow glacially eroded submerged valley that connects the Saguenay River at St. Fulgence to the St. Lawrence Estuary at Tadoussac (Figure 2.1,Figure 2.2).

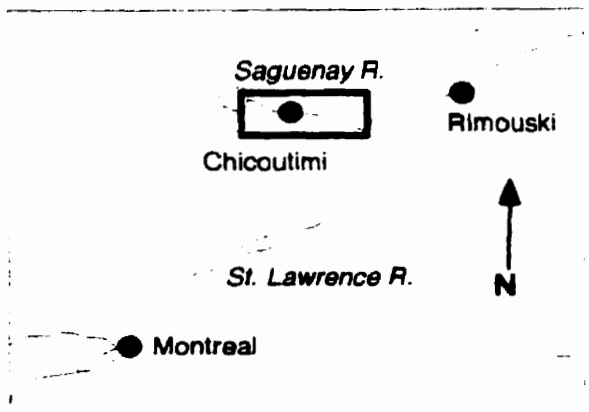

Figure 2.1 Regional setting of the Saguenay River and Fjord

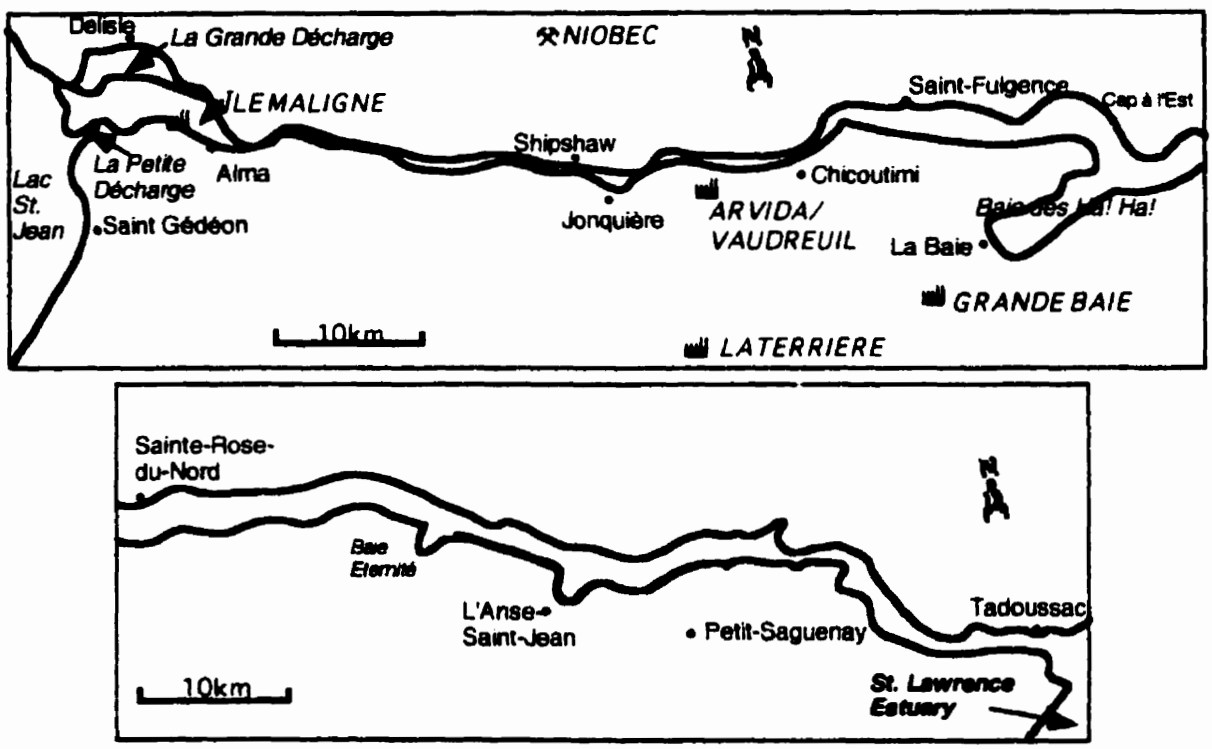

Figure 2.2 Saguenay River and Fjord. Alcan facility, mine.

It has a U–shape cross–section and is delineated by a shallow sill (20m) at the entrance to the Fjord. The Fjord itself is divided by a second sill (80m depth), 18 km upstream, into two distinct basins. The "exterior" basin reaches a maximum depth of 250 m. The larger "interior" basin extends from the sill westward to St. Fulgence reaching a maximum and nearly constant depth of 275m. The major tributary of the Fjord is the Saguenay River that accounts for 90% of the freshwater input to the Fjord. For the purposes of

identification, the hydrographic system is divided into three parts: the upper Saguenay between Lac Saint-Jean and the Shipshaw dam which is unaffected by marine waters and is characterized by a large elevation drop: 2) the middle Saguenay between the Shipshaw dam and Saint Fulgence, 3) and the Saguenay Estuary between Saint Fulgence and Tadoussac.

The water column of the estuary is characterized by a thin freshwater lens, a strong near-surface (10-15m) halocline, and well mixed waters at depths greater than 30 m. The bottom waters, originating from the St. Lawrence Estuary (Therriault & Lacroix, 1975; Seibert et al., 1979), have a salinity of about 30, are well oxygenated and display only minor annual temperature variations; -1 to 1 °C (Drainville, 1968; Sundby & Loring, 1978).

2.1.1 Industrial Activity

The watershed of the Saguenay Fjord is a heavily industrialized area. The industrial activity has historically been unregulated resulting in elevated levels of a variety of contaminants in both the waters and sediments of the Fjord (Fortin & Pelletier, 1995). In recent years, because of government regulations, large reductions in contaminant discharge have been achieved.

The industrial activity is dominated by the aluminum production facilities of Alcan. These facilities have introduced many contaminants to the Fjord including mercury, arsenic and aluminum. The facilities include a large inorganic chemical plan at Jonquière (Vaudreuil works) and four smelters (Arvida, Île Maligne, Grande Baie, and Laterrière). Alcan also operates its own transport facilities; a major port at La Baie (Port Alfred) and a railway (Saguenay and Roberval). The Vaudreuil works includes a large Bayer plant (conversion of bauxite to alumina (Alcan, 1990)) as well as plants for the production of aluminum fluoride and synthetic cryolite. A chloro-alkali plant (closed in 1976) operated for nearly 40 years at this site (Guay & Couillard, 1980). The smelters use

the Hall-Herault electrochemical process (Cundiff et al., 1985) to reduce alumina to metallic aluminum. The operational process differs between the smelters; the older plants (Arvida and Île Maligne) use the Söderberg process (Cundiff et al., 1985) and the modern plants use pre-baked anodes. The Arvida plant fabricates primary aluminum as well as anodes and cathodes for itself and the Île Maligne plant. The smelter at Île Maligne produces aluminum ingots (MOE, 1996). These plants are in the process of decommissioning; the Arvida plant already has 10 of 20 Söderberg potlines decommissioned (MOE, 1996). The remaining Söderberg lines at Arvida and the entire Île Maligne smelter are to be replaced by the new Alma smelter (completion 2001) (CMJ, 1998). The modern smelters all produce primary aluminum; the facility at Grande Baie also manufactures prebaked anodes. All facilities drain to the Saguenay River or to the Saguenay Fjord. There are significant differences between the older and modern plants in terms of effluent aluminum load (see Table 2.1). Unmeasured amounts of aluminum minerals may also enter the Fjord via wind and losses in transport and handling. Arsenic, an impurity of the primary ore material bauxite, is released from the Vaudreuil facility during the Bayer process. Historically this has been significant (see Table 2.1) but the effluent load has been greatly reduced by adsorption onto γ-alumina in decantation pools. (J. Labrie pers. comm.)

Of some importance are the five large pulp and paper mills located in the region. These plants have historically contributed primarily organic contaminants including dioxins and furans. Metals such as nickel, lead, zinc and copper have also been part of the effluents from these plants. A significant load of aluminum was formerly released from the Abitibi-Price mill at Alma (MOE, 1996).

The Niobec niobium mine and mill located 10 km north of Chicoutimi introduces a small amount of arsenic to the Fjord. The mine and mill have been operating since 1976 with a major expansion in 1981 (Gendron et al., 1983). The ore rock of this mine is reported to contain up to 20 ppm arsenic (Fournier, 1994). The mining and milling of the

ore results in an effluent load of 14.6 kg/year of arsenic. Additives used in the milling process contribute an effluent load of 197.1 kg/year of aluminum (Groupe LGL, 1989). The database on industrial effluent loads is sparse (Table 2.1) and effluent loads are highly variable in time.

Table 2.1 Industrial effluent loads (kg/day)

Plant (Year built)	Year	As	P	Al	Source
Alcan Arvida/Vaudreuil (1924)	1976	N/A		2000	Duchesneau & Riverin, 1976
	1988	1.2		2642	MOE, 1996
	1995	0.3		470	
Alcan Île Maligne (1944)	1988	–		7.8	MOE 1996
	1995	–		6.0	
Alcan Grande Baie (1980)	1988	–		1.3	MOE, 1996
	1995	–		1.2	
Alcan Laterriere (1989)	1993	–		1.1	MOE, 1996
	1995	–		1.5	
Niobec (1976)	1987	0.04		–	Groupe LGL, 1989
	1991	0.02		5.9	MOE, 1996
Cascades Jonquière	1989	–		81.2	Groupe LGL, 1989
	1995	–		–	MOE, 1996
Abitibi–Price Kenogami	1989	–		34.5	Groupe LGL, 1989
	1995	–		–	MOE, 1996
Abitibi–Price Alma	1989	–		12.5	Groupe LGL, 1989
	1995	–		25.7	MOE, 1996
Stone–Consolidated Pt Alfred	1989	–		89	Groupe LGL, 1989
	1995	–		19.5	MOE, 1996

2.1.2 Arsenic in the Saguenay Fjord Estuary

Arsenic levels in estuarine sediments collected near the water-sediment interface are reported to vary between 10 and 25 ppm (Belzile, 1988; Richard, 1997; Maher, 1984). Analysis of surficial sediments of the middle Saguenay River and the upper Saguenay Fjord (Ouellet, 1979; Primeau & Goulet, 1983; Mucci et al. 1999) have shown significant enrichment in arsenic in the Baie des Ha! Ha! (Figure 2.1) and seaward in the interior basin. Near normal levels occur in the Bras du Nord, the near shore area at La Baie, and with the exception of the immediate area around Arvida, the middle Saguenay River. Surface sediments (0-1 cm) recovered upstream of Baie Eternite have an arsenic concentration of 55 ppm (Gobeil, 1996). This is about 2 to 4 times what is observed in the St. Lawrence Estuary.

The source of the arsenic in the sediments is unclear. It has been attributed to anthropogenic contamination by Ouellet (1979) but no specific source was identified. The elevated levels around the outfall of the Vaudreuil works can be attributed to the former high effluent load from that plant, but the arsenic in the Baie des Ha! Ha! can not be directly traced to Vaudreuil since levels in the Bras Nord are typical for marine sediments. The arsenic associated with the bauxite shipped through the Fjord and off loaded at Port Alfred is a possible anthropogenic source. Dissolved arsenic in the waters of the river and the freshwater lens of the Fjord are amongst the lowest levels reported for industialized and "pristine" estuaries. Primeau and Goulet (1983) reported levels below 30 nM for waters of the Baie des Ha! Ha!. Levels as low as 1 nM in the Saguenay River increasing to a mean concentration of 19 nM at maximum salinity have been reported (Tremblay and Gobeil, 1990). Similar levels have been measured more recently (Alpay, unpublished data, Mucci et al. 1999). With the tremendous reduction of effluent arsenic in recent years, it can be surmised that current levels of anthropogenic arsenic are probably lower than anytime since 1924. The current, most likely arsenic source is seawater; oceanic seawater has an average concentration of 26 nM and an As/Cl ratio of ~5 x 10^{-6} (Onish, 1969). Levels in the St. Lawrence Estuary are reported at approximately 16 nM (Tremblay & Gobeil, 1990).

It is commonly accepted that arsenic will be "scavenged" by suspended particulate matter (SPM) in estuarine environments. Ferric oxides and hydroxides (Sadiq, 1990; Morse, 1994), manganese oxides and organic material have commonly been cited as important scavengers. The role of aluminum oxides and hydroxides is to be determined in this thesis. With the low concentration of dissolved arsenic in the Fjord, the sediment enrichment can not be attributed to the precipitation of an authigenic As-bearing phase. Since suspended particulate matter (SPM) levels in the Fjord and the St. Lawrence Estuary are nearly identical (0.6 and 0.7 mg/L) (Richard, 1997), arsenic accumulation in the sediments of the Fjord cannot be accounted for by this variable. Alternatively, the

SPM of the Fjord may have a greater scavenging efficiency for arsenic resulting from differences in composition, and the highly stratified nature of the estuarine water column. Burial rates are also similar, they vary from <0.2 to 1.1 cm/y in the St. Lawrence Estuary (Silverberg et al., 1990; Jennane, 1992) and are between 0.2 and 7 cm/y in the upper basin of the Saguenay Fjord (Perret et al., 1995).

2.1.3 PHOSPHORUS IN THE SAGUENAY FJORD ESTUARY

Phosphorus in the sediments of the Saguenay Fjord is slightly elevated in comparison to levels in the St. Lawrence Estuary. Levels at the water-sediment interface in the Fjord are as high as 0.15%; levels in the St. Lawrence Estuary are around 0.11% (Richard, 1997). The source of the phosphate is undoubtedly anthropogenic. The Lac St. Jean region is heavily farmed and thus the application of fertilizer represents a source of phosphate. The level of phosphate in the marine waters of the Fjord are less than that of the St. Lawrence Estuary (0.2 μM as opposed to 0.8 μM). Like arsenate, greater scavenging efficiency of phosphate by SPM in the Fjord has been proposed to explain the higher sediment concentrations (Lucotte & d'Anglejan, 1988; Richard, 1997)

2.1.4 PARTICULATE ALUMINUM IN THE SAGUENAY FJORD ESTUARY

Particulate aluminum concentrations in the freshwater lens of the Saguenay Fjord of up to 150.8 ppb in the freshwater lens can be calculated from the suspended particulate matter measurements and the elemental analyses of Sundby & Loring (1978) from samples taken in 1974. More recent analyses (samples taken in 1996) show that levels have fallen in recent years to a maximum of 100 ppb (Alpay, unpublished data). The amount of particulate aluminum in the freshwater lens decreases with distance from the Saguenay River. The majority of the particulate aluminum can be attributed to anthropogenic sources, specifically the smelter at Alma and the combined plant at Jonquière. Observed reductions can be attributed to improvements in environmental controls at Alcan facilities and consequent reductions in effluent loading. It should be

noted that the exact nature of the particulate aluminum has not been identified except for FEG-SEM/EDX of grains composed of aluminum and oxygen that may be gibbsite. Although gibbsite is theoretically unstable in seawater in the presence of silica, work by Crane (1998) has shown gibbsite to be metastable in seawater for periods of up to seven months. The material entering the Fjord is likely either gibbsite or γ-alumina since both are manufactured by Alcan. The stability of γ-alumina in seawater is unknown and has apparently not been. Aluminum has been detected in sediment analysis (Mucci & Edenborn, 1992). The aluminum may come from the feldspars and clay minerals in the sediments in addition to the aluminum minerals.

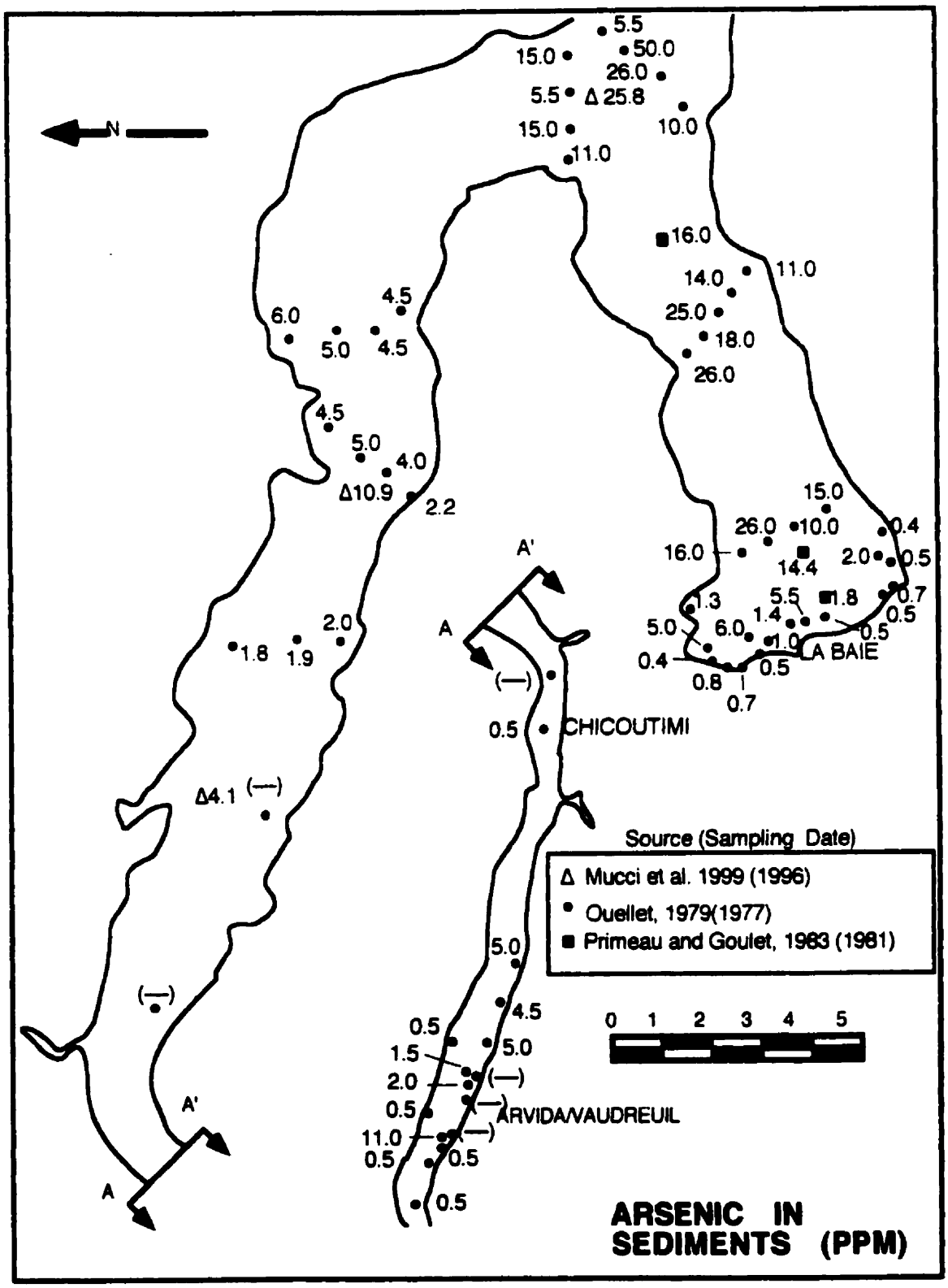

Figure 2.3 Arsenic in Saguenay Fjord sediments

2.2 Adsorption and the Solid-Solution Interface

Surface science and more specifically the characterization of mineral–solution interfaces is an area of extensive study supported by a voluminous literature. As any piecemeal review of such an extensive body of work would be likely inadequate, the following is derived mostly from the excellent reviews of Davis & Kent (1990) and Stumm & Morgan (1996).

2.2.1 The Hydrous Oxide-Solution Interface

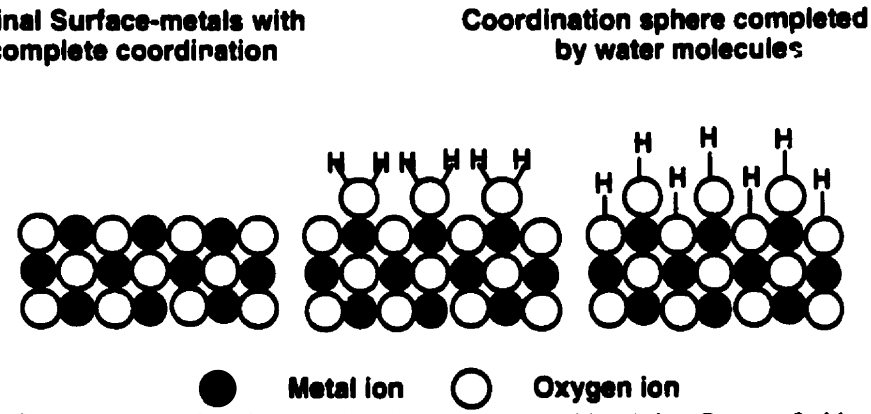

Figure 2.4 Development of surface hydroxyl groups on oxides (after Stumm & Morgan, 1996)

In the presence of water an oxide will become covered in surface hydroxyl groups (Figure 2.4). Schematically these groups are represented as variants of the functional group ≡S-OH. The full range of these groups is predicted by Schindler (1985).

2.2.2 Adsorption

Adsorption refers to the attachment of dissolved species to a solid surface such that the species do not enter or form the structure of a solid phase. Where such a distinction is not possible the more general term of sorption is commonly used as it includes co-precipitation and absorption.

2.3 Empirical Approaches to Adsorption Modeling

In many cases, a non-mechanistic approach to adsorption is all that is required for a model. These empirical approaches are widely used in geochemical transport or other

global models where the computational simplicity and low data requirements outweigh the greater applicability of an analytical approach. No attempt is made to describe the process by which adsorption occurs, the reliability of the predicted results is the goal. Such approaches provide a correlation or fitting coefficient between the amount of adsorbed solute and the solute concentrations in solution. The simplest of the correlations is the *partitioning coefficient*, K_d.

$$\Gamma_J = [J_{aq}]\, K_d \qquad [2.1]$$

where $[J_{aq}]$ = concentration of solute
Γ_J adsorption density (moles m^{-2} or mole g^{-1})

This coefficient gives a simple linear relationship between adsorption density and concentration. An adaptation of this equation, the general partitioning equation of Honeyman & Leckie (1986), accounts for proton exchange;

$$\Gamma_J = \frac{K_{part} \bullet_S [J]}{[H^+]^{\chi}} \qquad [2.2]$$

where χ = apparent ratio of moles of protons released per mole of solute J adsorbed.
Γ_s surface density of uncomplexed adsorption sites

Results of a large number of adsorption studies have been represented by the Freundlich and the Langmuir isotherms. The Freundlich isotherm is an exponential isotherm.

$$\Gamma_J = ([J_{aq}]\, K_f)^{\beta} \qquad [2.3]$$

where β = empirical parameter.

When the parameter is equal to 1 the Freundlich isotherm reduces to the simple partition isotherm. The Langmuir isotherm takes into account the finite number of adsorption sites on a surface. The Langmuir isotherm also assumes identical energies for all adsorption sites and monolayer coverage. The mass law equation is written as:

$$\Gamma_J = S_T\left[\frac{K_L [J_{aq}]}{1+K_L[J_{aq}]}\right] \qquad [2.4]$$

where S_T = density of all adsorptive sites

A number of other isotherms have been proposed which include additional adjustable parameters such as the Langmuir-Freundlich, Redlich-Peterson, Toth and Dubinin-Radushkevich isotherms (see Kinniburgh, 1986). Multiple site versions of the Langmuir and Freundlich isotherms have also been suggested (Kinniburgh, 1986). These isotherms have been used with variable success. However, with increasing parameters, the computational benefits of the empirical approach are diminished.

2.3.1 SURFACE COORDINATION THEORY

To design a mechanistic model of adsorption it is first necessary to develop a model of the forces and interactions at an interface. Three forces promote adsorption. In order of increasing strength they are van der Waals interactions, electrostatic forces, and chemical affinity. The forces are not exclusive of each other and so adsorption is the sum of the interaction of the three forces. van der Waals interactions are generally weak and are largely insignificant when the other forces are in operation. Electrostatic forces result from the allocation of surface and dissolved species of opposite charge. Chemical affinity refers to the formation of surface complexes with some degree of covalency. This type of adsorption, also known as chemisorption, is so strong that electrostatic or mass law constraints may not apply.

Rigorous interpretations of adsorption are based on the concept of surface coordination. Surface coordination extends the ion pairing and complex formation that occurs in solution to include chemical species on surfaces. The basic tenets of surface coordination theory are:

1. A surface is composed of specific functional groups that react with dissolved solutes to form surface complexes (coordinative complexes or ion pairs) in a manner analogous to reactions in homogeneous solution. A surface may have a single or multiple types of surface functional groups. The amount of functional groups is finite and is expressed as a density/

2. Equilibria of surface complexation and ionization reactions can be described by mass law equations with corrections for variable electrostatic energy.

3. Surface charge and surface electrical potential are necessary consequences of chemical reactions of the surface functional groups. Specific chemical interactions dominate the electrical properties; the electric field and electrostatic effects are secondary factors resulting from the surface coordination reactions.

4. Apparent binding constants of the mass law equations are empirical parameters related to thermodynamic constants via the activity coefficients of the surface species.

The surface hydroxyl groups of a hydrous oxide have similar donor properties as their dissolved solutes, such as hydroxides and carboxylates. The most important adsorption (surface complex formation) equilibria are (from Stumm & Morgan, 1996);

Acid Base Equilibria

$$\equiv S\text{-}OH + H^+ \leftrightarrow \equiv S\text{-}OH_2^+ \quad [2.5]$$

$$\equiv S\text{-}OH + OH^- \leftrightarrow \equiv S\text{-}O^- + H_2O \quad [2.6]$$

Metal Binding

$$\equiv S\text{-}OH + M^{Z+} \leftrightarrow \equiv S\text{-}Om^{(z-1)+} + H^+ \quad [2.7]$$

$$2 \equiv S\text{-}OH + M^{Z+} \leftrightarrow (\equiv S\text{-}O)_2M^{(z-1)+} + 2H^+ \quad [2.8]$$

$$\equiv S\text{-}OH + M^{Z+} + H_2O \leftrightarrow \equiv S\text{-}OMOH^{(z-2)+} + 2H^+ \quad [2.9]$$

Ligand Exchange

$$\equiv S\text{-}OH + L^- \leftrightarrow \equiv S\text{-}L + OH^- \quad [2.10]$$

$$2 \equiv S\text{–}OH + L^- \leftrightarrow \equiv S_2\text{-}L^+ + 2OH^- \quad [2.11]$$

Ternary Surface Complexation

$$\equiv S\text{-}OH + L^- + M^{Z+} \leftrightarrow \equiv S\text{-}L\text{-}M^{Z+} + OH^- \quad [2.12]$$

$$\equiv S\text{-}OH + L^- + M^{Z+} \leftrightarrow \equiv S\text{-}OM\text{-}L^{(z-2)+} + H^+ \quad [2.13]$$

where $\equiv S\text{–}OH$ = surface functional group
$\equiv M^{Z+}$ metal of charge Z
$\equiv L^-$ ligand

2.3.1.1 Inner and Outer-sphere Complexes

As illustrated by Figure 2.5, ions can also be part of the diffuse swarm. The chemical bonded ions represent inner-sphere adsorption whereas the ion pairing is referred to as outer–sphere complexation

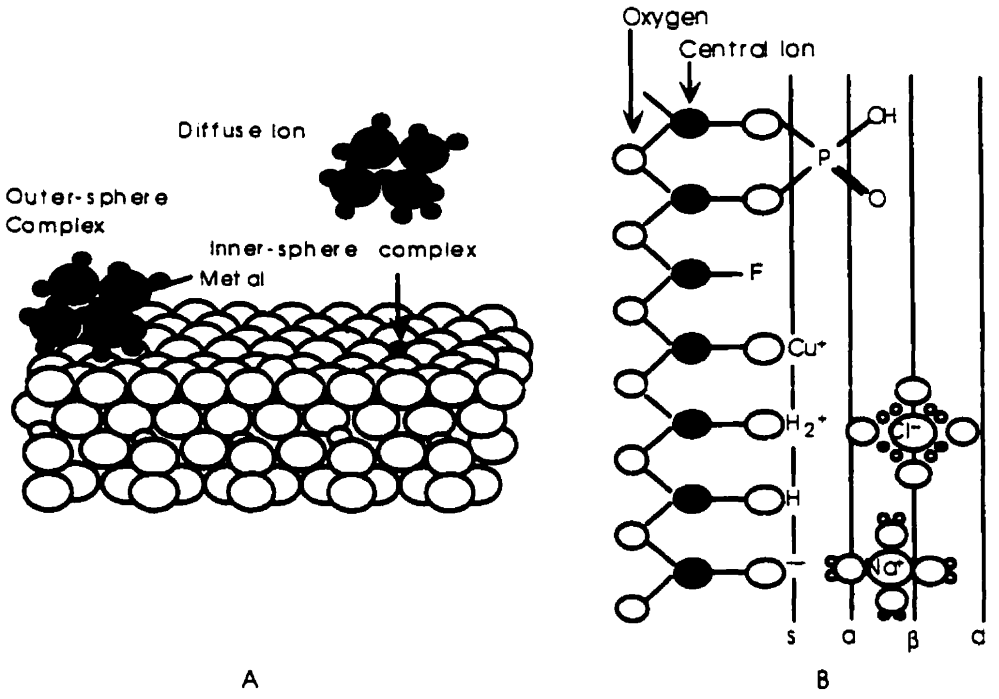

Figure 2.5 (A) Surface complex formation of an ion on a hydrous oxide surface. (B) Schematic portrayal of hydrous oxide surface. After Sposito (1989,1984)

In Figure 2.5B, the planes associated with surface hydroxyl groups ("s"), inner-sphere complexes (a), outer-sphere complexes ("β") and the diffuse ion swarm ("d") are shown. There is a great deal of difference between the two adsorption complexes so much so that inner–sphere and outer–sphere complexes of the same ion must be treated as different chemical entities. The two types can be distinguished by the effect of ionic strength on adsorption— a strong dependence on ionic strength is typically observed for outer-sphere adsorption. Outer-sphere adsorption is also less stable as it involves electrostatic bonding and so is influenced by a greater number of factors than inner-sphere adsorption.

2.3.2 Charge Distribution at Solid-Solution Interfaces

The boundary between any two distinct phases is an area of dissymmetry. In the case of the interface between a mineral and a solution, the dissymmetry is countered by a structural reorganization that reflects the competing interactions of the bulk phases. The structural reorganization results in a charge separation and the consequent creation of an electrical potential relative to the bulk solution phase.

Charges that develop on the surface of the mineral are of three types 1) *permanent* structural charge, 2) *coordinative* surface charge, and 3) *dissociated* charge. A permanent charge develops as a result of isomorphic substitutions in a mineral, such as the replacement of Al^{3+} for Si^{4+} in the crystal lattice of phyllosilicates. Such substitutions are rare in oxides and hydroxides and thus permanent surface charge is generally absent from such minerals. The coordinative charge is the charge directly associated with the surface. It results from the ionization of the surface functional groups (equations 2.5 and 2.6). The dependence of surface charge on pH is evident. The surface charge is also a result of the coordinative binding of a solute to the surface or adsorption (equations 2.7-2.13)

The total surface charge, the sum of permanent and coordinative charges, is expressed as a density, in units of charge per unit area. The net surface charge density of a hydrous oxide is given by

$$\sigma_p = F[\Gamma_H - \Gamma_{OH} + \Sigma(Z_M\Gamma_M) + \Sigma(Z_A\Gamma_A)] \qquad [2.14]$$

where σ_p = net surface charge density (C m^{-2})
F Faraday constant (96490 C mol^{-1})
Z valency of sorbing ion
Γ adsorption density (mol m^{-2}) of H^+, OH^-, metal ions, and anions

The net proton charge σ_H (C m^{-2}), the charge resulting from the binding of protons to the surface — also known as surface protonation— is

$$\sigma_H = F(\Gamma_H - \Gamma_{OH}) \qquad [2.15]$$

Similarly a coordinative complex charge is the sum of the densities of the adsorbing ions. To express a charge in terms of mass (i.e. C kg^{-1}) it is necessary to multiply the sorption density by the specific surface area (m^2 kg^{-1}) of a particle.

The charge that develops at the surface of a particle is balanced by the charge of ions in the diffuse swarm, which while free in solution, remain near enough to a surface to balance the surface charge thus

$$\sigma_p + \sigma_o = 0 \qquad [2.16]$$

where σ_D = diffuse charge

Each ion in the diffuse swarm contributes to the diffuse charge. The effective charge of an individual ion *i* can be apportioned by

$$\sigma_{Di} = \frac{Z_i}{m_s} \int_V [c_i(x) - c_{0,i}] dV \qquad [2.17]$$

where Z_i = valence of ion
$c_i(x)$ concentration of ion at point x in the solution
$c_{0,i}$ concentration of ion in bulk solution
m_s mass of solid adsorbent

The integral in equation 2.17 is applied over the entire volume of the aqueous solution containing the adsorbent. The equation represents the distribution of the charge of the ion in aqueous solution. The equation applies equally to all ions in solution including H^+ and OH^- and the total diffuse charge is the sum of the individual ion charges.

2.3.3 Point of Zero Charge

An important parameter in explaining the adsorption behaviour of a hydrous oxide is its point of zero charge. The *point of zero charge* (pzc) is the pH at which the net surface charge is equal to zero, thus

$$\text{at pzc: } \sigma_p = 0 \qquad [2.18]$$

This point is also refereed to as the isoelectric point (iep), the condition when particles will not move in an applied electrical field. A pzc established solely due to the binding of H^+ or OH^- may be distinguished as the *point of zero net proton charge* (pznpc),

$$\text{at pznpc: } \sigma_H = 0 \qquad [2.19]$$

2.3.4 Surface Coordination And Interface Models

Rigorous surface complexation models have been used in relatively simple systems. They have an advantage in that they can be applied under a wide range of conditions. Their drawback is that they require an extensive database. Underlying all

models is a particular interpretation of the solid–solution interface. As illustrated previously, the electric state of a surface is dependent on the distribution of free charge in its neighbourhood. The distribution is usually idealized as an *electric double layer*; the surface charge is seen as one layer and the second is the diffuse charge which is distributed diffusely in the liquid in contact. This is a representation of the Gouy-Chapman model.

2.3.4.1 GOUY-CHAPMAN MODEL

The Gouy-Chapman model relates surface charge density, σ_ρ, to the potential at the surface, ψ_0 (volt):

$$\sigma_\rho = \sqrt{8RTee_0c \times 10^3} \sinh\left(Z\psi_{\sigma}^{F} RT\right) \qquad [2.20a]$$

where

R		gas law constant (8.314 J mol^{-1} K^{-1})
T		Absolute Temperature (K)
ε		Relative dielectric constant of water (78.5 @ 25°C)
ε_0		Permittivity of free space ($8.854 * 10^{-12}$ C V^{-1} m^{-1} (C^2 J^{-1} m^{-1})
c		molar electrolyte concentration (M)
Z		valence of ion

Equation 2.20a is valid when the electrolyte is symmetrical (Z = ionic charge). The full derivation of the equation is available elsewhere (Sposito, 1984) At low potential, equation 2.20a can be linearized as

$$\sigma_\rho = \varepsilon\varepsilon_0 \kappa\psi_0 \qquad [2.20b]$$

The Debye parameter, κ, is defined by

$$\kappa = \sqrt{\frac{2F^2 I \times 10^3}{ee_0 RT}} \qquad [2.20c]$$

The double layer thickness in meters is the reciprocal of the Debye parameter. A schematic of the model is given below (Figure 2.6A).

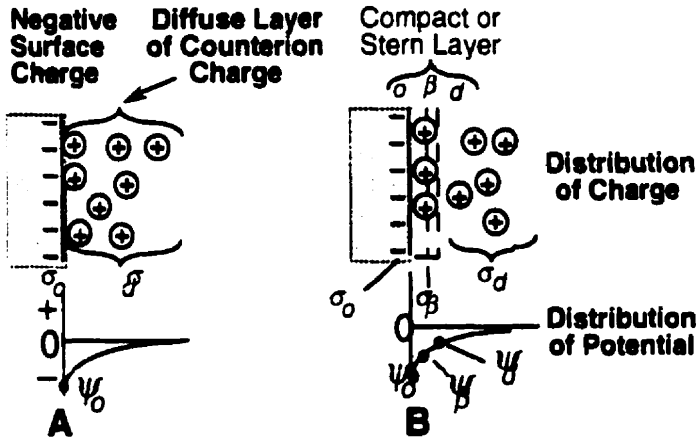

Figure 2.6 Schematic drawings of electrical double layer models. A: Gouy-Chapman B: Stern (after James & Parks, 1982)

2.3.4.2 STERN-GRAHAME MODEL

The Gouy-Chapman model is not adequate when the product of the distance from the surface and the Debye parameter is small and the surface potential is high. Under these conditions, the Gouy-Chapman model predicts excessively large local concentrations of ions near the surface. This prediction is the consequence of considering ions as point charges and neglecting their ionic diameter. Alternatively, Stern (1923) suggested dividing the interface into two regions, a compact layer of ions adsorbed at the surface and a second diffuse layer. The compact layer could include ions with specific (or inner–sphere) adsorption potential. This compact region is given a finite limitation on the concentration of ions within it (Figure 2.6B). Grahame (1947) expanded the model by dividing the compact region into two layers; an inner layer of specifically adsorbed ions and an outer layer of non–specifically adsorbed ions. These two layers are called the inner and outer Helmholtz planes respectively (IHP, OHP).

2.3.5 MODELS OF HYDROUS OXIDE–WATER INTERFACE

Stumm & Morgan (1996) argue that the oxide water interface requires its own model of interface structure to describe electrostatic energies of adsorption. Westall & Hohl (1980) have summarized the proposed models ranging from the simple to the

complex such as the Stern–Grahame based triple layer model. The central issue is how to relate chemical concepts of the interface to electrostatic principles.

Most models use one of the two classical EDL models to define the interface structure. This results in consideration of surface reactions and electrostatic corrections. All models reduce to a set of numerically solvable simultaneous equations. The equations include: (1) mass law equations, (2) mole balance equations for surface sites, (3) surface charge, and (4) structural constraint equations.

The majority of the models have used a diprotic representation of the oxide surface. Thermodynamic constants for the ionization reactions (equations 2.5, 2.6) can be determined. For equation 2.5 the constant is

$$K_{a1}^{0} = \frac{[\bullet SOH]\,[H^{+}]}{[\bullet SOH_2^{+}]} \frac{[gSOH]\,[gH^{+}]}{[gSOH_2^{+}]} \quad [2.22a]$$

In practice the activity coefficients of the surface species are not readily determinable so that it is necessary to define an intrinsic equilibrium constant.

$$K(int) = \frac{[\text{Products (including surface species)}]}{[\text{Reactants (including surface species)}]} \exp\frac{nF\psi_0}{RT} \quad [2.22b]$$

where n = number of protons in the reaction.

The standard state for adsorption equilibria is determined at the point of zero charge. This represents adsorption onto a surface of null net charge and is more akin to chemical adsorption than electrostatic adsorption.

The generalized form of surface coordination is as follows (Sposito, 1984):

$$a(\equiv SOH) + pM^{m+} + qL^{-} + xH^{+} + OH^{-} \Leftrightarrow \equiv (SO)_a M_p (OH)_y H_x L \quad [2.23]$$

$$b(\equiv SOH) + qL^{-} + xH^{+} \Leftrightarrow \equiv S_b H_x L_q^{\zeta} + bOH^{-} \quad [2.24]$$

where $\delta = pm + s - a - ql - y$ *and* $\zeta = x + b - ql$ are valences of the surface complexes formed. The valences contribute to the coordinative surface charge. All models treat adsorption of strongly bound inner-sphere complexes (specifically adsorbed) ions in accordance with equations 2.20 and 2.21. The models differ in their approach to weakly

bound ions and the EDL model used. The different models use electrostatic correction factors that are consistent with the interfacial structure of the EDL model.

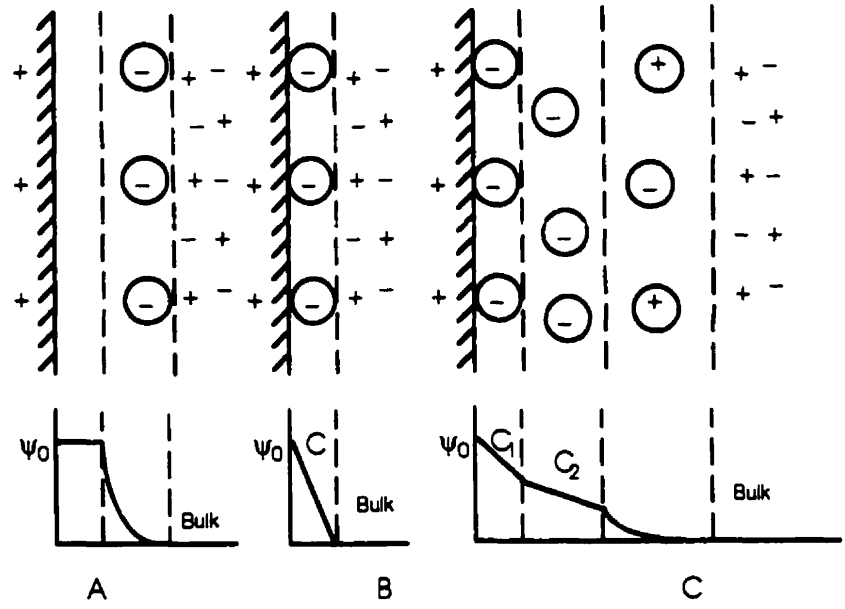

Figure 2.7 Schematics of surface complexation models A) Diffuse Double Layer Model B) Constant Capacitance Model C) Triple Layer Model (After Stumm & Morgan, 1996)

A simple model of the interface is obtained by including all surface species as part of σ_p and considers a single surface potential $\psi_0 = \psi_D$ and one charge density $\sigma_p = -\sigma_D$. Chemical inputs are total surface site density and mass law constants for specifically bound ions. This diffuse double layer model (DDLM) (Figure 2.7A) was developed by Stumm et al. (1970) and Huang & Stumm (1973). The DDLM incorporates the Gouy-Chapman model. The effect of ionic strength on adsorption is accounted for by the dependence of the surface charge on ionic strength (Equations 2.20 a-c). Surface reactions are described in terms of amphoteric hydroxyl groups and inner-sphere co-ordination reactions. The model incorporates two layers; a surface plane that encompasses proton transfer reactions and inner–sphere coordination complexes and a diffuse layer plane; this represents the distance of closest approach for all counterions.

The constant capacitance model (CCM) (Figure 2.7B) is a special case of the DDLM and is applicable to systems at high ionic strength. It was developed by Schindler & Kamber (1968) and Hohl & Stumm (1976). The EDL is approximated to a parallel

plate capacitor. The model considers only the surface plane for the adsorption of protons, hydroxyls and all inner-sphere adsorption. The relationship between coordinative charge, σ_o, and potential is

$$\sigma_o = C\Psi_o \qquad [2.25a]$$

where C = constant integral capacitance of mineral water interface (Farad m^{-2}).

The capacitance is effectively an empirical parameter found via trial and error. It can however be divided into two components: a Gouy (diffuse) component, C_G, and the Helmholtz (compact) component, C_H,

$$C^{-1} = C_G + C_H^{-1} \qquad [2.25b]$$

The Helmholtz capacitance can be described by:

$$C_H = \varepsilon'\varepsilon_0/d \qquad [2.25c]$$

where ε' = local value of the dielectric constant
d Stern layer thickness

Under conditions where the dielectric constant is independent of surface charge density, two domains of nearly constant capacitance under varying surface charge densities exist. When $C_G >> C_H$ (high ionic strength), $C \equiv C_H$, when $C_G << C_H$ (lower ionic strength), $C \equiv C_G$. If the surface potential is small (less than 25 mV), then $C_G \equiv \varepsilon\varepsilon_0\kappa = 2.3\sqrt{I}$ (25°C) . The model also requires constants for all mass law equations involving surface species.

The triple layer model (TLM) (Figure 2.7C), first proposed by Stern (1924), is a model that incorporates the Stern–Grahame electrical double layer model. The model allows a distinction between inner and outer–sphere complexes. This is accomplished by the incorporation of a layer for outer–sphere complexation (the inner Helmholtz plane (IHP) or β plate). The capacitance of the layer between the IHP and the plane of closest approach of dissociated counterions (outer Helmholtz plane (OHP)) is ignored. The model requires capacitances for the Stern layer and the IHP as well as mass law constants for all adsorption equilibria including the outer–sphere (i.e. ion–pairing) equilibria. Four

layer models (Bousse & Meindel 1986), that incorporate additional distinctions in adsorption type, have also been proposed but have met with limited success.

2.3.5.1 Computer Modeling

Modeling adsorption using mechanistic models requires the solution of a series of simultaneous equations. Solving the equations is computationally intensive and for this reason it often done by a computer model. An example of such a model is FITEQL (Herbelin & Westall, 1994; Westall, 1982) which calculates adsorption equilibrium parameters based on experimental data. The code uses a nonlinear squares method and can be run using a choice of adsorption models: constant capacitance, diffuse layer, Stern, and triple layer. In the gibbsite adsorption literature, FITEQL has been run exclusively in the constant capacitance mode.

2.4 Components of Experimental System

2.4.1 Phosphorus

Phosphorus is an essential nutrient to photosynthetic plants. It is often considered a contaminant since it promotes excessive plant growth and may lead to eutrophification of water bodies. It is common; 0.10% of the total mass of the Earth's crust is phosphorus and is found in most rock types. The number of phosphorous minerals is large (Koritnig, 1978) but apatite is the most common and is of greatest importance. Phosphorus is released into the aquatic environment through the weathering of phosphorus bearing rocks. Phosphorus has no volatile compounds; thus, there is no atmospheric transport except associated with particles. Anthropogenic sources include mining and subsequent industrial and agricultural use. The formerly wide spread use of phosphates in detergents was also a significant source.

Phosphorus is removed from solution by precipitation, biotic uptake, and adsorption. The ultimate fate of phosphorus is ocean sediments but the major nutrient status of phosphorus is indicative of the complexity of the phosphorus cycle. The only

stable redox state of phosphorus in aqueous solutions is +V, thus inorganic phosphorus is always present as phosphate and in turn the phosphate will be almost exclusively orthophosphate (HPO_4^{2-} at seawater pH). Phosphate can exist as the anion, as a complex with metal ions, or as an organic complex. The concentration of organic phosphorous often exceeds phosphate in oceanic surface waters.

Phosphorus concentrations in seawater range from 1 ppb to 50 ppb (Drever, 1988) although an extreme value of 370 ppb has been reported (Reedy et al., 1968). Phosphorus in near surface waters is controlled by biologic activity and at depth concentration is determined by the regeneration/degradation of settling organic matter and ultimately by the solubility of apatite. These controls result in a prototypical nutrient distribution in seawater; surface values are nearly zero and reach a maximum at about 1000 meters (Millero & Sohn, 1992).

2.4.2 ARSENIC

Arsenic is a metalloid that is notorious for its use as a homicidal poison; it has also been widely used as a broad–spectrum pesticide. Arsenic behaves similarly to phosphorus and will replace it in biochemical reactions leading to an inhibition of oxidative phosphorylation and growth (NRCC, 1978; Planas & Healy, 1978; Stryer, 1981), the cause of its acute toxicity. Arsenic is present in the Earth's crust at an average abundance of 1.8 ppm (Krauskopf, 1979) and locally can reach concentrations of up to 2900 ppm in iron–rich sedimentary rocks (Boyle & Jonasson, 1973). In nature, arsenic occurs occasionally as a solid in its elemental state but is most often found in combination with sulfur and or other metals (Boyle & Jonasson, 1973). It is released into aquatic and terrestrial environments as result of erosion of rocks and soil, volcanic emissions, and the release of soil gases. Anthropogenic sources, such as smelter emissions, fossil fuel consumption, and historical use of arsenical pesticides, represent significant inputs.

Arsenic is removed from solution by biotic uptake, adsorption, and precipitation. In most aquatic environments, precipitation will be insignificant since most arsenic minerals are highly soluble. The ultimate fate of arsenic is ocean sediments, however its reactivity ensures an extensive cycling through biotic and abiotic components of aquatic and terrestrial systems. The cycling of arsenic is complex; Lantzy & Mackenzie's (1994) "simple" model of the oceanic arsenic cycle involves 29 fluxes.

In the dissolved phase, arsenic can be present as inorganic arsenite (As(III)) and arsenate (As(V)) species as well as methylated arsenate compounds (Cullen & Reimer, 1989) (see Figure 2.8). Arsenic will initially hydrolyze to arsenite but, under oxygenated conditions, will oxidize further to arsenate species. The rate of oxidation is slow but it can be accelerated by chemical oxidants such as manganese or iron hydroxides (Oscarson et al., 1981a,b; De Vitre et al., 1991) or by bacterial activity (Cullen & Reimer, 1989). Increased salinity also promotes oxidation (NRCC, 1978). The reduction of arsenate to arsenite can occur as result of biochemical processes associated with phytoplankton blooms in oxygenated surface waters (Andreae, 1978).

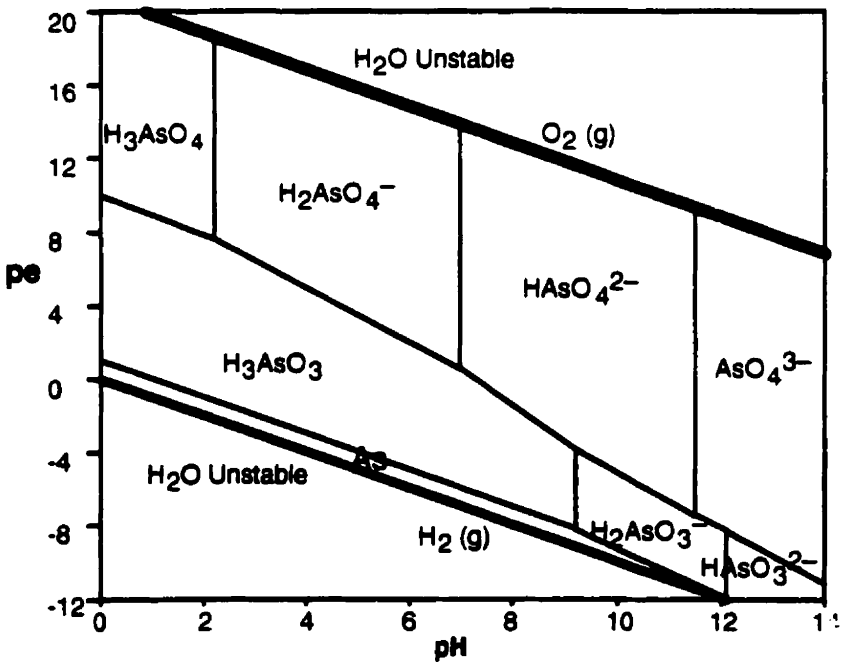

Figure 2.8 pe-pH diagram for As-H_2O system at 25° C. Dissolved [As] 0.7 µM
After Cherry et al. (1979)

Arsenic in seawater shows a nutrient type distribution with a shallow regeneration cycle (Bruland, 1983). Thermodynamics suggest that arsenate species should be the dominant species under oxygenated conditions and this is confirmed by speciation measurements conducted in a variety of aquatic environments (Abdullah et al., 1995; Riedel, 1993; Sadiq, 1992). The concentration of arsenic in seawater ranges from 13 to 53 nM and is not believed to be solubility limited although the thermodynamic database for arsenic mineral and solid phases is extremely limited. Over 100 arsenic minerals are known (Boyle & Jonasson, 1973) but data is available for less than 10% of the minerals. One solid phase that has been proposed as solubility limiting in fresh water is barium arsenate $Ba_3(AsO_4)_2$ (Wagemann, 1978; Crecelius et al., 1986). Crecelius et al. (1986) believe the calculation to be erroneous, and attribute the misinterpretation to major discrepancies in the thermodynamic data of Chukhlanstev (1956). There is no evidence for its geological occurrence. Under anoxic conditions, reduced sulfur limits arsenic solubility by the formation of arsenic sulfides (Figure 2.9). Coprecipitation and/or adsorption to iron sulfides represents a significant removal mechanism. Arsenic is known to be strongly associated with iron sulfides especially pyrite (Boyle & Jonasson, 1973). Authigenic framboidal pyrite found in the Saguenay Fjord (Mucci et al. 1999) and the Gulf of St. Lawrence (Belzile & Lebel, 1986) contains up to 1000 ppm arsenic.

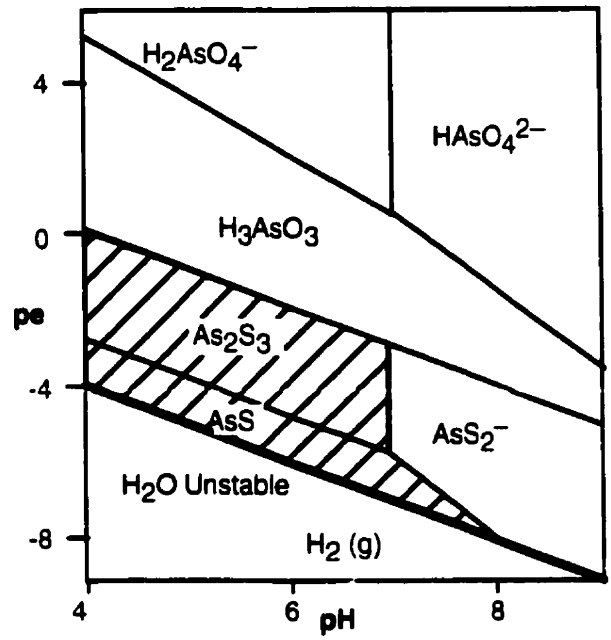

Figure 2.9 pe-pH diagram for As-S-H_2O system at 25° C. Total dissolved As species at 66 nM Total S species at 0.1 mM.
Hatched area represents presence of solid phases. After Cherry et al. (1979)

2.4.3 Gibbsite and Other Aluminum Oxides

Gibbsite [α-$Al(OH)_3$ or $Al_2O_3 \cdot 3H_2O$] is the most common of the hydrated aluminum oxide minerals. It is usually the major component of bauxite and is a common soil constituent. In its natural state it often contains traces of Fe, Si, Ca, and Mg (Palache et al., 1944). It is also found as a pure synthetic mineral, a product of chemically refined bauxite also known as alumina trihydrate.

Gibbsite is typically white in colour although the shade of white is variable. Iron in impure gibbsite leads to a reddish yellow colour. Polymorphs of gibbsite are bayerite and nordstrandite; bayerite differs from gibbsite in its layering pattern. Gibbsite has an ABBA pattern and bayerite is layered ABAB. Nordstrandite is an intermediate phase alternating gibbsite and bayerite layering (i.e. ABBAABAB) (Goldberg et al., 1996). Amorphous aluminum hydroxide has the same chemical formula but has no crystallinity. A gel of aluminum hydroxide and water forms when aluminum hydroxide is synthesized in the presence of boron (Beyrouty et al., 1984).

Other common aluminum oxides are gamma and alpha alumina (corundum) (γ-Al_2O_3, α-Al_2O_3), boehmite (γ-AlOOH) and diaspore (α-AlOOH). Gamma alumina is produced by the thermal dehydration of gibbsite and is the intermediate stage in the production of aluminum. It is suggested that the gamma alumina surface is similar to edge faces on gibbsite (explained below) and that studies of the alumina surface may be applicable to gibbsite with respect to patterns of adsorption behaviour rather than absolute measurements (Goldberg et al., 1996). The adsorption properties of alpha alumina have also received some attention, but the relationship to the adsorption behaviour of gibbsite is not as strong.

2.5 Gibbsite Crystallography

Gibbsite is a monoclinic mineral that typically forms tabular pseudo–hexagonal crystals.

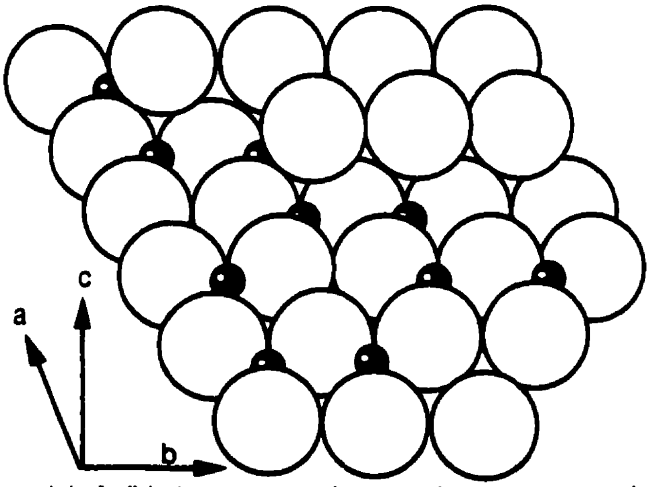

Figure 2.10 Sphere model of gibbsite structure. Large spheres represent hydroxyl ions, smaller spheres trivalent aluminum ions. Part of upper hydroxyl layer removed for clarity. (after Goldberg et al., 1996)

The larger OH^- ions are arranged in a close-packed double layer structure with the smaller Al^{3+} ions occupying the interstices between the two layers (Figure 2.10). Two types of interstices (cation sites) occur. The smaller tetrahedral sites are surrounded by four of the larger spheres, three in one layer, one on top. The larger octahedral sites are surrounded by six spheres; three from two adjacent layers. Al^{3+} ions occupy 2/3 of the octahedral

coordination sites. Each Al^{3+} ion is coordinated to six OH^- ions and each OH^- ion is shared by two Al^{3+} ions. Crystal growth occurs by layer extension (*a* and *b* direction) or by layer stacking (*c* direction). Surface hydroxyls of an ideal basal plane will coordinate to two Al^{3+} ions and edge plane hydroxyls will coordinate to one Al^{3+} ion. The structure of gibbsite can also be seen as a series of Al^{3+} rings. A single ring of 6 Al^{3+} ions is joined above and below by six pairs of bridging OH^- ions creating a $Al_6(OH)_{12}^{6+}$ functional unit (Figure 2.11A).

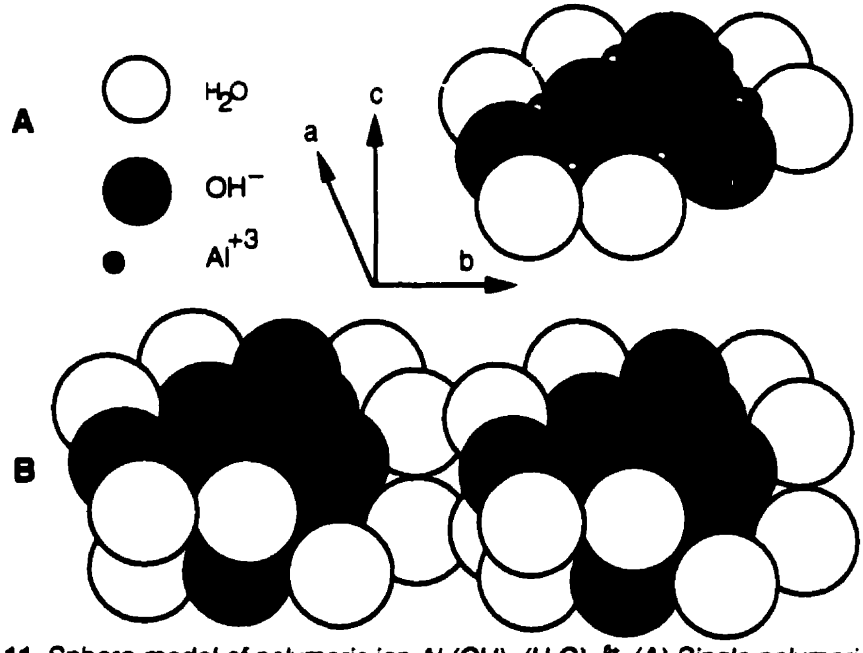

Figure 2.11 Sphere model of polymeric ion $Al_6(OH)_{12}(H_2O)_{12}^{6+}$. (A) Single polymeric ion with upper hydroxyl and water layer removed. (B) Two complete polymeric ions (After Goldberg et al., 1996)

The excess charge on each Al^{3+} retains a pair of water molecules (Figure 2.11). These "edge" sites are believed to be the only adsorption sites on gibbsite (Parfitt et al., 1977; Russell et al., 1974). The 001 surface, although forming the majority of the surface area of gibbsite, is inert with respect to adsorption. The $Al(OH)_6$ unit can also be viewed as a octahedron (Figure 2.12), the apices being the centre of an OH^- ion. Two octahedra are joined along one edge by sharing a pair of OH^- ions i.e. $Al(OH)_2Al^{4+}$. Six joined octahedra form the ring structure of the sphere model. This model shows the "holes" in the structure that occur due to the dioctahedral arrangement of Al^{3+}.

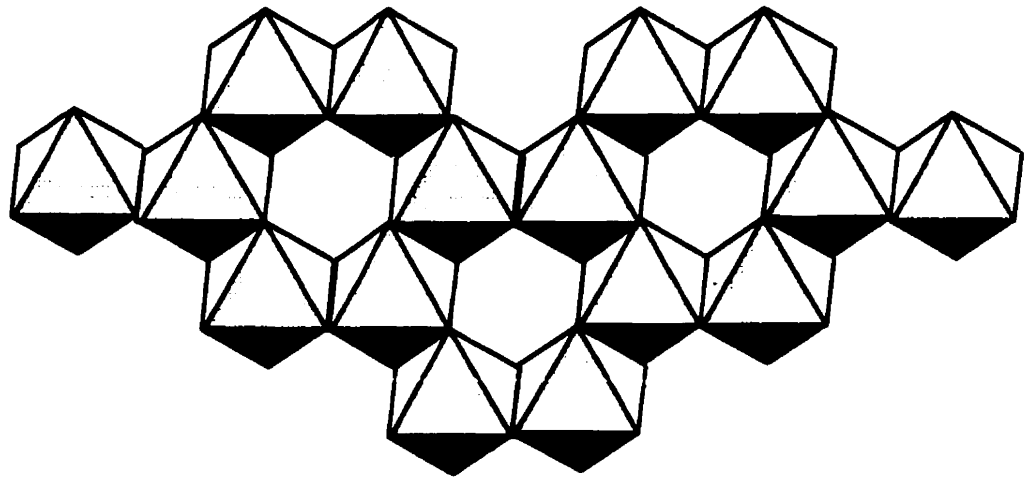

Figure 2.12 Octahedral model of gibbsite structure. Three coalesced $Al_6(OH)_{12}$ rings and two additional aluminum ions (After Goldberg et al., 1996)

2.5.1 GIBBSITE SURFACE PROPERTIES AND VARIABILITY

Production conditions in an industrial setting are poorly constrained; thus introducing variability in surface properties of the gibbsite. To a lesser degree, variability is also found in chemical grade gibbsite. Measurements of surface properties have revealed these differences (e.g., van Riemsdijk & Lijklema, 1980a; Parfitt et al., 1977). The variability can be traced to both the analytical method and to the gibbsite itself. Not only will gibbsite have a natural variability, additional variability is introduced by the gibbsite retaining a memory of its history (i.e synthesis, pretreatment, grinding) (Davis and Kent, 1990).

Specific surface areas for gibbsite have been reported in a range of 26 to 50.5 m^2/g. Unfortunately only one of these measurements was accompanied by a grain size measurement. Manning and Goldberg (1996) report a 45.0 m^2/g surface area for grains of less than 500 μm. Higher specific surface area values reported by Okazaki et al.(1989) appear to be measurements of amorphous aluminum hydroxide rather than gibbsite. A few low values have also been reported (Alvarez et al., 1976; Helyar et al., 1976a). Sources of variability in specific surface area are the grain size, the gibbsite itself as well as uncertainties associated to the measurement technique. If specific area is known,

adsorption behaviour can be normalized and results of different studies can be compared. However most results are reported in terms of mass.

Given that adsorption will only occur on edge sites, the percentage of specific surface area represented by edge faces is of great importance. Very few measurements have been made of this property. van Riemsdijk and Lijklema (1980a) calculated an edge area percentage of 14 based on shadowed electron micrographs and similar analyses by Russell et al (1974) and Parfitt et al. (1977a) yielded percentages of 7 and 20 respectively.

Parfitt et al. (1977a) estimated that the basal plane of gibbsite contains approximately 12 hydroxyl groups per nm^2 whereas edge planes contain 4 groups. Proton acceptor and donor sites are estimated at 2.8 and 5.6 sites per nm^2 respectively (Sposito, 1984). Directly measured isoelectric points via electrophoresis have been reported at pH = 9.6 (Goldberg et al., 1993a) and 10.0 (Kavanagh et al., 1975). Potentiometric titration measurements of the pH_{PZC} have yielded values of 7.8, 9.5 (Hingston et al., 1972) and 9.8 (Kavanagh et al., 1975).

2.5.2 GIBBSITE SOLUBILITY

The solubility of gibbsite is largely pH dependent. In fresh water, dissolved aluminum occurs as Al^{3+}, $AlOH^{2+}$, $Al(OH)_2^+$, $Al(OH)_3^0$, and $Al(OH)_4^-$ (Roberson & Hem, 1969). The total concentrations of all aluminum species are at a minimum at a pH of 6. Solubility increases rapidly with decreasing pH and at a lesser rate with increasing pH. In seawater, the presence of sulfate and fluoride anions increases solubility by complexation. Using the solubility constants of Stumm & Morgan (1996), the solubility of gibbsite in seawater can be calculated (Figure 2.13). The complexes increase solubility by about 1 log unit at pH 6 and by 1.25 log units at pH 4. At higher pH the influence of seawater anions becomes negligible.

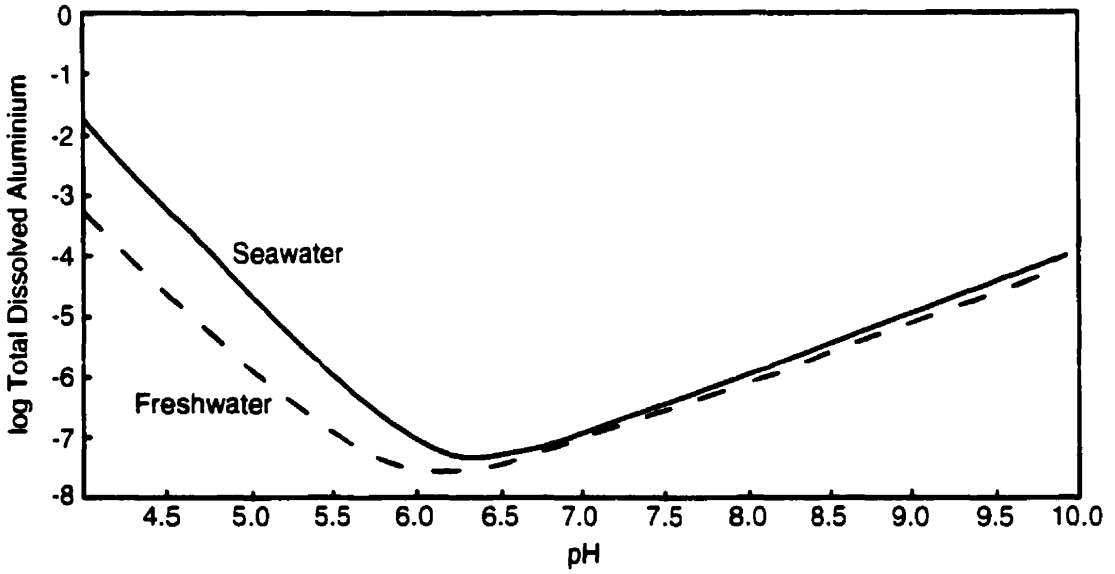

Figure 2.13 Calculated solubility of gibbsite in freshwater and seawater (S=35). Calculated using compilation of Stumm & Morgan (1996).

The kinetics of gibbsite dissolution are very slow. Su & Harsh (1994) report equilibrium from gibbsite dissolution in low pH solutions occuring at over 450 days. Gibbsite has been shown to remain stable in artificial seawater for periods up to seven months (Crane, 1998), even in the presence of high silica concentrations. Under these conditions, thermodynamics would predict its conversion to kaolinite or Na–montmorillionite

2.6 The Adsorption Behaviour of Gibbsite

The bound water molecules associated with unbalanced Al^{3+} ions can be replaced by an adsorbed single hydroxyl group (Goldberg et al., 1996).The resulting surface complex is an aluminol functional group (Al≡OH). The protonation and deprotonation reactions can be described by:

$$Al{\equiv}OH + H^{+} \Leftrightarrow Al{\equiv}OH_2^{+} \quad [2.26]$$

$$Al{\equiv}OH \Leftrightarrow Al{\equiv}O^{-} + H^{+} \quad [2.27]$$

and the general surface complexation reactions by:

$$Al{\equiv}OH + H_3X \Leftrightarrow Al{\equiv}H_2X + H_2O \quad [2.28]$$

$$Al{\equiv}OH + H_3X \Leftrightarrow Al{\equiv}HX^{-} + H_2O + H^{+} \quad [2.29]$$

$$Al{\equiv}OH + H_3X \Leftrightarrow Al{\equiv}X^{2-} + H_2O + 2H^+ \qquad [2.30]$$

where X = trivalent anion complex or single anion

2.6.1 PREVIOUS WORK

Previous investigations of the adsorption of arsenate and phosphate on gibbsite are listed in Table 2.2.

Table 2.2 Arsenate and phosphate adsorption studies on gibbsite

Authors	Adsorbent
Bache, 1964	PO4
Muljadi et al.,1966a,b	PO4
Hingston et al., 1971	AsO4
Kuo & Lotse, 1974	PO4
Kyle et al., 1975	PO4
Helyar et al., 1976a	PO4
Parfitt et al., 1977	PO4
van Riemsdijk & Lijklema, 1980a,b	PO4
Manning & Goldberg, 1996	AsO4 PO4

Studies conducted on alumina and on amorphous aluminum hydroxide have also been carried out; these have some applicability with respect to gibbsite.

Table 2.3 Adsorption studies on alumina; amorphous $Al(OH)_3$

Authors	Adsorbate	Adsorbent
Chen et al., 1972	PO4	α–Alumina
Huang, 1975	PO4	γ–Alumina
Anderson et al., 1976	AsO4	Al(OH)3
Peinemann & Helmy, 1977	PO4	? Alumina
Anderson & Malotky, 1979	AsO4	Al(OH)3
Anderson & Malotky, 1979	PO4	γ–Alumina
Lijklema, 1980	PO4	Al(OH)3
Bolan et al., 1986	PO4	Al(OH)3
Xu et al., 1988, 1991	AsO4	α–Alumina
Okazaki et al., 1989	PO4, AsO4	Al(OH)3
Violante et al., 1991	PO4	Al–oxide (?)

The conditions and the materials used in these studies vary; including time, concentrations, and the gibbsite itself. Most of these studies have determined the amount of arsenic lost from a solution and attributed the loss to adsorption. A notable exception is the work of Xu et al. (1988, 1991) who used the radioisotope ^{75}As as a tracer and measured the activity of ^{75}As adsorbed onto the gibbsite.

The studies have shown relatively consistent adsorption envelopes for all aluminum substrates (Hingston et al., 1971; Chen et al., 1972; Huang, 1975; Anderson et al., 1976; Xu et al., 1981; Okazaki et al., 1989; Violante et al., 1991; Manning & Goldberg, 1996). Peak adsorption is observed at pH 4 to 5; adsorption declines linearly from that point as pH increases but some adsorption still occurs up to pH of 10 (Figure 2.14). No data were found describing adsorption above a pH of 10. The finite quantity of the adsorbate within the experimental system allows for the complete adsorption of the adsorbate. This is seen on an adsorption envelope as a flat line. As pH increases, adsorbates will remain in solution and so the envelope returns to a normal shape (Anderson et al., 1976, Manning & Goldberg, 1996). The adsorption envelopes appear to be independent of PZC, there is no narrow adsorption edge which should otherwise be present at pH 9-10. This is indicative of inner-sphere adsorption where changes in adsorption with pH are related to adsorbate speciation. This concept is developed further in the discussion of the results of this study

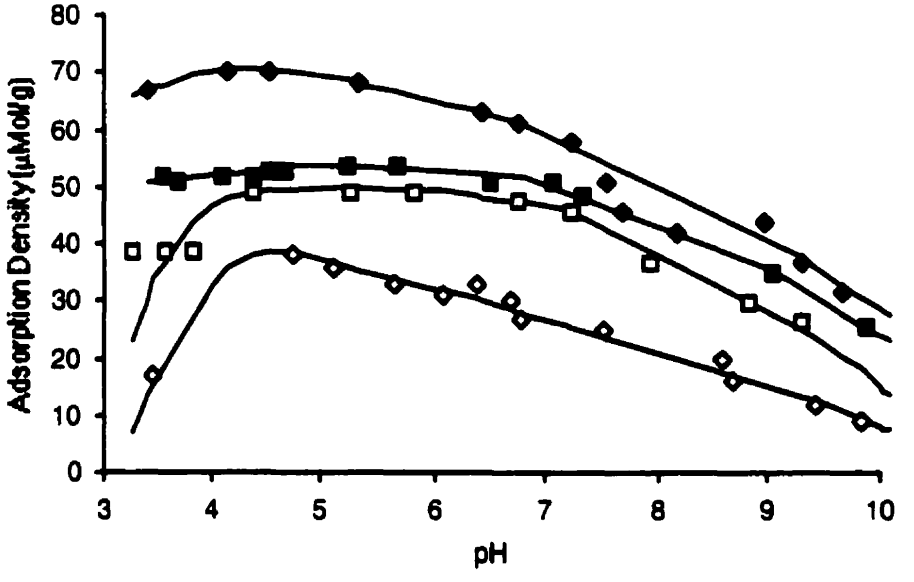

Figure 2.14 Adsorption envelope of arsenate and phosphate to gibbsite■ 133 µM PO4 ❑ 133 µM AsO4 ◆ 266 µM AsO4 (Manning & Goldberg, 1996) ι 270 µM AsO4 (Hingston 1971)

The kinetics of adsorption differ between arsenate and phosphate. Arsenate adsorption is a straight forward, one-step and rapid process. Anderson et al. (1976) observed arsenate adsorption to amorphous aluminum hydroxide being essentially complete after 24 hours. Xu et al. (1988), at a lower sampling rate, show adsorption being completed after 5 days. This rapid equilibration was also observed by Livesey & Huang (1981) in adsorption studies on Al-rich soils. The kinetics of phosphate adsorption are greatly complicated by the precipitation of aluminum phosphate solid phases. As a result it is more accurate to describe the process as phosphate sorption — Sorption being a general term to describe all ion-surface interactions. The process has been broken down into two steps by van Riemsdijk & Lijklema (1980a); an initial rapid adsorption and a slower precipitation of an aluminum phosphate phase. Bache (1964) theorized that a third additional step also occurs, the slow adsorption of phosphate to the precipitate. Helyar et al. (1976a) report phosphate sorption to gibbsite to be incomplete after periods of more than 96 hours. Similarly Kuo & Lotse (1974) observed sorption being incomplete at 48 hours, whereas Kyle et al. (1975) allowed for an equilibration period of 141-191 hours before conducting their isotopic exchange studies. Temperature studies show increased phosphate adsorption to gibbsite at higher temperature (Muljadi et al., 1966b; van Riemsdijk & Lijklema, 1980b). No published work has been found on the influence of temperature on arsenate adsorption to gibbsite or other aluminum minerals.

Previous arsenate and phosphate adsorption studies have been mostly undertaken at concentrations two or three orders of magnitude larger than concentrations normally encountered in natural environments. Adsorption of phosphate to gibbsite has been described by the Langmuir isotherm in many studies (Figure 2.15) (Bache, 1964; Muljadi et al., 1966a; Helyar et al., 1976a; Parfitt et al., 1977). This treatment has also been applied to results of studies carried out on α-alumina (Chen et al., 1973), γ-alumina (Huang, 1975) and non-crystalline aluminum oxide (Violante et al., 1991). The Langmuir isotherm model is also applicable to lower concentrations as well (Figure 2.16).

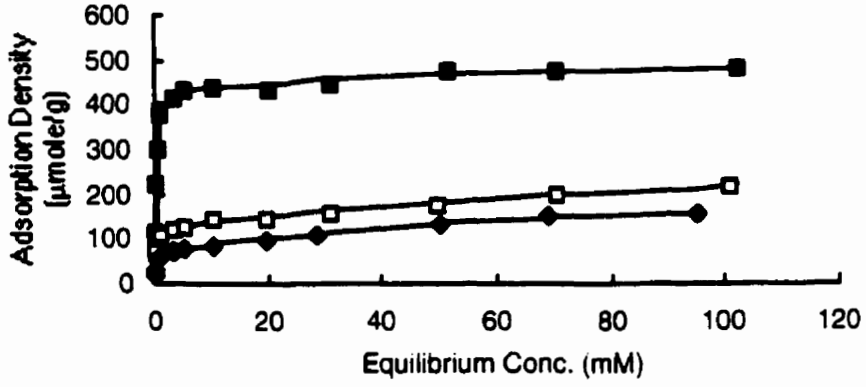

Figure 2.15 Adsorption of phosphate to gibbsite in low ionic strength solutions. ❐ pH 5 ■ 9 ◆10. Data from Muljadi et al. (1966a)

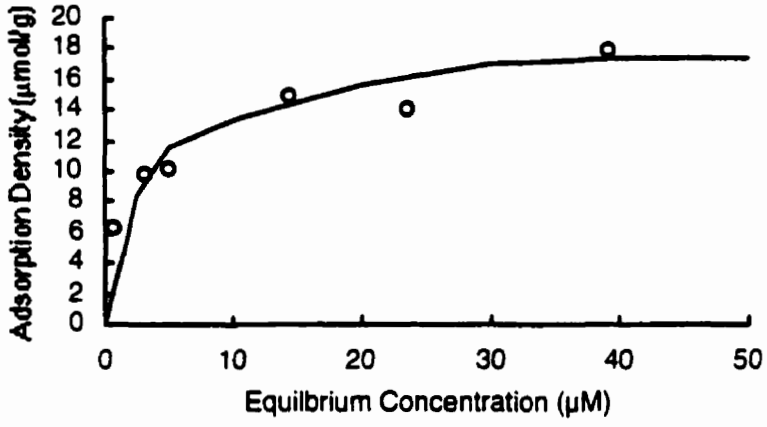

Figure 2.16 Adsorption of phosphate to gibbsite (pH 5.5) Data from Helyar et al. (1977a)

Adsorption isotherms for arsenate adsorption to gibbsite are less well established. In fact, none of the published data have been modeled in terms of isotherms. Isotherms have been reported for other aluminum substrates. The work of Anderson et al. (1976) and Anderson & Malotky (1979) on amorphous aluminum hydroxides shows that adsorption can be described by the Langmuir isotherm. However, at concentrations below 50 µM, the adsorption data can also be described with some success by simple linear isotherms (Figure 2.17).

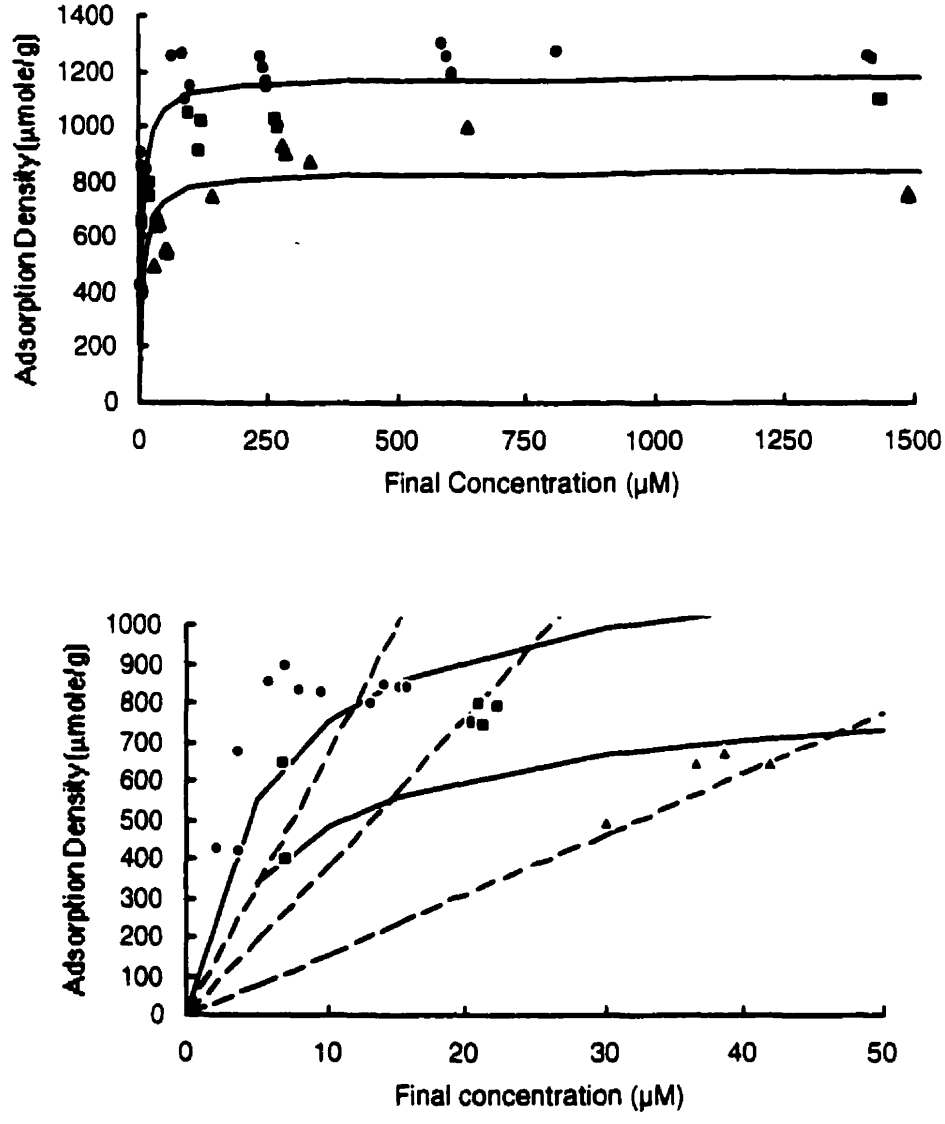

Figure 2.17 Adsorption of arsenate onto amorphous aluminum hydroxide ● pH 7 ■ 7.5 ▲ 8. Data from Anderson et al. 1976 and Anderson & Malotky 1979. Solid lines are Langmuir isotherms for pH of 7 and 8 of Anderson et al, 1976; dashed lines are simple linear isotherms calculated from concentrations below 50 µM.

2.6.1.1 Arsenite Adsorption

It is readily apparent from work on iron oxyhydroxides (Pierce & Moore, 1982) that arsenite adsorption is much less than that of arsenate. Manning & Goldberg (1997) showed that on amorphous aluminum hydroxide arsenite adsorption was 20 to 60% less than that of arsenate. Raven et al (1998) have shown arsenite to adsorb more strongly by

feriihydrate when the initial arsenic concentration is high. But the adsorption of arenite may in fact be the formation of ferrric arsenite.

2.6.2 Surface Coordination Modeling of Adsorption to Gibbsite

The constant capacitance model of Stumm et al. (1980) has been used to model arsenate and phosphate adsorption on natural soils, aluminum and iron oxides and hydroxides (Goldberg & Sposito, 1984; Goldberg, 1986a, b; Goldberg & Glaubig, 1988; Manning & Goldberg, 1996). These studies have all used the FITEQL computer code (Westall, 1982) to derive surface complexation constants from experimental data.

The studies have all used a capacitance value of 1.06 F m^{-2}. The values of the intrinsic protonation–deprotonation constants (K^+ and K^-)were an average of the intrinsic protonation–deprotonation constants of various aluminum oxides reported in the literature. The study of Manning and Goldberg (1996) treated the constants as adjustable parameters; they were constrained by pH_{PZC} so that

$$PZC = 0.5[|\log K^+| + |\log K^-|] \qquad [2.32]$$

In all cases, a fixed and consistent surface site density was used. A summary of the values found are listed in Table 2.4 where log K_i is the intrinsic constant for the complexation reaction

$$\equiv Al\text{–}OH + H_3(As,P)O_4 \Leftrightarrow \equiv Al\text{–}H_{3-i}(As,P)O_4 + H_2O + (1-i)H^+ \qquad [2.33]$$

Table 2.4 Surface coordination modeling results

Source	Data Source	log K^+	log K^-	Species	log K_1	log K_2	log K_3
Goldberg & Sposito, 1984	Parfitt, 1977	7.38	-9.09	PO_4	9.46	5.26	0.62
Goldberg & Sposito, 1984	Hingston et al., 1974	7.38	-9.09	PO_4	11.11	3.98	-3.75
Goldberg & Sposito, 1984	Helyar et al., 1976a	7.38	-9.09	PO_4	9.01	2.56	N/A
Manning & Goldberg, 1996	Manning & Goldberg, 1996	9.10	-10.5	PO_4	9.90	3.20	-4.70
Goldberg, 1986a	Hingston et al., 1971	7.38	-9.09	AsO_4	9.72	3.41	-3.58
Manning & Goldberg, 1996	Manning & Goldberg, 1996	9.10	-10.5	AsO_4	8.60	2.20	-5.70

None of the constants are reported with uncertainties. No numerical assessment of the goodness of the fits to the model was reported but visually the models of Manning & Goldberg (1996) and Goldberg (1986a) appear to reproduce the data sets although the fit is weaker at lower pH. As there were no figures of the relevant data presented in Goldberg & Sposito (1984) it is impossible to assess the quality of fit of the model. The assumptions made in the model such as the value for capacitance and the intrinsic protonation and deprotonation conditions are probably responsible for the discrepancies in the constants since theoretically they should all be the same.

2.7 Adsorption in the Presence of Seawater Constituents

Although aluminum phases have often been cited along with iron and manganese oxides as active "scavengers" for a variety of elements, adsorption studies in seawater are rare. Choi & Chen (1979a), as part of a wastewater treatment study, evaluated the ability of bauxite and alumina to remove fluoride in diluted artificial seawater. Balistrieri & Murray (1982) have studied the adsorption of heavy metals (Cu, Pb, Zn, and Cd) on goethite in seawater. Adsorption behaviour in seawater should be different from that of freshwater due to a markedly different chemical composition and a considerable increase in ionic strength. Adsorption may be directly or indirectly affected by the compositional difference. Choi & Chen (1979a) reported that salinity had no effect on fluoride

adsorption to alumina nad bauxite. Balistrieri & Murray (1982) report that seawater has a variable effect on the adsorption of the trace metals; they concluded that sulfate increases adsorption of cations, magnesium decreases it and chloride has no effect. The overall effect of the seawater is related to the pH of the normal adsorption edge of the metals. Metals with adsorption edges at pH from 3 to 6 have increased adsorption density; metals with adsorption edges from pH 6 to 9 have dimminished adsorption. The two studies suggest that the effect of seawater on adsorption can not be generalized; each adsorbate-adsorbent combination will react differently. The lack of direct studies necessitates a look at related studies; these studies can provide useful information as to what might be expected in seawater

2.7.1 Ionic Strength

Surface complexation theory predicts that ionic strength in an indifferent electrode should increase adsorption below the point of zero charge by increasing positive surface charge (Bowden et al., 1977) but experimental evidence (Hayes et al., 1988) shows no effects on inner–sphere adsorption for $.001 < I < 1$. This was confirmed by studies of the adsorption of copper (Okazaki et al., 1986) and boron (Goldberg et al., 1993b) to gibbsite for $0.1 < I < 1$.

2.7.2 Solution Interactions

Arsenate and orthophosphate in seawater may be unavailable for adsorption because of ion pairing and complexation with seawater ions. There is significant ion pairing between orthophosphate and seawater ions. At a pH of 8.2, 65% of phosphate is in ion pair complexes (Turner et al., 1981); a feature made apparent by the variation of apparent or stoichiometric dissociation constants of phosphoric acid with salinity (Kester & Pytkowicz, 1967). The same relationship has been predicted but not observed for arsenate (Lowenthal et al., 1977). There is some disagreement with respect to arsenic complexation in seawater. Turner et al. (1981), through a calculation involving 58 trace

elements in seawater, shows that only free arsenate ions form. However a second chemical speciation calculation (Crecelius et al., 1986) produces arsenic-fluoride complexes ($HAsO_3F^-$ and AsO_3F^{2-}) at fluoride levels (1.58 ppm) similar to seawater; the complexes account for up to 10% of the total As(V).

2.7.3 COMPETITIVE ADSORPTION

Table 2.5 Adsorption studies on gibbsite and alumina involving major seawater ions

Hingston et al., 1972	gibbsite	F^-, SO_4^{2-}, Cl^-
Huang & Stumm, 1973	γ-alumina	Mg^{2+}, Ca^{2+}, Sr^{2+}
Helyar et al., 1976a	gibbsite	Ca^{2+}, Na^+, K^+, Mg^{2+}, HCO_3^-
Helyar et al., 1976b	gibbsite	Sr^{2+}
Choi & Chen, 1979a	activated alumina	F^-
Choi & Chen, 1979b	activated alumina	$B(OH)_4^-$
Hingston, 1981	gibbsite	F^-
Farrah et al., 1987	gibbsite	F^-
Hao & Huang, 1986	γ-alumina	F^-
Xu et al., 1988	α-alumina	SO_4^{2-}
Goldberg et al., 1993a, b	gibbsite	$B(OH)_4^-$

The physical limit in the number of adsorption sites generates competition for the sites. Competitive adsorption studies between arsenate, molybdate, and phosphate in soils (Roy et al., 1986) and oxides (Manning & Goldberg, 1996) have indicated that adsorption of any one anion is significantly diminished by the presence of the other anions. Davis & Kent (1990) suggest that essentially all electrolyte ions will form complexes with surface hydroxyls on oxides; the level of adsorption of any one ion will be a combination of concentration and chemical affinity. Ions that are not electrostatically adsorbed (specific adsorption) will be adsorbed out of proportion to their concentration.

Chloride is reported to adsorb non–specifically to gibbsite (Hingston et al., 1972). Adsorption of arsenate to a high Al soil was unaffected by the addition of chloride (Livesey & Huang 1981). Sulfate is reported to show a similar behaviour (Hingston et al., 1972, Livesey & Huang, 1981). Xu et al. (1988) have shown that at lower pH (below 6) sulfate can reduce arsenate adsorption on alumina; however increasing the sulfate concentration does not further reduce adsorption. Bicarbonate at solution activity levels

of 1 to 5.8 $*10^{-4}$ M (artificial seawater is 2 * 10^{-3} M) has no measurable effect on phosphate adsorption (Helyar et al., 1976a). No work on bromine adsorption to gibbsite or other aluminum minerals has been found; chemical periodicity suggests that bromide behaviour would be similar to chloride. Boron exists as an anion in solution and its adsorption to aluminum oxides has received some attention. An inner–sphere adsorption mechanism has been suggested with peak adsorption occurring between pH 6 and 8 (Goldberg et al., 1993a). Boron adsorption to alumina is reported to decrease with increasing salinity (Choi and Chen, 1979b).

Of all seawater anions, it would appear that fluoride is the anion that will compete most effectively for adsorption sites. The studies of Hingston (et al., 1971, 1981) have shown strong adsorption of fluoride to gibbsite in weak electrolyte solutions (Figure 2.18). The data of Farrah et al. (1987) indicate a significant removal of fluoride from a solution containing gibbsite. The authors suggest that the removal is due to the formation of aqueous aluminum fluoride complexes that are not directly detectable. Kuo & Lotse (1974) show fluoride causing desorption of phosphate from gibbsite. The removal of fluoride from solution by activated alumina is well known; it is used widely in wastewater treatment (Choi and Chen, 1979a; Hao & Huang, 1986). Choi & Chen (1979a) show that fluoride removal by alumina is rapid and is unaffected by salinity. Fluoride is an essential component of the electrochemical production of aluminum. Molten cryolite [Na_3AlF_6] and small amounts of non–decomposing fluoride additives (e.g. aluminum, calcium, magnesium, lithium) act as a solvent for the alumina. The interaction between fluoride and aluminum is illustrated by the complexation of aluminum and fluoride. As shown earlier, the complexation is strong. It is responsible for an increase in gibbsite solubility in seawater as well as interfering in fluoride analysis.

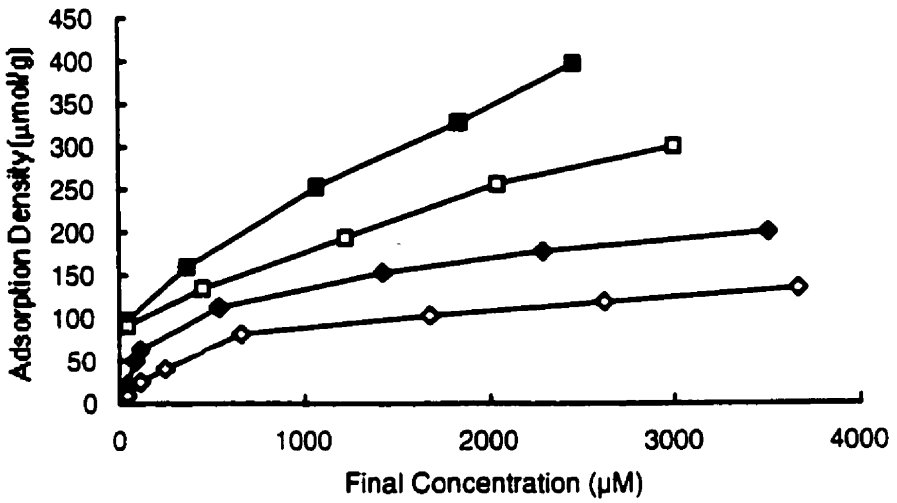

Figure 2.18 Adsorption of fluoride to gibbsite.
pH 6 ■ 6.5 ❑ 7 ◆ 8 ◇. Data from Hingston (1981)

Cations can also be adsorbed by gibbsite from seawater solutions. Magnesium, calcium, and strontium, in order of strength, are all reported to be specifically adsorbed on γ–alumina with adsorption increasing greatly at pH greater than 8 (Huang & Stumm, 1973). The adsorption of the univalent cations has not been investigated directly but their lack of effect on phosphate adsorption (Helyar et al., 1976a) suggests that adsorption is minimal and non–specific.

Increased phosphate adsorption has been attributed to the presence of major seawater ions. Chen et al. (1972) observed that adsorption of phosphate to α alumina increases with the addition of calcium and magnesium chloride. The same effect was observed by Helyar et al. (1976a) on gibbsite upon the addition of $CaCl_2$ at lower pH (i.e. 5.5). Strontium nitrate also has been shown to increase adsorption at pH 5.5 (Helyar et al., 1976b). Although not directly stated, the two sets of authors attribute the increase to the formation of ternary surface complexes. Chen et al (1972) have suggested that at higher pH divalent cations increase phosphate adsorption by decreasing repulsion between the negative surface and negative adsorbents. This is similar to the formation of a type A ternary complex (Stumm & Morgan, 1996);

$$\equiv Al\text{-}OH + Ca^{2+} + HPO_4^{2-} \leftrightarrow \equiv Al\text{-}OCa\text{-}HPO_4^{-} + H^{+} \qquad [2.33]$$

Helyar et al. (1976a) propose the formation of a surface complex that involves two phosphate ions and a central divalent cation of appropriate size, charge and co–ordination properties. Thus, phosphate is able to occupy a surface at a greater density. This is equivalent to a type B ternary complex (Stumm & Morgan, 1996);

$$2(\equiv Al\text{-}OH) + 2HPO_4^{2-} + Ca^{2+} \leftrightarrow \begin{matrix} \bullet Al\text{-}HPO_4^{-} \\ \bullet Al\text{-}HPO_4^{-} \end{matrix} > Ca^{2+} + OH^{-} \qquad [2.34]$$

2.7.4 Kinetic Effects

A study of phosphate and arsenate adsorption onto oxic estuarine sediments of the Saguenay Fjord in artificial seawater (Harris, 1996) shows arsenate adsorption equilibrium being reached within 24 hours. Phosphate showed a rapid initial adsorption step of 24 h followed by a gradual uptake that continued up to 40 days. As the mineralogical composition of the sediments was not determined, it is not possible to assess the direct relevance of the study to adsorption to gibbsite or even the influence of seawater of the kinetics. A study of phosphate adsorption to goethite in artificial seawater (Shaw, 1996) showed equilibrium being reached within 7 days. This is in agreement with experiments in low ionic strength solutions. There is however no distinguishable break in the removal; i.e. adsorption and precipitation can not be distinguished.

Chapter 3 Materials and Methods

3.1 Materials

All reagents used were reagent grade or better. Specific grades used for various procedures or techniques are described in the relevant section. Nanopure™ water was used for all solutions except where indicated. All glassware and reusable plasticware were rinsed with Nanopure™ water after soaking in a 10% nitric acid bath for at least 12 hours.

3.1.1 Gibbsite

Gibbsite (Aluminum trihydrate) was obtained from Alcan. The gibbsite was a bulk sample of the gibbsite produced at the Vaudreuil plant. The gibbsite is powdered to a size of less than 500 microns. The gibbsite was white in colour with a slight pink tone. Powder x–ray diffraction analysis (Figure 3.1) showed a perfect match to reference gibbsite (JCPDS 29–0041).

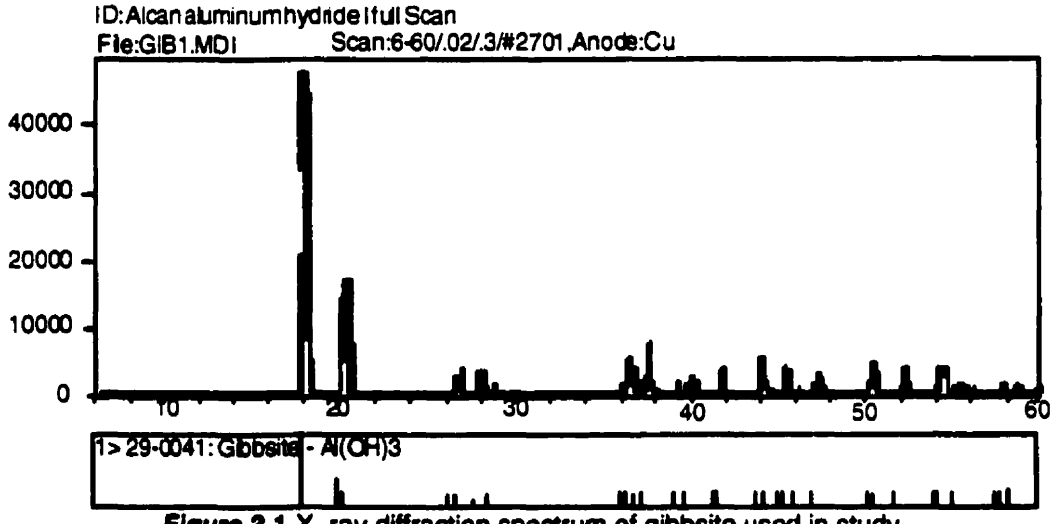

Figure 3.1 X–ray diffraction spectrum of gibbsite used in study

The x-ray fluorescence analysis (Table 3.2) indicates that the gibbsite is essentially pure with minor silica and sodium impurities. Phosphorus (as P_2O_5) is reported at 0.005 % and arsenic is below the detection limit of 1 ppm.

Table 3.1 X-ray diffraction peak index

Alcan aluminum hydrate		**JCPDS 29-41 (Gibbsite)**	
d (inter-planar spacing Å)	I% (peak intensity / max peak intensity)	d	I%
4.8698	100.0	4.853	100
4.3965	33.1	4.380	36
2.3903	19.0	2.389	16
2.4596	12.8	2.456	12
2.0528	12.7	2.052	12
1.8085	9.9	1.8074	10
3.3218	9.4	3.318	9
1.9978	9.1	1.9973	8
4.3256	8.7	4.328	18
1.7547	8.0	1.7542	9
2.1692	8.1	2.169	7
3.1911	7.7	3.189	7
1.6864	7.6	1.6871	7

Table 3.2 Gibbsite geochemistry (XRF)

SiO_2	0.25%	CaO	0.03 %	Cu	10 ppm
TiO_2	0.009 %	Na_2O	0.35 %	Ni	3 ppm
Al_2O_3	64.94 %	K_2O	0.03 %	Sb	2.8 ppm
Fe_2O_3	0.08 %	P_2O_5	0.005 %	Ge	2.7 ppm
MnO	0.03 %	Cr_2O_3	15 ppm	LOI	34.34%

The specific surface area of the gibbsite was not determined but a gibbsite of similar grain size was found to have a N_2 BET surface area of 45 m^2/g (Manning & Goldberg 1996).

Initial experiments revealed significant surface contamination by phosphate. A cleaning procedure was thus instituted; gibbsite was cleaned by soaking in 1 N HCl for 24 hours followed by multiple rinsing with Nanopure™ water. The gibbsite was then dried at 110° C in an oven for a period of 24 hours. Subsequent experiments indicated that most of the surficial phosphate had been removed.

3.1.2 Artificial Seawater

Artificial seawater was prepared in 20 kg batches according to the method of Kester et al. (1969) except that $NaHCO_3$ was added only as required to adjust pH (see

below). The seawater was prepared using doubly distilled water. The stock solutions of volumetric salts ($MgCl_2$, $CaCl_2$, $SrCl_2$) were standardized by titration against a silver nitrate solution itself standardized against a solution of NaCl of known concentration. The salinities of the two batches prepared for this study respectively were 34.6 ± 0.5 and 34.4 ± 0.4 as determined by titration with a silver nitrate solution standardized against IASPO standard seawater.

3.2 Adsorption Experiments

Arsenate and phosphate seawater solutions were prepared by diluting 10 mM stock solutions obtained by dissolution of the following salts $As_2O_5 \bullet \sim 3H_2O$ and KH_2PO_4 in Nanopure™ water. The stability of the phosphate stock solution required that it be prepared fresh for each experiment. The arsenic stock solution stored under refrigeration was stable for periods of up to 6 months. To prepare an experiment, stock solutions were diluted in artificial seawater to an intermediate concentration of 100 µM. From the intermediate solution, nominal concentrations of 1, 2, 5, 10, 20 and 50 µM were produced. The set nominal concentrations varied to a small degree between experiments. pH was adjusted to the desired value by addition of either a 10% HCl solution, $NaHCO_3$ or Na_2CO_3. Treated gibbsite was weighed and added to acid-washed glass or disposable polystyrene 50 ml centrifuge tubes. Forty ml of the experimental solutions were then added to the tubes. A single experiment used adsorbate-Nanopure™ water solutions that were pH adjusted in the same manner as the seawater solutions. Glass tubes were used for phosphate because phosphate is known to adsorb strongly to most plasticware (Murphy & Riley, 1956; Morse et al., 1982). The use of disposable plastic tubes for arsenic eliminated the possibility of contamination from improperly washed glassware and was operationally more efficient; in addition previous studies of arsenate adsorption have utilized plastic reaction vessels (Hingston et al., 1971; Manning & Goldberg, 1996). The majority of experiments were carried out with 50.0 ± 0.5 mg of gibbsite but the influence

of varying the solid/solution ratio was investigated by running experiments at 100.0 and 200.0 ± 0.5 mg. Glass tubes were sealed by double layers of Parafilm™; polystyrene tubes with the supplied screw caps.

Experiments were run to determine the rate and extent of adsorption of arsenate and phosphate onto gibbsite from seawater. A single experiment was run in Nanopure™ water for comparison purposes. The adsorption envelope approach taken in previous studies is of limited use in a study of seawater since the pH range of marine waters is narrow. Alternatively, initial pH levels were set between 6.5 and 8.5 to cover the range of values found in natural marine environments where final pH varied between 7 and 8. Experiments were run both at room temperature (20 ± 2 °C) and in a refrigerator at 3° ± 1° C. The higher solid/solution ratio experiments were only run at room temperature. To establish the extent of adsorption to the walls of the containers the seawater-adsorbate solutions were added to tubes in the absence of gibbsite and carried through the equilibration periods. Enough tubes for each concentration/temperature combination were prepared to cover sampling at selected dates. Initial experiments were run for 28 days with sampling times at 1,3,7,14 and 28 days. As steady state conditions were established within a few days for arsenic, later experiments were run for 7 days with sampling at 1, 3, and 7 days. The phosphate experiments were also shortened to the same length to permit a comparison between the adsorbates. (External factors caused two experiments to be extended to 8 and 14). The final experiments were sampled only at 7 days. All tubes were shaken by hand at least once per day. At the beginning of each experiment aliquots of the pH-adjusted seawater-adsorbate solutions were taken for immediate analysis (phosphate) or were preserved for later analysis (arsenate).

On sampling dates, centrifuge tubes and pH buffers were temperature equilibrated by resting in a water bath for 2 hours at 20°C. This might have shifted adsorption equilibrium for the 4° experiments to a small degree. In the case of experiments

conducted at room temperature, the equilibration was not required since the buffers and the samples had temperatures that were within 1° C of each other.

All pH measurements were carried out using an Accumet™ 25 pH meter with an AgCl/Ag ORION™ combination electrode and temperature probe. The meter was calibrated using three NIST–traceable buffers of 4.00, 7.00, and 10.00. The pH of a TRIS buffer solution prepared in artificial seawater (Hannson, 1973; Dickson, 1992) was also determined in order to convert all measurements to the total hydrogen concentration scale. The difference between pH_{sw} and pH_{NIST} was between 0.1 and 0.2. The Nanopure™ water experiment pH are reported on the NIST scale/.

Initially, following pH measurements, slurries were centrifuged at 1500 rpm for 15 minutes before sampling but this step later proved to be unnecessary. After settling, samples were withdrawn from the tubes with a 10 ml plastic syringe. After rinsing the syringe with the experimental solution an aliquot was filtered through a 0.45 micron MSI Acetate Plus or Millipore HA filter into either a 30 mL Nalge™ high density polyethylene bottle (arsenate) or a 20 mL glass test tube (phosphate). At least 10 ml was taken for each analysis. Samples for arsenic and aluminum analysis were preserved by the addition of a 1% equivalent volume of concentrated high purity HCl (i.e. 0.1 ml to 10 ml) and refrigerated. Insignificant losses of As(V) have been reported for 100 nM artificial seawater solutions stored in glass, high density polyethylene and PTFE containers for periods up to 28 days (Massee et al., 1981). Phosphate analyses were carried out on the sampling day.

Table 3.3 List of experiments

#		Ratio	Conc.	Time	Final pH	T	Comment
1	AsO_4	1.25	1,2,5,10,20	28	7.7-7.9	Both	pH uncontrolled
2	PO_4	1.25	1,2,5,10,20	28	2.3-7.8	Both	pH uncontrolled
3	PO_4	1.25	0	16	7.6-7.9	Both	Indicated surface PO4
4	PO_4	1.25	0,1,2,5,10,20	28	5.0-6.8	Both	pH uncontrolled
5	AsO_4	1.25	1,2,5,10,20	28	7.8-8.4	Both	
6	PO_4	1.25	0,2,5,10,20	14	6.2-8.3	Both	Affected by Ice Storm
7	AsO_4	1.25	1,2,5,10,20	7	7.7-8.0	Both	
8	PO_4	1.25	0,2,5,10,20	7	7.8-8.0	Both	
9	PO_4	1.25	0,2,5,10,20	7	7.9-8.1	Both	
10	AsO_4	1.25	1,2,5,10,20	8	7.8-8.2	Both	
11	AsO_4	1.25	1,2,5,10,20	8	6.9-7.8	Both	1 μM samples low pH
12	PO_4	1.25	0,2,5,10,20	7	7.6-8.4	Both	
13	AsO_4	2.5,5	1,2,5,10,20	7	7.6-8.0	23°	
14	PO_4	2.5,5	0,2,5,10,20	7	7.0-7.7	23°	
15	AsO_4	2.5	1,2,5,10,20,50	7	6.9-7.0	23°	
16	AsO_4	2.5	1,2,5,10,20,50	7	7.1-7.4	23°	
17	PO_4	1.25	2,5,10,20,50	7	7.0-7.6	23°	
18	PO_4	1.25	2,5,10,20,50	7	7.5-7.8	23°	
19	AsO_4	1.25	5,10,20,50	7	6.9-8.4	23°	Data In-Fill Exp.
20	AsO_4	1.25	1,2,5,10,20,50	7	7.4-7.8	23°	Nanopure™ water
21	PO_4	1.25	2,5,10,20	7	-	23°	Experiment Failed

3.3 Analysis

3.3.1 X-Ray Diffraction

The X-ray diffraction analysis was conducted by the author using the facilities of the Geochemical Laboratories in the Department of Earth and Planetary Science McGill University. A 12 kW rotating anode RIGAKU D/Max 2400 X–ray diffractometer was used. A single sample of the aluminum trihydrate supplied by Alcan was analyzed in a backfilled aluminum mount. The scan was from 2–theta values of 6 to 60. The step size was .02° and a scan time of .3 seconds for a scan speed of 4°/minute. A copper x–ray source was used and the analysis was conducted at 40 kV and 160 mA.

3.3.2 X-Ray Fluorescence

The X-ray fluorescence analysis was performed by the Geochemical Laboratories at the Department of Earth and Planetary Sciences McGill University. The instrument used was a Philips PW2400 3 kW automated XRF spectrometer system with a Rhodium

60 kV end window x–ray tube. Major elements (e.g. Si, Al, Fe) were analyzed using 32 mm diameter fused beads prepared from the sample powder and a lithium tetraborate mixture at a ratio of 1:5. Trace elements (e.g. As, Cd, Ni, Sn) were determined from 40 mm diameter pressed pellets prepared with a mixture of sample powder and Holchat Wax Micropowder™ (5:1 ratio). The instrument is calibrated using IS–40 Certified International Reference Materials. Accuracy is reported as being within 0.5% for silica; within 1% for other major elements and within 5% for trace elements. Instrument precision is reported by the Geochemical Laboratories to be within 0.6% and overall precision is within 1% for beads and within 0.65% for pellets. Detection limits (ppm) are as follows;

Table 3.4 X-ray fluorescence detection limits (ppm)

SiO_2	60	Na_2O	75	V	10	Cd	2.0
TiO_2	35	K_2O	25	Zn	2	I	1.0
Al_2O_3	120	P_2O_5	35	LOI	100	Sb	0.5
Fe_2O_3	30	Co	10	Mo	1.0	Sn	1.0
MnO	30	Cr_2O_3	15	Pb	1.0	Ag	2.0
MgO	95	Cu	2	As	1.0	Ge	1.0
CaO	15	Ni	3	Se	1.0		

3.3.3 ARSENIC

Analysis for total arsenic was conducted by the author using the hydride generation/atomic absorption spectrometric (AAS) method of Aggett & Aspell (1976) using a Perkin Elmer 5100 AAS equipped with a FIAS 200 flow injection system and an AS 90 autosampler. No attempt was made to determine the arsenic speciation. Analysis was carried out within two months of sampling. Samples were diluted volumetrically with Nanopure™ water to nominal concentrations of less than 10 ppb (max. dilution factor 500). The operational range of the method is 2–20 ppb. Aqueous standard solutions were prepared on the day of analysis from a certified reference standard of 1000 ppm. Standard concentrations were usually at 2,4,6,8,10,12,14 and 16 ppb. Standard calibrations were always at an R^2 level of at least 0.999. Samples were run in triplicate;

samples with RSD% values above 10 were re-analyzed when possible. Outliers at values greater than 4 standard deviations from the mean were rejected. Concentrations were determined by multiplying by the dilution factor and taking into account the addition of the HCl preservative.

3.3.4 Soluble Reactive Phosphate (SRP)

Phosphate was measured on the day of sampling, as it proved impossible to preserve the samples without precipitation of an unknown white solid and/or considerable loss of phosphate. Phosphate was analyzed by the heptamolybdate spectrophotometric method of Koroleff (1976) with the following modifications; no turbidity reagent was used and a 10 mm cuvette was used. The use of a smaller cuvette results in an increase in the detection limit of the method to 0.1 μM. The upper limit of the method is reported as 28 μM. The spectrophotometer was a Bausch and Laumb Spectronic 21 with standard glass cuvettes. Calibrations were conducted for each analytical session using dilute KH_2PO_4 solutions (1 to 25 μM) prepared on the day of the analyses. Standards were analyzed in triplicate and correction for blanks was made on individual cuvette-position combinations. R^2 of the calibration curve was always above 0.9990 and generally above 0.9995. Samples were measured in duplicate and RSD% values were generally under 5%

3.3.5 Aluminum

A small number of samples were analyzed for aluminum to establish the general level of aluminum within the samples. Aluminum analysis was conducted within one month of sampling using the catechol violet spectrophotometric method of Dougan & Wilson (1974). This method has an operational range of up to 400 ppb. Based on a molar extinction coefficient of 6.94×10^4 l/mole•cm, the lower detection limit is 78 ppb. The method is subject to minor interference from fluoride and phosphate although the effect is unimportant for the purposes here. Calibration curves were established by the use of standards (1–250 ppb) prepared on the day of analysis from a 1000 ppm stock standard

aluminum solution. Standards were analyzed in triplicate and correction for blanks was made on individual cuvette–position combinations. R^2 values were always above .9900. Since the required precision of aluminum analysis was not high, only single determinations of samples were made. The spectrophotometer was a Bausch and Laumb Spectronic 21 with standard 10 mm glass cuvettes.

3.3.6 FLUORIDE

The possibility of fluoride adsorption was investigated by analyzing the later arsenate experiments for fluoride. Preserved samples were analyzed within 1 month of sampling. Fluoride analysis was performed using a Fisher™ Fluoride Ion selective electrode, an ORION™ Double Junction Reference Electrode and an Accumet™ 25 pH/ion meter. The general theory for the operation of the electrode is given in Frant & Ross (1966). The measurements were carried out in the presence of the sodium citrate total ionic strength adjusting buffer (TISAB I) of Frant & Ross (1968). This buffer has been often used for seawater fluoride analysis (Warner, 1969;1971a, b) and is reported to be effective in minimizing aluminum interference (Kauranen, 1977).

The samples were analyzed using the standard addition method of Warner (1971a) except that a different quantity of sample was analyzed. This method is preferred to the potentiometric method of Warner (1971a) since the total concentration of soluble fluoride in seawater is available without a calculation involving salinity. The necessary calculations are performed by the ion meter but the result must be multiplied by the dilution factor introduced by the addition of the buffer.

To determine the response slope of the electrode, standards of 200,100,50 and 25 μM were prepared from a 0.1 M fluoride standard stock solution supplied with the electrode. The response of the electrode was determined on the day of the analysis. The slope for all segments was within the operating guidelines of –59 ± 4 mV (Fisher Scientific, 1990). The ion meter did not achieve stability at times of up to 30 minutes.

Because of this, measurements were made on a timed basis. Initial readings were taken after 5 minutes of immersion of the electrodes and the final reading was taken 5 minutes after the standard addition was made. Given the lack of stability of the ion meter and the unknown effects of storage on F^- the accuracy of the fluoride measurements is questionable.

3.4 Data Treatment

Adsorption density was calculated by subtracting the concentration of a sample from the initial concentration of the batch and dividing by the solid/solution ratio (r).

$$\Gamma = \frac{C_i - C_f}{r} \qquad [3.1]$$

where Γ = adsorption density
C_i initial concentration
C_f final concentration

Percentage removal of an adsorbate has been used as a measure of adsorption in studies under seawater conditions (Shaw, 1996; Harris, 1996), but the low levels of adsorption that were found and the computational difficulties inherent in comparing such results to previous studies led to the use of a more conventional adsorption density measurement. In this study the absence of a specific surface area measurement necessitated the use of a mass/mass density expressed in terms of micromoles of adsorbate per gram of gibbsite.

The lack of pH control resulted in a scattering of pH values. To have sufficient data points to plot isotherms it was necessary to use relatively large pH groupings. The groupings were a half pH unit wide thus 7.00 ± 0.25, 7.5 ± 0.25, 8.0 ± 0.25. Since there was a near symmetrical distribution about the central values artifacts induced by this treatment are minimal.

Isotherms were fitted to the data using least squares regression using Microsoft Excel™. The empirical parameter for the Freundlich isotherm equation was fitted for

each data subset by the goal seeking function of the program. The fits of Langmuir isotherms were checked by the linearization method of Vieth & Sposito (1977).

3.5 Sources of Error

Most errors other than random errors will be positive and would suggest greater adsorption than actually happened. This is due to the indirect nature of the measurements; the total loss of the adsorbate is assumed to be due to adsorption. Random error is always present in analysis and is minimized by the use of multiple analytical determinations and statistical treatment.

Error introduced by the presence of impurities in the reagents is corrected for by the use of blanks and by the analysis of the initial arsenate or phosphate seawater solutions. Losses of adsorbate other than by adsorption are possible but were accounted for by the use of blanks. Errors of this type would increase apparent adsorption.

Negative errors would result from the unintentional addition of phosphate or arsenate to the reaction vessels. These additions could be the result of contaminated plasticware or glassware, or contamination from airborne dust. Both possibilities were minimized by the cleaning and the sealing of reaction vessels. The influence of organisms could create positive or negative errors. The experiments were not conducted under sterile conditions and any biotic influence would be uncontrolled. Any influence of this type would probably be irreproducible.

Chapter 4 Results and Discussion

4.1 Adsorption Isotherms

4.1.1 ARSENATE

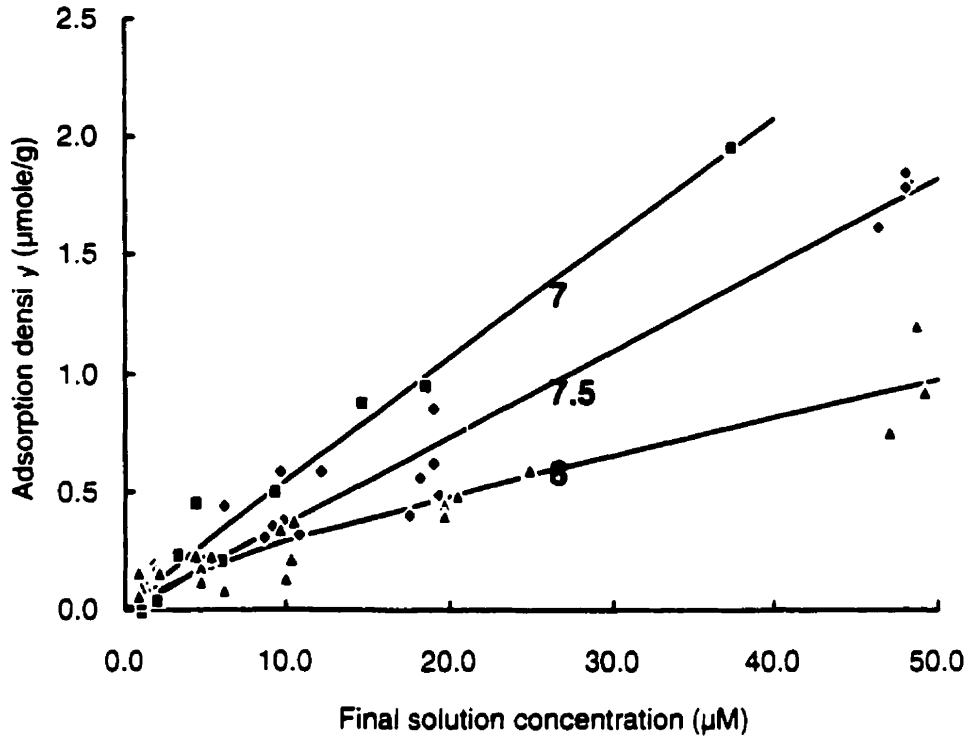

Figure 4.1 Arsenate adsorption in artificial seawater after 7 days and 23 ± 1°C pH ■ 7 ◆ 7.5 ▲ 8.

Arsenate adsorption on gibbsite from artificial seawater at pH 7, 7.5 and 8 can be reasonably represented by Freundlich isotherms (Figure 4.1 and Table 4.1). Some of the scatter in the data is attributable to the broadness of the pH groupings (see Table 4.2). At concentrations greater than those used in this study, adsorption behaviour might be described by a Langmuir isotherm as reported in studies carried out in dilute solutions (Anderson et al, 1976; Anderson & Malkoty, 1979) since at low concentrations the shape of a Freundlich isotherm is similar.

Table 4.1 Parameters of arsenate isotherms

pH	K_f	Uncertainty	exponential parameter	R^2
7	$5.82*10^{-2}$	$0.22*10^{-2}$	0.97	0.9741
7.5	$3.65*10^{-2}$	$0.12*10^{-2}$	1.00	0.9310
8	$5.15*10^{-2}$	$0.24*10^{-2}$	0.75	0.8925

Table 4.2 Arsenate isotherm pH group data

pH	# of points	mean	maximum	minimum	RSD
7	11	7.0	7.24	6.80	2 %
7.5	20	7.5	7.69	7.35	1
8	20	8.0	8.24	7.75	2

The influence of pH is clear even if it is not directly quantifiable by the Freundlich isotherm (the exponential parameter is not held constant). Recalling the Freundlich isotherm equation described earlier,

$$\Gamma_J = ([J_{aq}]K_f)^{\beta} \qquad [2.3]$$

it can be seen that if the exponential parameter of the Freundlich isotherm (β) is set to 1 then the isotherm is reduced to the simple linear isotherm. For the isotherms in Figure 4.1, the reduction to a simple linear isotherm results is a near linear relationship (R^2 = 0.9997) between the partitioning coefficient K_f and pH.

Table 4.3 Parameters of simple arsenate isotherms

pH	K_d	Uncertainty	R^2
7	$5.28*10^{-2}$	$0.20*10^{-2}$	0.9740
7.5	$3.65*10^{-2}$	$0.12*10^{-2}$	0.9310
8	$2.11*10^{-2}$	$0.12*10^{-2}$	0.8498

Results of the experiment carried out in Nanopure™ water show that the arsenate adsorption to gibbsite at pH 7.5 can be fitted using a Langmuir isotherm with an excellent goodness of fit (R^2 = 0.97) (Figure 4.2). Recalling the Langmuir isotherm equation,

$$\Gamma_J = S_T\left[\frac{K_L[J_{aq}]}{1+K_L[J_{aq}]}\right] \qquad [2.4]$$

the Langmuir coefficient (K_L) is 4.36 and the total site density (S_T) is 2.26 μmole/g.

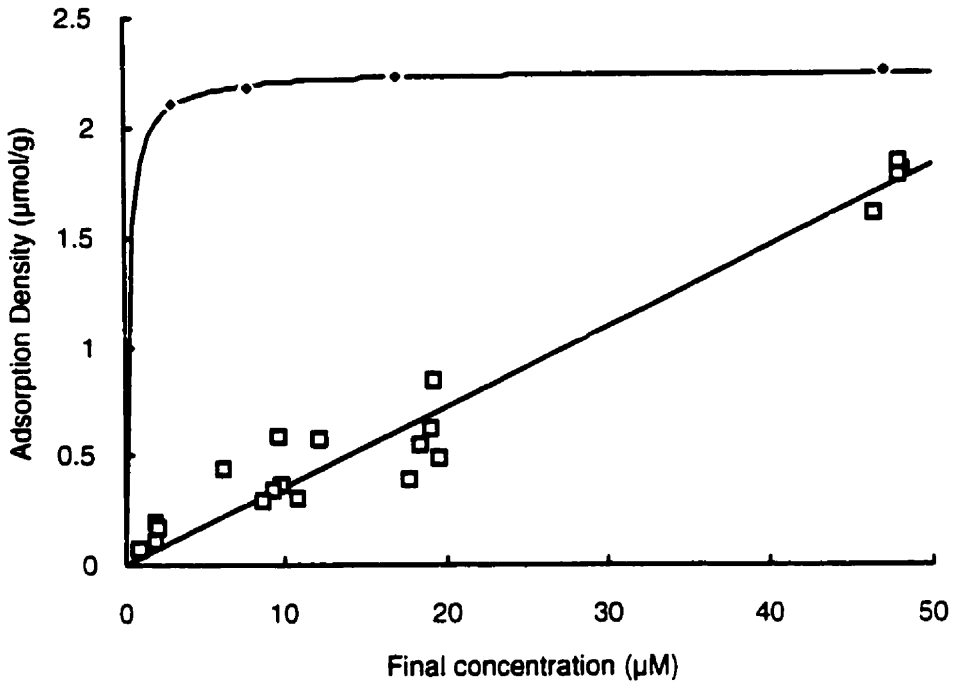

Figure 4.2 Adsorption of arsenate to gibbsite from Nanopure™ water and artifical seawater at pH 7.5 and 23°C after 7 days ● Nanopure™ water ✱ artificial seawater.

The adsorption pattern of the freshwater experiment is consistent with results of other studies (Anderson et al., 1976; Anderson & Malkoty, 1979). The specific adsorption of arsenate to gibbsite is illustrated by the limited effect that concentration has on adsorption behaviour (Figure 4.2). The apparent maximum adsorption density of the gibbsite (2.26 µmol/g) is much lower that densities reported previously but as noted (see Section 2.5.1) the great variability in surface properties makes inter-experiment comparisons impractical. Hingston (1981) suggests that anion adsorption to gibbsite conforms to a Langmuir isotherm at low concentrations but adsorption density never reaches a maximum and that adsorbtion densities will increase linearly with conentration. If this explanation is true then the plateau apparent in Figure 4.2 can only be regarded as an artifact of the limited concentration used in the experiment. In either case it is apparent that the calculation of maximum adsorption density is dependent on the range of concentrations used.

A comparison of the adsorption isotherms in artificial seawater and in Nanopure™ water (Figure 4.2) clearly shows that some property of the artificial seawater is responsible for the diminished adsorption density. The strong relationship between adsorbate concentration and adsorption density observed in the experiments conducted in artificial seawater is not observed in the Nanopure™ water experiment.

Blanks showed no significant deviations from the initial solution concentrations. Thus all removal processes are related to adsorption to the gibbsite and there was no detectable contamination.

4.1.1.1 Estimation of Specific Surface Area

The measurement of specific surface area of the gibbsite was not made primarily because of difficulties in gaining timely access to analytical facilities. In addition, the specific surface area is not a requirement of the modeling approach that was chosen so that the knowledge of the specific area was not critical. In an experimental study of the adsorption of arsenate to gibbsite, Manning & Goldberg (1996) used a gibbsite with similar grain size as that used in the present study (less than 500 microns). This gibbsite had a measured specific surface area of 45 m^2/g. The similarity of the gibbsite with respect to the grain size allows for an estimate of specific surface area to be made.

The calculated maximum adsorption density from the Nanopure™ water experiment suggests that the specific surface area is lower than the 45 m^2/g reported by Manning & Goldberg (1996). Their gibbsite at a pH of 7.5 shows an adsorption density of ~ 60 μmol/g at a final concentration of 150 μM and ~ 40 μmol/g at a final concentration of 33 μM (Figure 4.3). Fitting an isotherm through two data points has no merit; there is however no other adsorption study which used different initial arsenate concentrations and for which the specific surface area of the gibbsite was determined. With this in mind, the data of Manning & Goldberg show a trend that could be described by a Langmuir or a Freundlich isotherm but no definitive limitation of site density can be

made. The maximum observed density of 60 μmol/g is more than 10 times greater than what was observed for the gibbsite used in this study. This difference is greater than the range of gibbsite specific surface areas reported in the literature (10-60 m^2/g). It is more likely that most of the difference in the maximum adsorption densities is accounted for by a difference in the percentage of specific surface site area provided by the edges of the gibbsite crystals, the only adsorption sites on the gibbsite crystal. The difference in the specific surface area or the edge area could be attributable to differences to the synthesis conditions of the gibbsite. The Alcan gibbsite was synthesized from bauxite on an industrial scale, whereas the gibbsite of Manning & Goldberg (1996) was synthesized from aluminum chloride at laboratory scale. There are also differences in the treatment of the gibbsite; the gibbsite of Manning & Goldberg (1996) was ground by mortar and the Alcan gibbsite was not. The grinding creates additional edge surface area. The experimental procedure may be partly responsible for the decreased adsorption density. The study of Manning & Goldberg was only conducted for 4 hours and experiments were continually agitated during that time, whereas the experiments in this study were conducted over 7 days and were only shaken once per day. Although the gibbsite used in the present study became well dispersed upon agitation, the settling of the gibbsite will bring grains into contact. The settled gibbsite particles will have a large percentage of their surface area in contact with one another and this may prevent adsorption. However given the form of the gibbsite (plates) the majority of the intergrain contact will be between the non-adsorbing faces of the gibbsite. There will be some degree of contact of the edge faces but the pattern will be random and unlikely to repeat itself after agitation. Thus, intergrain contact can not account for the order of magnitude difference in maximum adsorption density.

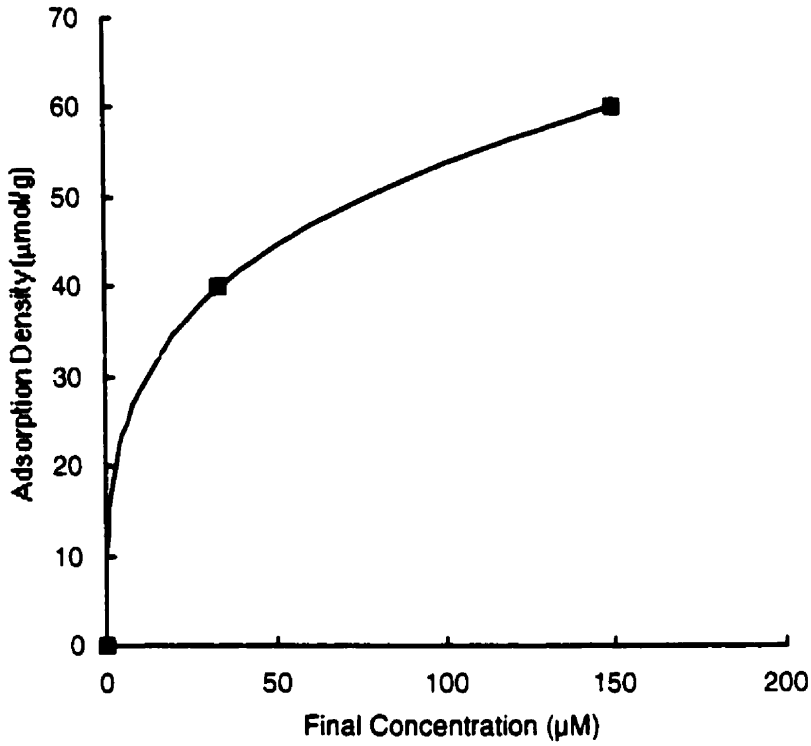

Figure 4.3 Adsorption of arsenate to gibbsite from a 0.1 N NaCl solution at 22°C after 4 hours. Calculated from experimental data of Manning & Goldberg (1996)

4.1.2 PHOSPHATE

The data describing phosphate adsorption had a greater degree of scatter and efforts to derive a well–fitted isotherm were less successful (Figure 4.4 and Table 4.4). An insufficient number of data points precluded an isotherm for pH 7. The grouping for pH 8 includes two data points greater than 8.25 (Table 4.5). Adsorption at both pH levels could be fitted with a Freundlich isotherm although the correlation coefficient for pH 7.5 is low.

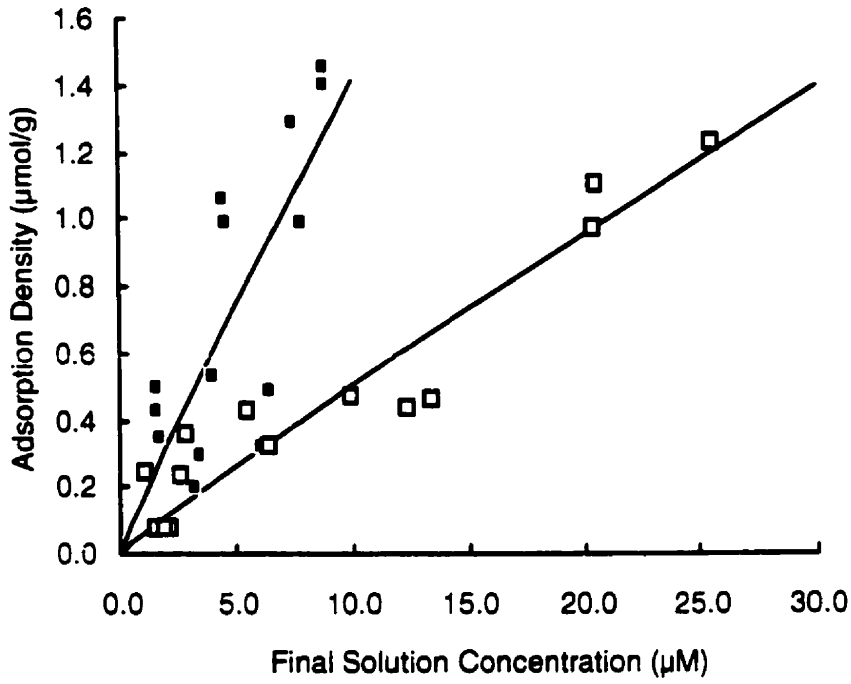

Figure 4.4 Adsorption of phosphate to gibbsite in seawater at 23°C after 7 days pH 7.5 ■ 8.0 □

Table 4.4 Parameters of phosphate adsorption isotherms

pH	K_f	Uncertainty	exponential parameter	R^2
7.5	0.170	0.016	0.92	0.562
8	0.061	0.003	0.75	0.895

Table 4.5 Phosphate isotherm pH group data

pH	# of points	mean	maximum	minimum	RSD
7.5	15	7.5	7.73	7.26	2%
8	14	8.0	8.5	7.75	3%

The blanks were, within 10%, the same as the original solutions. Thus, all phosphate removal is related in some manner to the presence of the gibbsite.

4.1.3 Comparison Between Arsenate and Phosphate Adsorption

Phosphate adsorption density is greater than that of arsenate, the difference decreases as pH rises (Figure 4.5). Phosphate has been previously reported to adsorb to gibbsite and amorphous aluminum hydroxide at greater densities than arsenate (Manning & Goldberg, 1996; Okazaki et al., 1989; Hingston et al., 1971). There is thus a greater

affinity between the gibbsite surface and phosphate. The physical cause of this is unknown although Hingston (1981) suggests that it is related to steric (i.e., size) effects. A phosphate surface complex will occupy less space (45 Å/anion) than an arsenate surface complex (61 Å/anion). It is suggested that a fluoride complex will occupy even less space (20 Å/anion). A more detailed discussion of the adsorption mechanism and inter comparisons appear in Section 0. Since the adsorption of anions is coupled with a release of OH^- ions, adsorption is favoured by lower pH

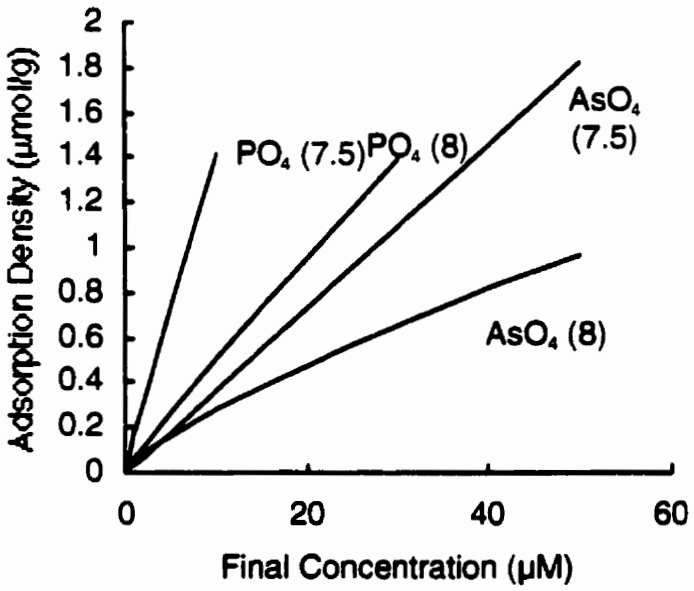

Figure 4.5 Comparison of adsorption of phosphate and arsenate to gibbsite in artificial seawater at 23°C. pH groupings in parenthesis.

4.1.4 FLUORIDE

The relatively constant initial concentration of fluoride (66–72 µM) found in the artificial seawater does not offer an adequate database for the construction of an isotherm to model fluoride adsorption. The analysis of fluoride in the experimental system was an extension to the original scope of the thesis and so there was a wide disparity in the storage of the samples which may explain the poor quality of the data. Nevertheless, a correlation between fluoride adsorption density and pH was noted for experiments run in

the presence of 20 μM As (Figure 4.6). The samples of this set received identical treatment in terms of storage. The observed trend agrees with the pH relationship established in dilute solution studies (Hingston et al., 1972; Hingston, 1981; Farrah et al., 1987).

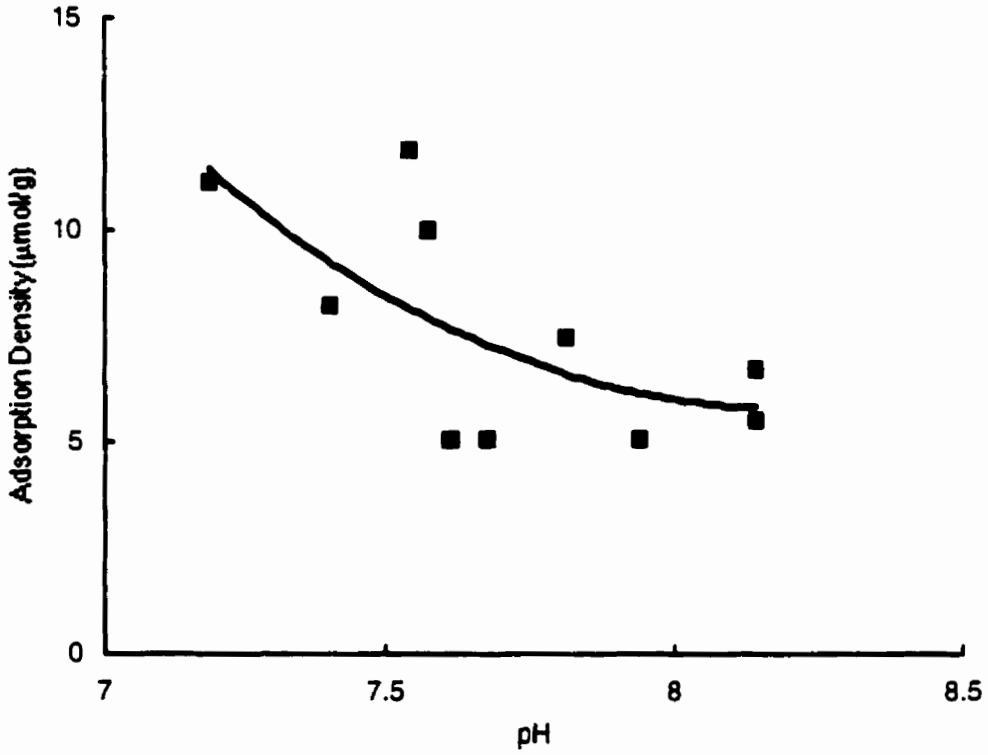

Figure 4.6 Fluoride adsorption to gibbsite from artificial seawater. Fluoride ~ 70 μM, arsenate ~ 20 μM

4.2 Speciation of Adsorbates and Surface Complexes

The narrowness of the pH range used (7-8) makes a full consideration of adsorption envelopes irrelevant. However, since the adsorption envelope reflects the speciation of both the solute and the surface it is important to consider the relationship of pH with adsorption. The speciation of the solutes and the gibbsite surface are shown as Bjerrum plots in Figures 4.7-4.9.

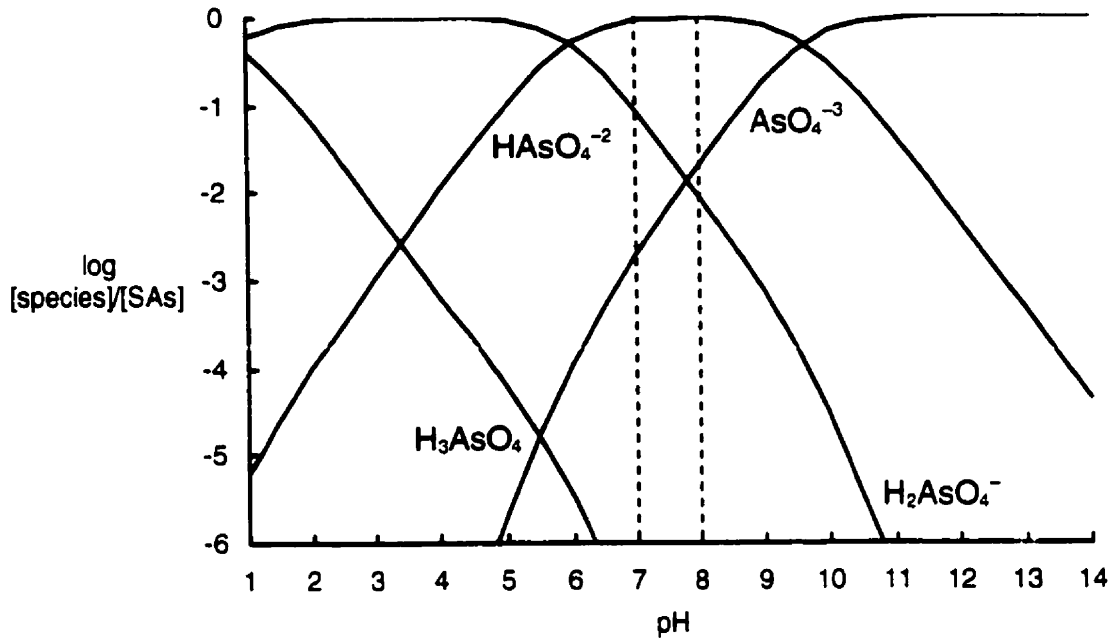

Figure 4.7 Bjerrum plot for arsenate (50 µM) in seawater. pK_1 1.828, pK_2 5.966, pK_3 9.656 on total proton scale. Constants from Lowenthal et al. (1977). Converted to total proton scale with constants of Dickson & Riley (1979a).

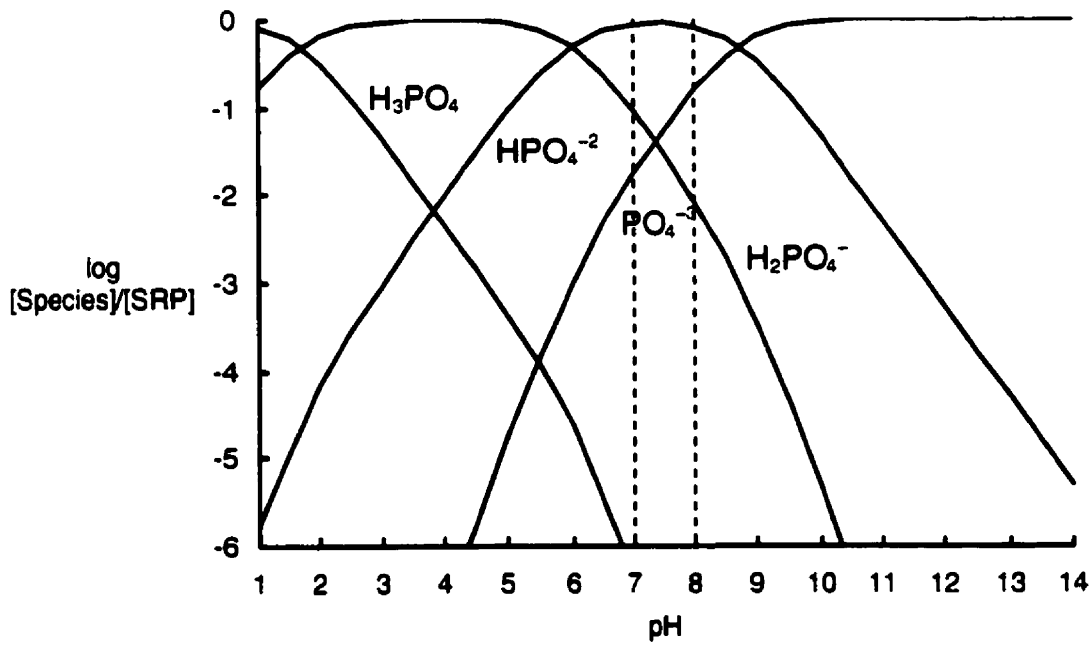

Figure 4.8 Bjerrum plot for phosphate (50 µM) in seawater. pK_1 = 1.68 pK_2 = 6.00 pK_3 = 8.71 on total proton concentration scale. Dissociation constants from Dickson & Riley (1979b) Converted to total proton scale with constants of Dickson & Riley (1979a)

Although the monoprotic species dominate over the pH range investigated in this study, the decline in adsorption densities, expressed as smaller distribution coefficients, with an increase of pH coincides with a decline in the relative concentrations of the diprotic species. The pH range examined coincides with the pH range where diprotic concentrations are decreasing and monoprotic concentrations are relatively constant. Although a full adsorption-pH relationship was not developed, the relationship is similar to what is seen in low ionic strength solutions (see Section 0). Whereas there is no direct evidence of the preferentially adsorption of the diprotic species, the data suggest it.

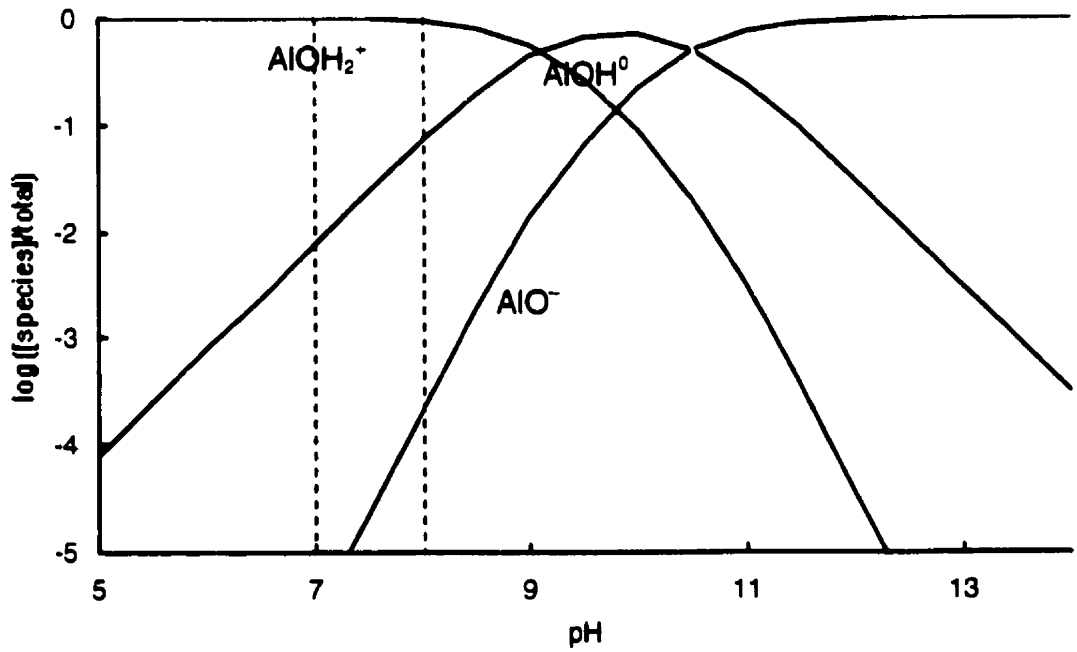

Figure 4.9 Speciation of gibbsite surface species. Intrinsic constants from Manning & Goldberg (1996)

The gibbsite surface over the pH range of the present study is dominated by the $AlOH_2^+$ species (Figure 4.9). The relative abundance of this surface species only declines at a pH that is much closer to the PZC (~9-10 for gibbsite).

The adsorption behaviours of arsenate and phosphate suggest that they are not dominated by electrostatic interactions or outer-sphere complexation. Adsorption declines slowly in the 7-8 pH range used in this study as reflected in smaller distribution

coefficients as pH increases. An outer-sphere adsorption mechanism would show a rapid decline in adsorption densities as pH nears the PZC (~9–10 for gibbsite) and would occupy a narrow pH range. This is reflective of a change in surface speciation as illustrated in Figure 4.9. In contrast, inner-sphere adsorption is believed to be partially covalent in nature and essentially independent of surface charge, thus the adsorption envelope is not dictated by the PZC of gibbsite (pH_{PZC} = 9–10) but by adsorbate speciation. The decline in adsorption with increasing pH is related to the decline of the concentration of the preferentially adsorbed species. Hingston (1981) has shown that the pH of inflexion points of anion inner–sphere adsorption envelopes coincide with the pK_a values (i.e. $pK_a = -\log K_a$) of the corresponding conjugate acids (Figure 4.10). In the case of arsenate and phosphate, adsorption declines in concert with the decline of the diprotic species concentration. This is seen by the pK_2 for orthophosphate shown in Figure 4.10.

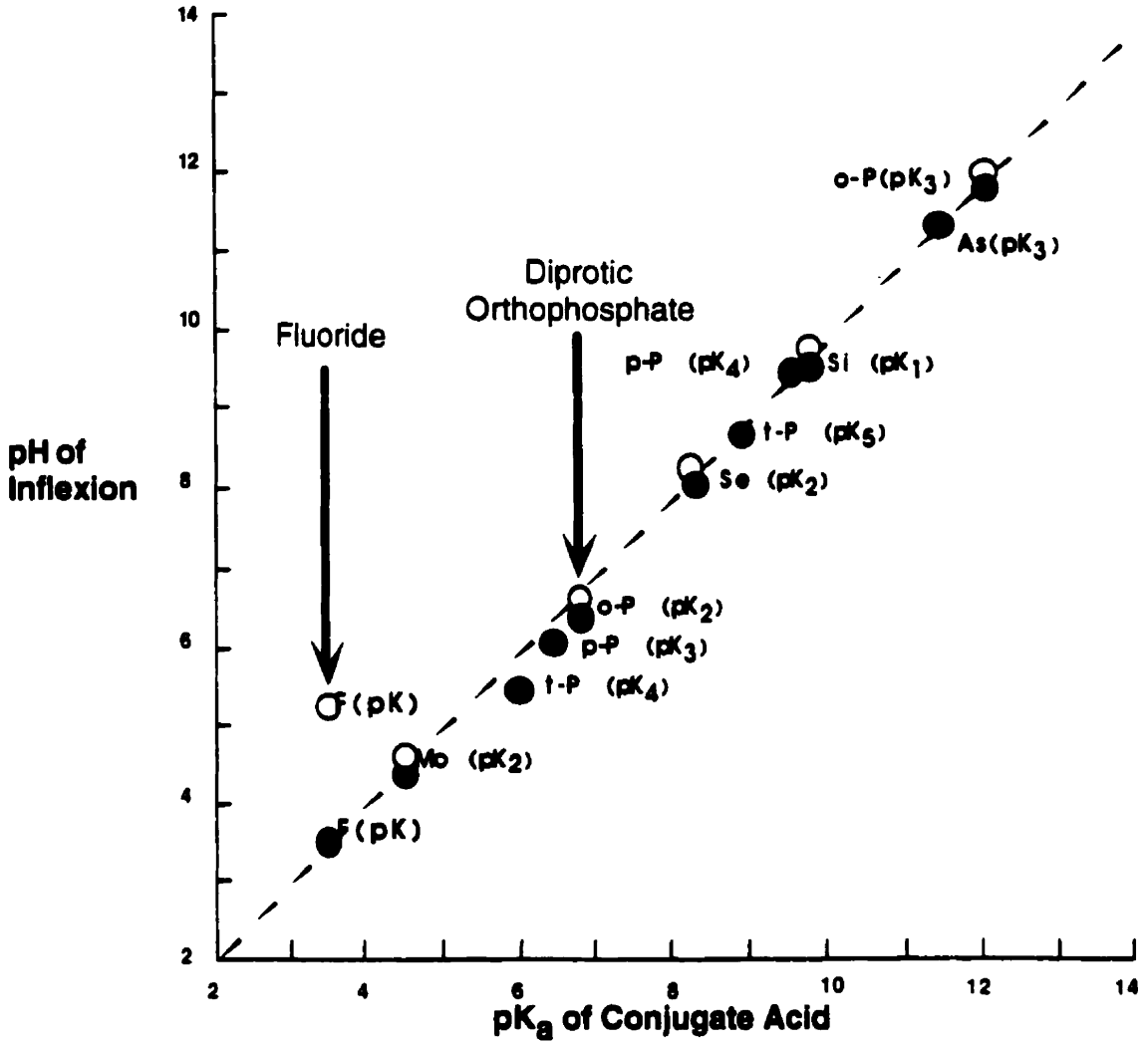

Figure 4.10 Relationship between pK_a and pH at the change of slope of adsorption envelopes. Adsorbents ●, goethite; ○ gibbsite. Adsorbates: F *fluoride*; Mo, *molybdate*; t–P, *tripolyphosphate*; p–P, *pyrophosphate*; o–P, *orthophosphate*; Se, *selenite*; Si, *silicate*; As, *arsenate*. (From Hingston, 1981).

The adsorption of fluoride is also believed to be inner–sphere (Hingston, 1981); the observed decline in adsorption density is attributable to a change in fluoride speciation (Figure 4.11). Hingston et al. (1972) show peak fluoride adsorption at pH 5 and decline in adsorption in both directions with respect to pH. The decline at lower pH, however, is poorly defined. Furthermore, Farrah et al. (1987) show no decline in adsorption with decreasing pH and a decline in adsorption with increasing pH beginning at a pH of 4 to 5. Taken together the two studies would suggest that HF^0 is the species being preferentially adsorbed.

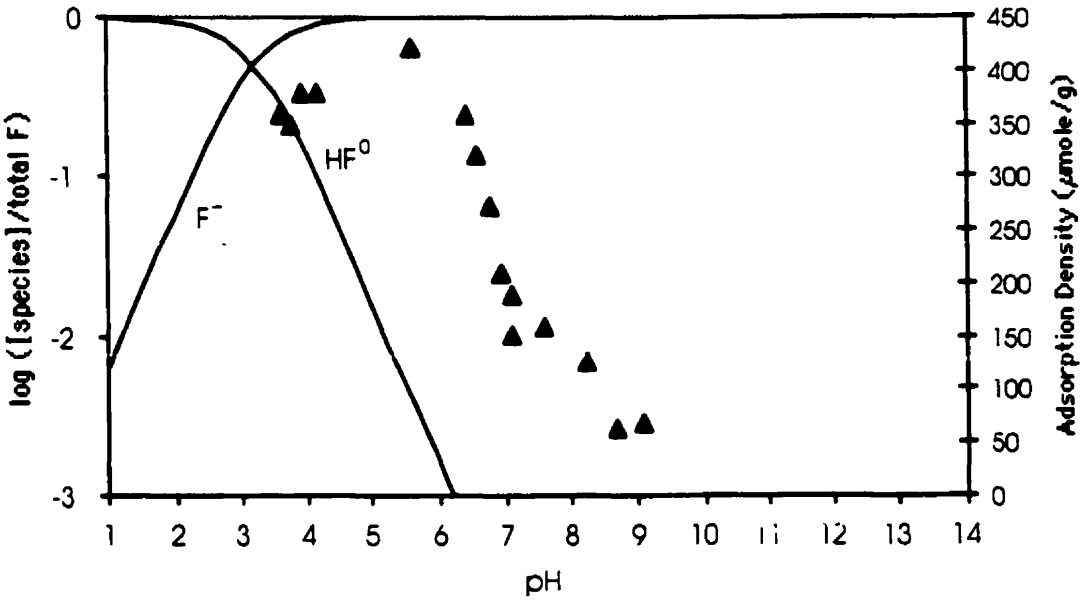

Figure 4.11 Bjerrum diagram of fluoride and adsorption of fluoride to gibbsite. Dissociation constant from Stumm and Morgan (1996). Adsorption data from Hingston et al. (1372)

Fluoride adsorption to gibbsite is notable in its deviation from the direct correspondence of pH of inflexion points and pKa values (Figure 4.10 and Figure 4.11). This difference appears to be the result of an unspecified strong chemical interaction between fluoride and aluminum in addition to adsorption. This anomalous behaviour is not observed for adsorption onto goethite whereas gibbsite behaves normally with other adsorbates. One possible cause of the discrepancy may be associated with analytical uncertainties. The difficulty in measuring fluoride in the presence of aluminum has been noted (Warner. 1969; Kauranen, 1977). The fluoride in alumino–fluoride complexes is undetectable by an ion–selective electrode (Pickering, 1986; Farrah et al.. 1987). If adsorption is measured indirectly then the fluoride that is in alumino–fluoride complexes would be included in the quantity of adsorped fluoride and thus adsorption would be overestimated. The overestimate of adsorption will shift the adsorption envelope. HF^{o} dissociates and presumably desorbs at higher pH and the free fluoride would complex with dissolved aluminum. As the solubility of aluminum is dictated by pH, increasing pH will diminish the concentration of dissolved aluminum. In turn, a decrease in dissolved aluminum

concentration results in a reduction in the aamount of the alumino–fluoride complexes thus leaving a greater concentration of the free fluoride ion. This explanation assumes that gibbsite will dissolve. However, as noted earlier, the dissolution of gibbsite is slow and it is not likely that great quantities of aluminum will be present during the short time frames of the adsorption experiments. In addition, the interference of aluminum is minimized by the prevention of the formation of the complexes by the addition of TIASB I (Kauranen, 1977) during the analyses. Interference by fluoride on the analysis of aluminum by the catechol violet spectrophotometric method is minor (Dougan & Wilson, 1974), so it is not likely that aluminum levels have been underestimated. The low concentrations of HF^0 at pH >5 suggests a mechanism other than adsorption to explain the experimental results. The removal of fluoride is potentially due to the precipitation of cryolite (Na_3AlF_6). Its formation could occur in low ionic strength solutions in the presence of sodium (from a supporting electrolyte) (Figure 4.12). Cryolite is manufactured synthetically from gibbsite according to the reaction that also dictates the stability fields,

$$6HF + Al(OH)_3 + 3NaOH \leftrightarrow Na_3AlF_6 + 6H_2O \qquad [4.1]$$

Once formed, the cryolite could remain in association with gibbsite by some weak force or it might exist as separate particles, which would be difficult to detect optically since cryolite has almost the same refractive index as water.

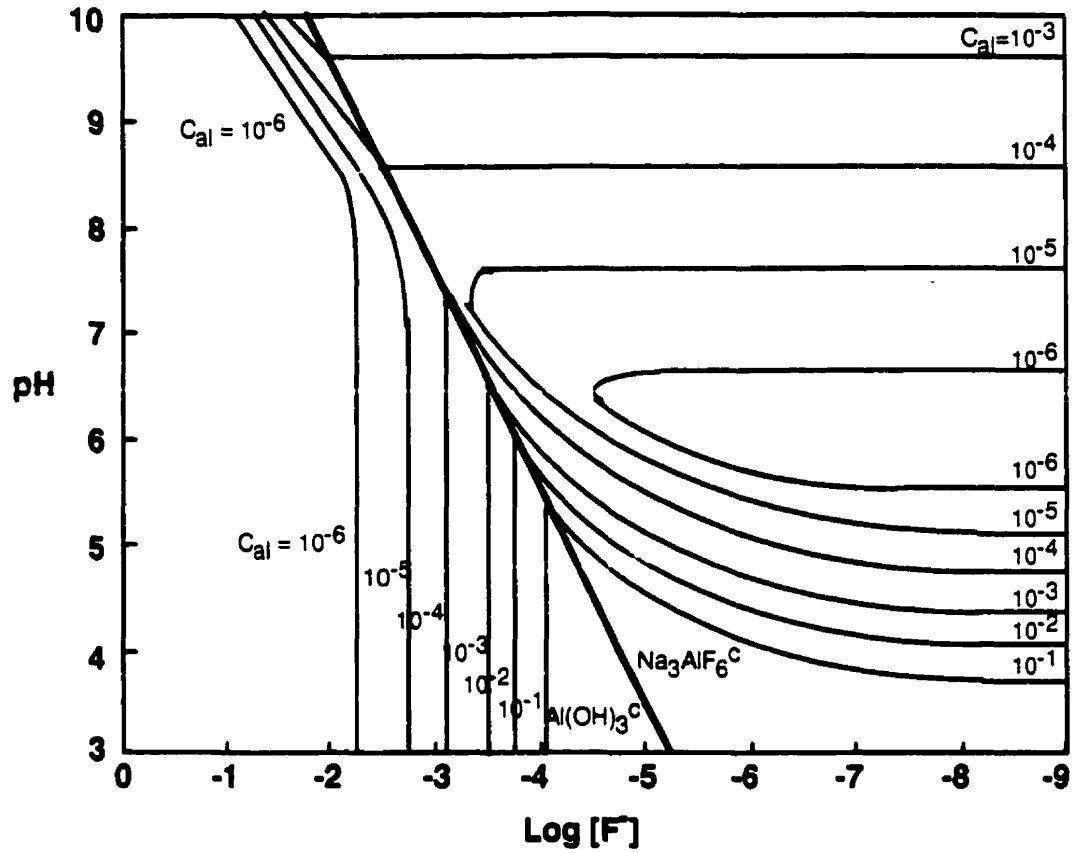

Figure 4.12 Stability fields of cryolite and microcrystalline gibbsite and their solubilites in relation to pH and [F⁻] at 25°C and 1 atmosphere total pressure. Ionic strength 0.10 , ([Na] = 0.1 M). From Roberson & Hem (1969).

The stability line will shift to the right (decreasing fluoride) with the increased level of sodium in seawater. The concentration of total fluoride in the artificial seawater is 70 nM (~1.3 ppm). Based on thermodynamic considerations alone it would not be possible to form cryolite in seawater from gibbsite since the free fluoride concentration is lower than the stability field of cryolite. In seawater and in the presence of aluminum the majority of fluoride ions will be present as ion pairs and aluminum–fluoride complexes. However as equilibrium with gibbsite was not achieved and aluminum concentrations were very low (see below), a large portion of fluoride (49%) would be present as free fluoride (Millero & Schreiber, 1982). On the other hand, the electrostatically positive surface of the gibbsite over the pH range of this study could act as a concentration mechanism for fluoride and thus create a localized concentration of fluoride sufficient to allow the precipitation of cryolite. The adsorption behaviour of fluoride onto gibbsite from artificial

seawater has not been investigated. If the behaviour is similar to that in dilute solutions then the co–precipitation of cryolite is a possibility. The formation of cryolite has not been detected in fluoride adsorption studies (Hingston et al., 1972; Farrah et al., 1987) but in these studies the surface was not directly investigated. X–ray diffraction analysis of gibbsite that was in an artificial seawater for periods of up to 7 months showed no evidence of cryolite formation (Crane, 1998). However, the rinsing of the gibbsite to remove residual sea salts could dissolve traces of cryolite which might prcipitate. In addition, cryolite may be undetectable by X–ray diffraction. Only one of the 4 primary diffraction peaks of cryolite would be detectable in a gibbsite–seawater system. The strongest peak coincides with the major peak for halite, the major residual sea salt. The second peak would have a 2–theta value of 73, which is outside of the range examined. The fourth peak is close to the strongest peak for gibbsite. A peak corresponding to the third peak of cryolite is sometimes present but at small amplitude and within background noise (Crane, 1998). Thus, no definite conclusion on the presence of cryolite can be made based on available x–ray diffraction spectra.

4.2.1 Proposed Surface Coordination Equilibria

To determine the most likely coordination reaction it is necessary to take into account the changes that occurred in pH during the experiment and the surface charge of the gibbsite following adsorption. pH in the experiments varied, but in general it rose by 0.2 to 0.8 units over the 7 days of equilibration. Since the adsorption of anions is coupled with a release of OH^-, the adsorption of anions is indicated. Given these considerations it can be surmised that adsorption reactions involving the release of protons are relatively unimportant. The surface charge after adsorption was not measured andit is not clear what the charge should be. Since the triprotic species are not important in the pH range of this study they do not need to be considered. The limited pH range of the present study does not allow for the role of the triprotic species at lower pH to be established. The

orientation of the adsorbate ions (4 oxygens around a central atom) allows for bidentate (2 surface sites) complexes but effectively prevents the formation of tridentate complexes. The adsorption equilibria that can be considered based on the rise in pH are:

$$\equiv Al\text{–}OH_2^+ + H_2X^- \Leftrightarrow \equiv Al\text{–}H_3X^+ + OH^- \quad [4.2]$$

$$\equiv Al\text{–}OH_2^+ + HX^{-2} \Leftrightarrow \equiv Al\text{–}H_2X + OH^- \quad [4.3]$$

$$2\equiv Al\text{–}OH_2^+ + HX^{-2} \Leftrightarrow (\equiv Al)_2\text{–}H_2X^+ + H_2O + OH^- \quad [4.4]$$

$$\equiv Al\text{–}OH_2^+ + X^{-3} \Leftrightarrow \equiv Al\text{–}HX^- + OH^- \quad [4.5]$$

$$2\equiv Al\text{–}OH_2^+ + X^{-3} \Leftrightarrow (\equiv Al)_2\text{–}HX + OH^- \quad [4.6]$$

There are many other possibilities, such as those involving an uncharged surface species ($\equiv Al\text{–}OH^0$). However, since adsorption decreases with increasing pH as $\equiv Al\text{–}OH^0$ becomes more important, such reactions will probably be unimportant. Given the observed relationship of adsorption density and diprotic adsorbate abundance, reaction 4.2 is likely predominant although other adsorption reactions may be taking place. The adsorption lf unprotonated phosphate ion should be considered at the higher pH range of this study.. The experiments at higher pH occasionally showed minor declines in pH (less than 0.2 units. The cause of this decline was not established. The pH decline is probably not due to a change in surface speciation since at the pH of the experiments (8-8.2) the quantity of negatively charged species is insignificant. A realistic possibility is that inner–sphere adsorption of magnesium, calcium and strontium to gibbsite causes desorption of protons and thus decreases pH. The specific adsorption of seawater cations to γ–alumina has been reported to increase greatly above a pH of 8 (Huang & Stumm, 1973). Such a reaction would be similar to equation 4.7.

$$\equiv Al\text{–}OH_2^+ + Ca^{2+} \Leftrightarrow \equiv Al\text{–}OH\text{–}Ca^{2+} + H^+ \quad [4.7]$$

It is also possible that the decline in pH is related to the buffering of the system by the carbonate ion present in the solution. The pH of natural seawater is 8.1 at 25°C and 1 atm. (pH_{NTIS} = 8.2). The precise structure of surface complexes can not be determined

without a direct characterization of the surface complexes. Brown (1990) gives a review of studies involving this type of characterization.

It is unlikely that the adsorption of fluoride can be described based on a single equilibrium given the previously mentioned strong chemical interaction. Based on the Bjerrum plot of fluoride speciation and the observed decline in adsorption with increasing pH above 5 (Hingston et al. 1972; Farrah et al., 1987) it would appear that HF_2^- is the adsorbed species. This equilibria could be described by a combination of the following reactions

$$\equiv Al\text{–}OH_2^+ + HF^0 \Leftrightarrow \equiv Al\text{–}HF^- + H_2O \qquad [4.8a]$$

$$\equiv Al\text{–}OH_2^+ + HF^0 \Leftrightarrow \equiv Al\text{–}F + H_2O + H^+ \qquad [4.8b]$$

Note the similarity of these reactions with reaction 4.1.

4.3 Temperature Effects

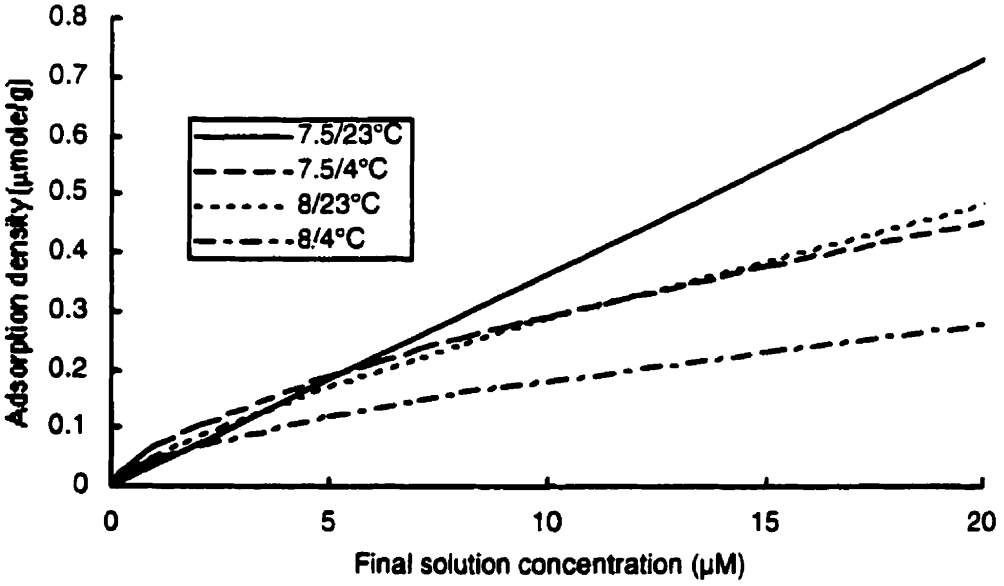

Figure 4.13 Arsenate adsorption onto gibbsite from artificial seawater as a function of temperature at pH 7.5 and 8. Data points removed for clarity

Arsenate adsorption is diminished at the lower temperature (Figure 4.13). The adsorption of phosphate is also diminished at the lower temperature but the change is insignificant (Figure 4.14).

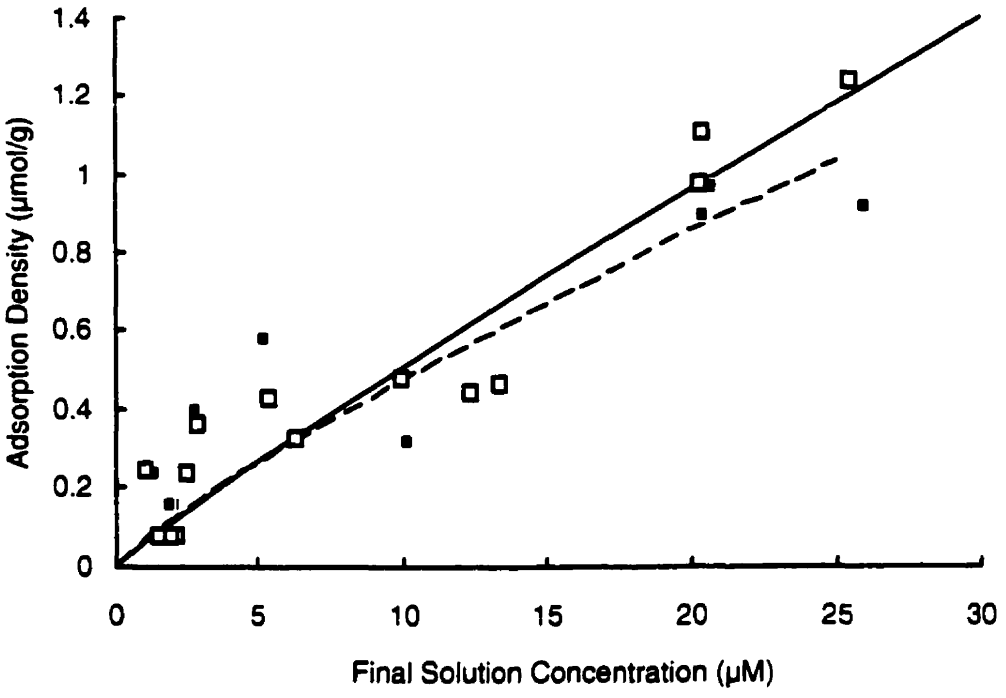

Figure 4.14 Phosphate adsorption onto gibbsite from artificial seawater as a function of temperature at pH 8 solid line and ■ 23°C, dashed line and ❐ 4°C

An increase in adsorption with temperature has been reported previously for phosphate onto gibbsite in dilute solutions (Muljadi et al., 1966b; van Riemsdijk & Lijklema, 1980b). The variation in adsorption with temperature at equilibrium is a reflection of the thermodynamics of the reaction. The rise in adsorption with temperature indicates that the specific adsorption reaction is endothermic. The smaller temperature dependence of phosphate adsorption indicates that the heat of the reaction is smaller than that of arsenate adsorption. The cause of the smaller temperature dependence is unknown. These results contrast with those reported in earlier studies (Muljadi et al., 1966b; van Riemsdijk and Lijklema, 1980b) where the temperature dependence was observed to be much greater. The complex nature phosphate sorption (see section 4.4) might be partly responsible as

the multiple stages of sorption could have different temperature dependencies. The shorter length of the earlier experiments may have prevented all stages of phosphate sorption from occuring.

4.4 Adsorption Kinetics

It is difficult to determine the effect of seawater on the kinetics of adsorption since the kinetics in freshwater have not been quantified. Only guideline ranges are available. Arsenic adsorption from seawater appears to reach equilibrium between 3 and 7 days and > 95% of adsorption occurs within 3 days (Figure 4.15); this is in the same range as the times reported in low ionic strength solutions (Anderson et al. 1976; Xu et al. 1988; Livesey & Huang. 1981). The experiments that ran to 28 days showed no significant change in adsorption density after 7 days.

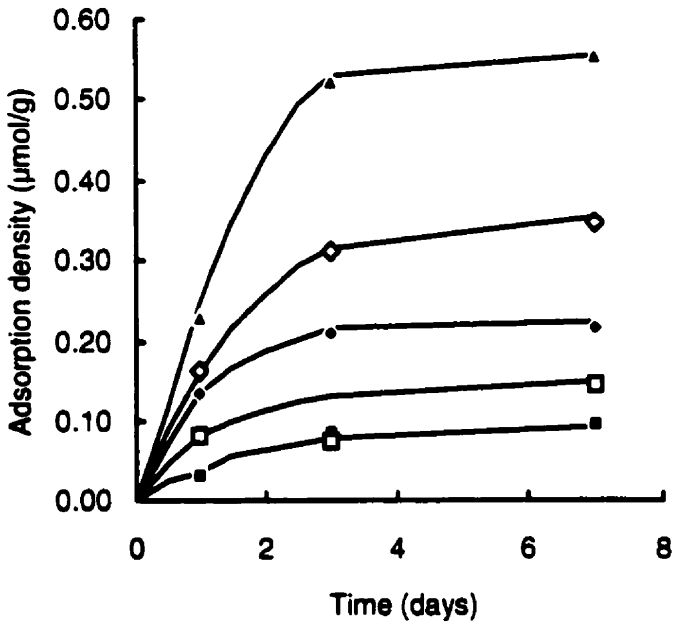

Figure 4.15 Kinetics of arsenate adsorption to gibbsite from seawater at 23°C and pH 7.5. ■ 1 µM ❑ 2 µM ◆ 5 µM ι □0 µM ▲ 20 µM.

As reported for experiments in low ionic strength solutions (Bache 1964; Helyar et al., 1976a; van Riemsdijk & Lijklema, 1980a), the kinetics of phosphate adsorption are of greater complexity. It is clear that steady state conditions were not achieved within 7

days (Figure 4.16). The two parts of the "sorption" process can not clearly be distinguished. It is possible that adsorption is complete by day 7 and the remaining "sorption" is co–precipitation. The 'co–precipitate' has never been identified in experimental work but previous studies on the adsorption kinetics of phosphate to gibbsite suggest its presence (Bache, 1964; van Riemsdijk & Lijklema (1980a). The precipitate has been proposed to be variscite ($Al(OH)_2H_2PO_4$) (Bache, 1964) and tarankite ($H_6K_3Al(PO_4)_8$) (van Riemsdijk & Lijklema, 1980a). van Riemsdijk & Lijklema (1980a) suggest that the formation of the co–precipitate is analogous to the formation of rust on a metal, slowing the precipitation reaction by acting as a physical barrier. The two stage "sorption" process is also supported by the need for rate equations with multiple constants (Kuo & Lotse, 1974).

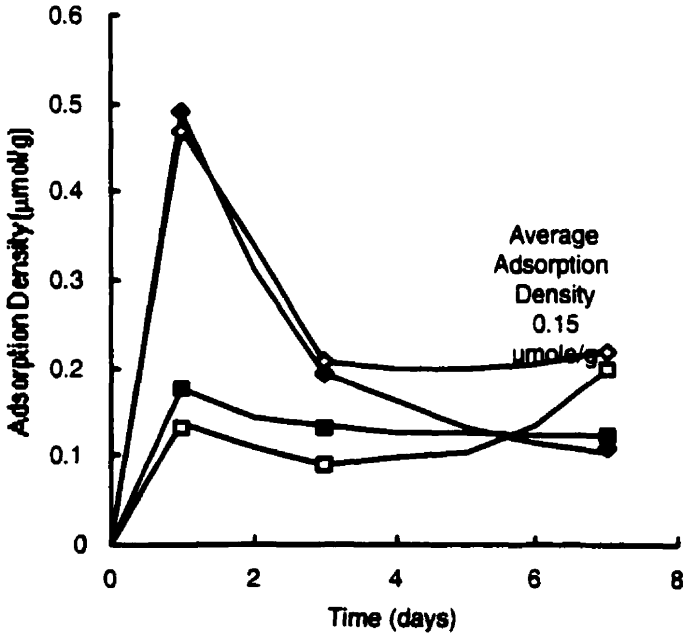

Figure 4.16 Kinetics of phosphate adsorption to gibbsite in seawater at 23°C and pH 7.5. □2 µM ■ 5 µM ▵ 10 µM ◆ 20 µM

Further complexity of phosphate kinetics is that the majority (around 70%) of the experiments show peak phosphate adsorption after one day. Figure 4.16 shows an experiment where all concentrations showed this behaviour. Phosphate was released back

to the solution at day 3. At day 7 there was no consistent behaviour; in some cases phosphate was partially removed whereas in others further desorption occurred. In the absence of other studies on phosphate adsorption from complex electrolyte solutions, one can only speculate about possible causes. There are two possible causes for this behaviour, competitive adsorption and removal mechanisms other than adsorption/desorption.

Competitive adsorption in this case may be a result of three separate factors: kinetics, abundance, and affinity. Desorption of phosphate has not been observed in other phosphate adsorption studies in dilute solutions. This suggests that the presence of the seawater ions may be responsible for desorption. The adsorption of the major seawater constituents might be slower that of phosphate. A combination of low adsorption affinity and high abundance of other seawater ions could result in desorption of phosphate. The ability of F^- and EDTA to desorb phosphate has been noted previously (Kuo & Lotse, 1974). The speed of the phosphate adsorption could be related to its affinity. Its subsequent desorption may be explained by the greater abundance but lower adsorption affinity and reaction kinetics of the major seawater anions. One would expect the electrostatic interaction between cations and the surface to be minimal since the surface of the gibbsite is positively charged up to its PZC of ~9–10.

Other removal processes could be responsible but they would have to be related to other interactions to the gibbsite surface. Biological activity is one possibility. Organisms such as bacteria attached on the surface could rapidly take up phosphate leading to a rapid population growth; this growth would be followed by a crash and a consequent release of phosphate upon the decay of the organisms. The source of organisms is unclear. It could be associated with the gibbsite but given the highly alkaline and high temperature conditions of gibbsite synthesis such a possibility is remote. Bacteria may have been introduced into the solution and in addition the experimental system was not sterile.

4.5 Solid:Solution Ratio

Variations of the solid:solution ratio have no effect on adsorption density for either phosphate or arsenate (Figure 4.17).

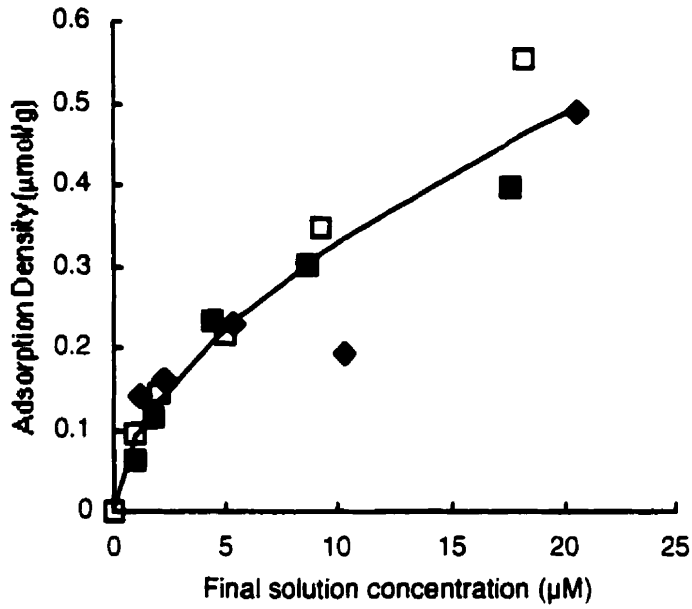

Figure 4.17 Adsorption of arsenate to gibbsite from artificial seawater at variable solid:solution ratios and pH (7.4–8.1) ◆1.25 g/L ❑ 2.5 g/l ■ 5 g/L.
Freundlich isotherm K_f=0.087 n=0.57 R^2=0.877

The solid:solution ratio does however affect the adsorption kinetics in a minor way. The reaction at higher solid:solution ratios is slower; this is probably due to a greater percentage of the solids being unexposed to the solution (due to intergrain contacts).

4.6 Aluminum Levels

The limited number of aluminum analyses that were performed showed very low levels of dissolved aluminum (Figure 4.18), well below those thermodynamically predicted for equilibrium of gibbsite in seawater (calculated from compilation of Stumm & Morgan, 1996). Given the slow dissolution of gibbsite reported elsewhere (Su & Harsh, 1994; Crane, 1998) it is likely that these levels reflect non–equilibrium conditions. It is unlikely that adsorption of arsenate, phosphate or other ions impeded dissolution since adsorption was minimal. The presence of fluoride is more likely to promote

dissolution by increasing solubility. The low levels of aluminum suggest that the dissolution of gibbsite was minimal and so can not be a cause of diminished adsorption.

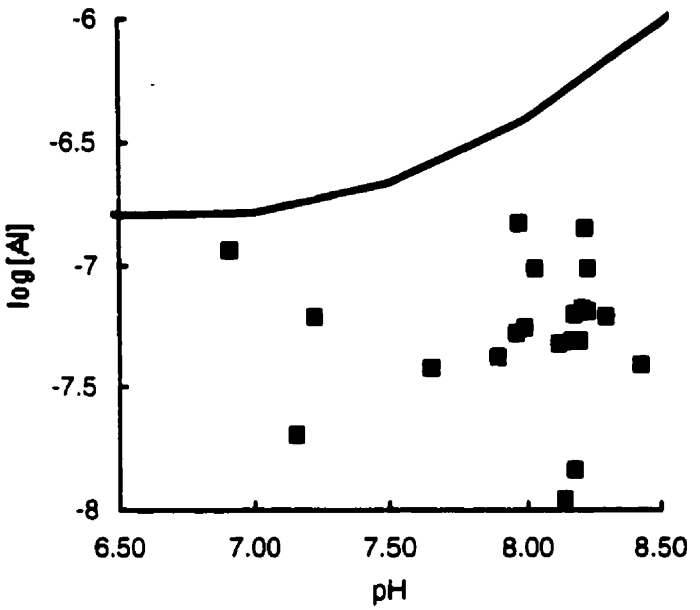

Figure 4.18 Measured dissolved aluminum in experimental artificial seawater solutions. The line represents equilibrium concentration in seawater with respect to gibbsite. Constants from compilation of Stumm & Morgan (1996)

4.7 Application of Results

4.7.1 Diminished Adsorption Density

It is clear that the presence of seawater salts diminishes the adsorption density of gibbsite for both arsenate and phosphate. The limited adsorption can not be attributed to experimental error since the non–random errors will tend to over–estimate adsorption rather than underestimate it. Contamination by arsenic or phosphate is unlikely given the precautions taken.

The exact cause of the diminished adsorption density has not been established. It is clear that fluorite will adsorb to gibbsite to some degree but the lack of precision of the ion selective electrode method precludes an accurate measure of adsorption. The addition of activated (finely divided) alumina is commonly used as a treatment method to remove fluoride from industrial waste waters (Choi & Chen, 1979a). The soil science literature

also abounds with evidence of the adsorption of fluoride to gibbsite (Farrah et al., 1987; Hingston et al., 1972; Hingston, 1981). Major ionic constituents of seawater (especially Na, Cl, and SO_4) may also compete for sites with arsenate or phosphate, although they most likely have a smaller affinity for the gibbsite surface. Their abundance could overwhelm the relatively small amounts of phosphate or arsenate (e.g. $[Cl^-]/[AsO_4] \cong 10^4$). The aqueous complexation and ion pairing of the adsorbates might also explain their limited adsorption from seawater. Phosphate is known to form ion pairs in seawater in great abundance. Calculations show that approximately 70% of HPO_4^{2-} in seawater is present as ion pairs, mostly with Ca^{2+} and Mg^{2+} (Milliero & Sohn, 1992). The ion pairing of arsenate is undocumented but most likely is of the same magnitude.

4.7.2 Adsorption to Gibbsite as a Vector to Sediments

The small amount of adsorption that occurs in seawater leads to the conclusion that adsorption to gibbsite is not a significant mechanism for the enrichment of phosphate and arsenate in Saguenay Fjord sediments. The maximum adsorption found in this study was 1.97 μmol/g at a concentration of ~50 μM As and pH 7.5. At concentrations (1 μM) closer to, but still two orders of magnitude greater than normal marine waters (~50 nM), adsorption is in the range of 0.10 – 0.40 μmol/g. The adsorption level at maximum arsenic concentration (17 nM) in the Fjord, calculated from the Freundlich isotherm for pH 7.5, is $6.5 * 10^{-4}$ μmol/g. The time needed for the enrichment to occur, if adsorption to gibbsite is the only enrichment process, can be calculated. It is necessary to take into account the diagenetic concentration process.

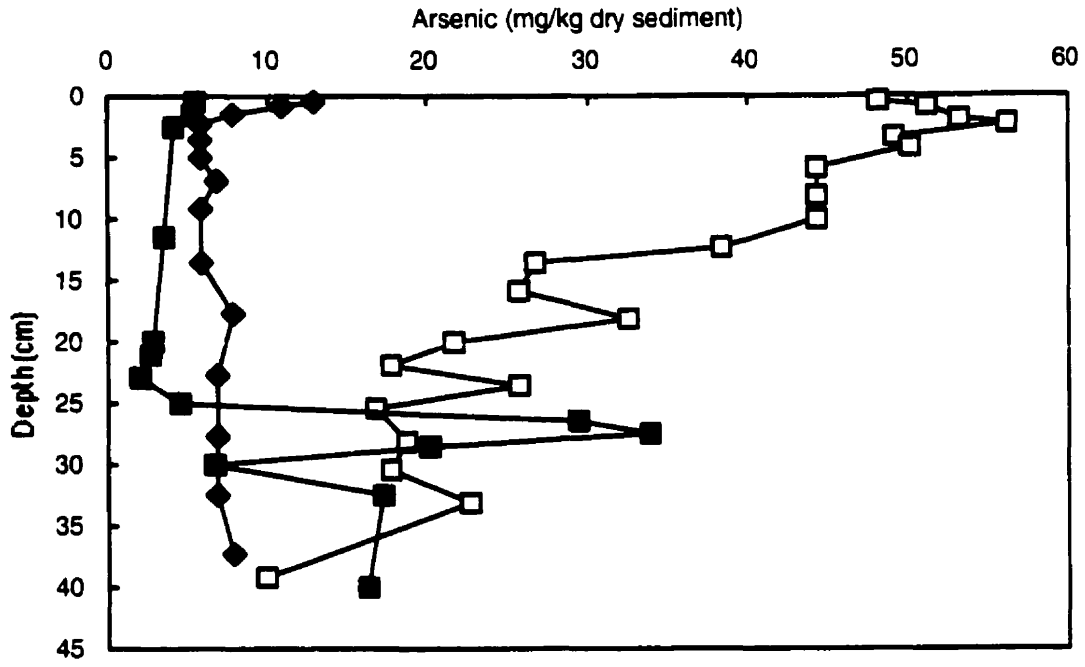

Figure 4.19 Sediment profiles of arsenic.
■ Baie des Ha! Ha! post flood (Mucci, unpublished data)◆ St. Lawrence Estuary (Gobeil, 1996) ❑ Saguenay Fjord 48° 21.2' N 70° 24.5' W (Upper Basin(Gobeil, 1996). Spike at 25 cm in Baie des Ha! Ha! is pre–flood originial sediment–water interface.

The processes of diagenesis lead to a concentration of arsenic near the sediment–water interface (Figure 4.19). A detailed explanation of the process is given elsewhere (Aggett & O'Brien, 1985). In summary, arsenate deposited in association with an adsorptive mineral phase may be reduced to arsenite upon burial in the anoxic zone of the sediments. Arsenite, having a smaller adsorption affinity then arsenate, would desorb and enter pore waters. As the arsenite and diffuses upward it could oxidize to arsenate. This reaction would be accelerated by the presence of maganese oxide. The arsenate may then readsorb to adsorbtive mineral phases.

The diagenetic enrichment process necessates an assumption of steady state deposition. That is to say the amount of arsenic buried is equal to the amount of arsenic reaching the sediment water interface. This assumption allows an input to be calculated by multiplying [As] at depth by the sedimentation rate. The average concentration of arsenic over the first 40 cm of sediments in the Interior basin of the Saguenay Fjord is

between 5 and 10 ppm (Figure 4.19). Given that arsenic is abundant in the crust of the earth, some amount of this arsenic is "natural. The arsenic is deposited by processes that act in all estuaries. Sediments in the St. Lawrence Estuary samples show average concentrations of 2 to 5 ppm over 40 cm. (Belzile, 1988, Gobeil, 1996; Richard, 1997). Coastal sediments of the Amazon shelf show similar concentrations (Sullivan & Aller, 1996). Arsenic levels in undifferentiated shales are reported to range between 6 and 18 ppm (Onish & Sandell, 1955). The midpoint of the estuarine sediment range (3.5 ppm) is probably a good approximation of the natural steady state level of arsenic in sediments. The exchangeable arsenic associated with suspended particulate matter in the Saguenay Fjord is much larger (28 ppm (Mucci et al. 1999)) then the arsenic at depth in the sediments. A degradation of the SPM at the sediment-water interface may be responsible for a release of exchangeable arsenic. As a result the exchangeable arsenic associated with SPM is not a good measure of arsenic input.

The average rate of sedimentation in the Saguenay Fjord is taken to be 0.3 cm/y (Perret et al. 1995; Mucci, pers. comm.) and the Alcan plant at Jonquière has been operating for ~75 years which means that about 22.5 cm of sediments have accumulated over this period. At a density of 1.375 $t \cdot m^{-3}$, the middle of the standard range for dry, mud-sized sediments, and approximating the area of the interior basin of the Fjord to 100 km^2 — an approximation made by Gobeil (1996) and sufficient for the purposes of this calculation— the amount of excess arsenic in the sediments of the Fjord is,

$$(7.5 - 3.5)\ ppm \times 1.375\ t \cdot m^{-3} \times 10^8\ m^2 \times 0.225\ m = 1.2 \times 10^2\ t \quad [4.9]$$

Using the calculated adsorption density reported above, the amount of gibbsite required to adsorb the excess arsenic can be calculated to be,

$$1.2 \times 10^2 t / 6.5 \times 10^{-4}\ \mu mol/g = 2.5 \times 10^9 t \quad [4.10]$$

The total load of all measured effluent aluminum, calculated from the highest recorded effluent levels (Groupe LGL, 1989; MOE, 1996), is 521 t/year. The exact nature of the

released aluminum is unknown but given the low solubility of aluminum compounds it is likely to be particulate. The aluminum effluent load has not been constant over time, nor have the plants been operated for the same lengths of time. The measured load does not include aluminum introduced to the Fjord from the loss of bauxite, gibbsite and alumina at the various storage and transport facilities of Alcan. The uncertainties associated with the effluent load require that the result of the calculation be treated as an order of magnitude. For the adsorption of arsenate to gibbsite to be the sole cause of the enrichment of the sediments, the time required would be

$$\frac{2.5 \times 10^{9}\ t}{521\ t \cdot y^{-1}} = 4.8 \times 10^{7}\ y \qquad [4.11]$$

As the oldest industrial plant has only been operating for 75 years, adsorption of arsenate to gibbsite could only be responsible for less than 0.0002% of the enrichment.

The nature of the particulate aluminum in the water column is not known so it may be that the phase can adsorb a greater quantity of arsenate. To be responsible for 1% of the enrichment within a reasonable time (75 years) the adsorption ability of the aluminum phase would have to be 4 orders of magnitude greater than that of gibbsite. The possibility can not be dismissed out of hand since adsorption of arsenate to amorphous aluminum hydroxide has been reported as high as 1600 μmol/g (at low pH and high solution concentration) in low ionic strength solution (Anderson & Malotky, 1979).

A similar calculation can be made for phosphate. The steady state concentration of phosphate in the sediments of the Fjord at the confluence of the Baie des Ha! Ha! and the North Arm is 300 ppm (Richard, 1997). The same author reports levels in the St. Lawrence estuarine sediments at 150 and 225 ppm. In the absence of other data, the midpoint of these two numbers is taken as the natural level. Using the same numbers as for the arsenic calculation (Sediment depth 0.225 m, area of Fjord 10^8 m^2, sediment density, 1.375 t/m^3), the excess phosphate is estimated at:

$$(300-188\ ppm)\ X\ 0.225\ m\ X\ 10^{6}\ m^{2}\ X\ 1.375\ t/m^{3} = 3.8\ X\ 10^{3}\ t \quad [4.12].$$

At a calculated adsorption density of $5.9\ X\ 10^{-2}\ \mu mol \bullet g^{-1}$ (SRP = 0.2 μM and pH 7.5) the quantity of gibbsite required would be;

$$\frac{3.8\ X\ 10^{3}\ t}{5.9\ X\ 10^{-2}\ \mu mol \bullet g^{-1}} = 2.1\ X\ 10^{6}\ t \quad [4.13]$$

At the same aluminum effluent load (521 t/y),

$$\frac{2.1\ X\ 10^{9}\ t}{521\ t \bullet y^{-1}} = 4.0\ X\ 10^{6} y \quad [4.14]$$

are required to supply this amount of gibbsite to the Fjord. Only 0.002% of the required gibbsite would have been supplied in 75 years. An alternative aluminum phase would require an adsorption density 3 orders of magnitude greater to account for 1% of the phosphate enrichment. As is the case for arsenate, such a possibility can not be immediately discounted. In both cases, it is likely that the competitive adsorption that affects gibbsite will affect any other aluminum phase. The increased adsorption density would require more than a simple multiplication of the specific surface area. Note that the above calculations were undertaken using adsorption densities calculated at 23°C. Actual water temperatures in the Fjord are much colder (bottom waters average 1°C). Thus the adsorption densities are overestimated and the results of the calculations are underestimates.

The residence time of particulate aluminum in the freshwater lens, calculated based on freshwater input, is on a scale of days (Fortin & Pelletier, 1995). Based on the renewal rate of the bottom waters (Gratton, 1995; Therriault & Lacroix, 1975), the residence time in the marine waters is certainly less than 1 year. Arsenic and phosphate that is adsorbed to gibbsite before it enters the marine waters would still be subject to the influence of the seawater as the gibbsite settles. The ions present in the seawater could cause the desorption of the arsenate and phosphate. Fluoride has been shown to cause desorption of phosphate (Kuo & Lotse, 1974)..

4.7.3 ALTERNATIVE VECTORS

Even if adsorption onto gibbsite or other aluminum solid phases is not responsible for the enrichment of the sediments, adsorption might still be responsible. It is commonly accepted that iron oxyhydroxides strongly adsorb arsenate and phosphate (Pierce & Moore, 1982; Bowell, 1994; Lucotte & d'Anglejan, 1988). Large particulate iron anomalies have been observed in the Fjord ($[Fe]_{tot}/[Fe]_{diss} > 1$) (Richard, 1997; A. Mucci pers. comm.). These may originate from the iron associated with the bauxite off loaded by Alcan at Port–Alfred (La Baie) or produced authigenically following mixing of freshwater with seawater (Sholkovitz, 1978). The effect of seawater on adsorption to goethite appears to be less than the effect on adsorption to gibbsite. Adsorption of phosphate to goethite from seawater at solid/solution ratios and adsorbate concentrations similar to those of this study is reported to be very efficient (>80 % adsorption) (Shaw, 1996). Preliminary work by Y. Gao (pers. comm.) shows similar behaviour for arsenate and only minor differences between adsorption affinity from seawater and from low ionic strength solutions.

Adsorption to manganese oxides also is a possibility. Adsorption of arsenic to manganese oxides is well documented (Oscarson et al., 1981a,b, 1983). Particulate manganese is found at elevated levels in the Saguenay Fjord: 1090 ppm in the freshwater lens and 3500 ppm in the marine waters (Cossa & Poulet, 1978). The high particulate manganese levels result from the precipitation of dissolved manganese or the coagulation of colloidal manganese oxides following estuarine mixing (Sholkovitz, 1978). The source of the dissolved manganese is a combination of both anthropogenic and natural sources. The most important anthropogenic sources are the pulp and paper mills and the Niobec mine (Group LOL, n.d.; MOE, 1996).

A further possibility is adsorption to organic substances. Thanabalasingam and Pickering (1986) have investigated arsenic sorption to humic acids and report arsenate and arsenite adsorption densities at pH 8 for initial arsenic concentrations of 5– 100 μM

to range from 80 to 120 μmol/g. They report that fluoride causes significant desorption of arsenic, but they do not suggest that fluoride is adsorbing. There are, however, a myriad of other organic compounds in the Saguenay Fjord both natural and anthropogenic that might serve as vectors of arsenic and phosphate to the sediments. Any such compounds must be particulate or be coagulated upon seawater mixing to serve as a vector. The total organic content of sediments in the Saguenay Fjord is 2-3% (Ouellet, 1979) and a peak of 14% was found in La Baie near the Stone-Consolidate Mill (Ouellet, 1979). Such measurements are in line with normal levels of organic content. In geochemical sampling associated with gold exploration, positive arsenic anomalies have been found to be associated with swamps (D. Walker, pers. comm.), an environment that is associated with high levels of dissolved organic compounds.

Potentially, any process that introduces deposits arsenic or phosphate to the sediments could be responsible for the enrichement. It may also be a combination of a number of processes. The enrichment would be the result of a greater amount of arsenic and phosphate being deposited than what is "normal" for an estuary. The unique conditions of the Saguenay Fjord must play a major role in the enrichemnt of the sediments.

Chapter 5 Conclusions

The objective of this research was to establish the importance of gibbsite as a potential vector for phosphate and arsenate to the sediments of the Saguenay Fjord. The objective was achieved by conducting laboratory batch adsorption experiments of arsenate and phosphate to gibbsite from seawater under conditions that simulated the natural environment. The influences of temperature and solid:solution ratios were examined. The kinetics of the reactions were also established. The conclusions that can be drawn are summarized below.

Phosphate adsorption to gibbsite from seawater was slightly greater than arsenate. This observation is consistent with results of studies carried out in low ionic strength solutions (Manning & Goldberg, 1996; Okazaki et al., 1989; Hingston et al., 1971). Arsenate adsorption at the low concentrations used in this study can be modeled adequately by a Freundlich isotherm. Phosphate adsorption data also fit a Freundlich isotherm but parameters carry larger uncertainties. Adsorption densities decline with increasing pH for both phosphate and arsenate. The adsorption of both arsenate and phosphate are significantly diminished in seawater compared to freshwater. The limited adsorption in seawater is believed to be largely a result of competition with major seawater ionic constituents, especially fluoride, for surface sites. Fluoride adsorption was inadequately characterized in this study to form a definite conclusion although it appears that fluoride behaviour in seawater is similar to what is observed in dilute solutions (Hingston, 1981). Nevertheless, the aqueous complexation of arsenate and phosphate can not be discounted as a cause of diminished adsorption.

Seawater has no distinguishable influence on the kinetics of the arsenate adsorption reaction. Adsorption equilibrium for arsenic was reached within times (i.e. 3–7 days) similar to those reported in low ionic strength solutions. Phosphate showed kinetic behaviour that can not be explained by a simple mechanism and is possibly the result of an interaction of the different adsorption kinetics of competing ions.

Both arsenate and phosphate adsorption densities decreased with decreasing temperature. The influence of temperature on phosphate adsorption was less than that of arsenate. The temperature relationship is consistent with what has been observed in low ionic strength solutions (Muljadi, 1966b; van Riemsdijk & Lijklema, 1980b). No solid/solution ratio effects were detected other than an artifact which could be ascribed to increased intergrain contacts at higher ratios.

Dissolved aluminum concentrations were below thermodynamically predicted levels for seawater in equilibrium with gibbsite. The low levels reflect the slow rate of gibbsite dissolution, as observed in other studies (Su & Harsh, 1994; Crane, 1998). The low levels of arsenate and phosphate adsorption suggest that adsorption did not hinder dissolution.

The adsorption densities of arsenate and phosphate onto gibbsite from seawater are small at natural concentrations. The Freundlich distribution coefficient for arsenate in artificial seawater was 3.83×10^{-2}. In Nanopure™ water, the data was fitted to a Langmuir isotherm. The value of the Langmuir coefficient was 4.36. A direct numerical comparison is not possible, but graphically the difference is striking. The adsorption density in seawater is from 2 to 0.5 orders of magnitude less than in the Nanopure™ water. Settling of gibbsite through the water column cannot be a significant vector of arsenate and phosphate to the Saguenay Fjord sediments and thus cannot explain their enrichment in this environment. Vector phases would need to have adsorption densities at least 1000 times greater than gibbsite to be of any significance to the enrichment for phosphate or arsenate. This assessment was based on conditions that are at the extreme ranges of conditions in the Saguenay Fjord and would tend to exaggerate adsorption. Actual adsorption in the Fjord would likely be much less. Potential vector phases could be detrital or authigenic iron oxides which are present in the Fjord.

5.1 Suggestions for Future Work

Although the very low level of adsorption is clear, a tighter set of data might be desirable. Some changes in the experimental methods might help. Direct measurements of adsorption using radiolabeled adsorbents (i.e. ^{74}As) as in the work of Xu et al. (1988, 1990) would eliminate a data reduction step and its consequent error. Accuracy of arsenic measurements might be improved by the use of an analytical method that covers the concentration range without a dilution step. The adsorption of phosphate could be determined with greater precision and accuracy by changes in experimental and analytical methods. Interpretation of phosphate adsorption data would be improved by a complete sterilization of all components. This would eliminate the potential role of bacterial uptake. Analyzing for total phosphorus (not just soluble reactive phosphate) may also be desirable, as it would give a more refined estimate of phosphate sorption. The conversion of phosphate to organic phosphorus could be evaluated. In the case of fluoride analysis, it is clear that the ion selective electrode method is inadequate for adsorption studies and an alternate method such as ion chromatography should be used. The influence of fluoride could also be determined by running experiments in fluoride–free seawater.

The full development of a surface complexation model is unwarranted in this study given the insignificance of gibbsite as a potential vector of contaminants to the Saguenay Fjord sediments. However if it were to be developed it would require an extensive experimental program to determine a) adsorption of all major seawater ions to gibbsite in a indifferent electrolyte at the ionic strength of seawater and b) the quantification of interactions of arsenate and phosphate with seawater ions. It would also be necessary to strictly control pH with indifferent seawater buffers.

Identification of the nature and quantities of aluminum phases in the water column of the Saguenay Fjord would allow for more conclusive statements on the role of particulate aluminum. The levels of particulate aluminum have likely been highly variable with time due to a considerable anthropogenic influence. In the absence of

historical data, it is unlikely that an accurate reconstruction of the release of aluminum phases to the Fjord can be made. The Saguenay Flood of 1996 eroded more than 6 x 10^6 metric tonnes of post–glacial sediments that were redeposited in the Baie des Ha! Ha! and the North Arm of the Fjord burying the indigenous contaminated sediments under 30–50 m of "clean" silty clays. It will now be possible to monitor the levels of dissolved and associated arsenic in both the water column and the sediments of the Saguenay Fjord with time. This knowledge combined with a more extensive characterization of the composition of the waters of the Saguenay Fjord could lead to the identification of the exact mechanism of enrichment. It will also be possible to determine if the mechanism is still operating.

References

Abdullah, M.I., Shiyu, Z. & Mosgren, K. (1995)
Arsenic and selenium species in the oxic and anoxic waters of the Oslofjord, Norway. *Marine Poll. Bull.* **31**, 116-126.

Aggett, J. & Aspell, A.C. (1976)
The determination of arsenic (III) and total arsenic by atomic adsorption spectroscopy. *Analyst.* **101**, 341-347.

Aggett, J. & O'Brien, J.A. (1985)
Detailed model for the mobility of aresnic in lacustrine sediments based on meaurements in Lake Ohakuri. *Environ. Sci. Technol.* **19**, 231-238.

Albert, W.B. (1932)
Arsenic toxicity in soils. *South Carolina Agriculture Experimental Station 45th Annual Report*. 44-46.

Alcan (1990)
Metallurgy of Aluminum. Publication 16M/XI-73-Rev 20M/V-79 40M/II-81-Rev 30M/XI-90. Alcan Public Relations Group: Montreal.

Alpay, S., Mucci, A. & Hillaire-Marcel, C. (1998)
Particulate and colloidal+dissolved species within a well-stratified extuarine environment: Preliminary results. Contributed oral presentation. AGU/ASLO Ocean Sciences Meeting, Februray 9-13, San Diego, California.

Alvarez, R., Fadley, C.S., Silva, J.A. & Uehara, G. (1976)
A study of silicate adsorption on gibbsite ($Al(OH)_3$) by X-ray photoelectron spectroscopy. *Soil Sci. Soc. Am. J.* **40**, 615-617.

Anderson, M.A., Ferguson, J.F. & Gavis, J. (1976)
Arsenate adsorption on amorphous aluminum hydroxide. *J. Colloid Interface Sci.* **54**, 391-399.

Anderson, M.A. & Malotky, D.T. (1979)
The adsorption of protolyzable anions on hydrous oxides at the isoelectric pH. *J. Colloid Interface Sci.* **72**, 413-427.

Andreae, M.O. (1978)
Distribution and speciation of arsenic in natural waters and some marine algae. *Deep Sea Res.* **25**, 391-402.

Bache, B.W. (1964)
Aluminum and iron phopshate studies relating to soils II Reactions between phosphate and hydrous oxides. *J. Soil Sci.* **15**, 110-116.

Balistrieri, L.S. & Murray, J.W. (1982)
The adsorption of Cu, Pb, Zn, and Cd on goethite from major ion seawater. *Geochim. Cosmochim. Acta.* **46**, 1253-1265

Belzile, N. (1988)
The fate of arsenic in sediments of the Laurentian Trough. *Geochim. Cosmochim. Acta.* **52**, 2293-2302.

Belzile, N. & Lebel, J. (1986)
Capture of arsenic by pyrite in near-shore matine sediment. *Chem. Geol.* **54**, 279-281.

Belzile, N. & Tessier, A (1990)
Interactions between arsenic and iron oxyhydroxides in lacustrine sediments. . *Geochim. Cosmochim. Acta.* **54**, 103-109.

Beyrouty, C.A., van Scoyoc, G.E. & Feldkamp, J.R. (1984)
Evidence supporting specific adsorption of boron on synthetic aluminum hydroxides. *Soil Sci. Soc. Am. J.* **48**, 284-287.

Bolan, N.S., Barrow, N.J. & Posner, A.M. (1985)
Describing the effect of time on sorption of phosphate by iron and aluminum hydroxides. *J. Soil Sci.* **36**, 187-197.

Bousse, L. & Meindel, J.D. (1986)
The importance of Ψ_o/pH characteristics in the theory of the oxide electrolyte interface. in Davis, J.A.; Hayes, K.F (eds.) *Geochemical Processes at Mineral Surfaces* . ACS Symposium Series 323. American Chemical Society: Washington DC 79-98.

Bowden, J.W., Posner, A.M. & Quirk, J.P. (1977)
Ionic Adsorption on Variable Charge Mineral Surfaces. Theoretical-Charge Development and Titration Curves. *Austral. J. Soil Res.* **15**, 121-136.

Bowell, R.J. (1994)
Sorption of arsenic by iron oxides and oxyhydroxides in soils. *App. Geochem.* **9**, 279-286.

Boyle, R.W. & Jonasson, I.R. (1973)
The geochemistry of arsenic and its use as an indicator element in geochemical prospecting. *J. Geochem. Exploration.* **2**, 251-296.

Brown, G.E. (1990)
Spectroscopic studies of chemisorption reaction mechanisms at oxide-water interfaces. **in** Hochella, M.F.; White, A.F. (eds) *Mineral-Water Interface Geochemistry* Reviews. in Mineralorgy 23. Mineralogical Society of America: Washington DC. 310-363.

Bruland, K.W. (1983)
Trace elements in seawater. **In** Riley, J.P. and Chester R. (eds.) *Chemical Ocenaography volume 8.* Academic Press: Toronto 157-220.

Chen, Y. R., Butler, J.N. & Stumm, W. (1972)
Adsorption of phosphate on alumina and kaolinite from dilute aqueous solutions. *J. Colloid Interface Sci.* **43**, 421-436.

Cherry, J.A., Shaikh, A.U., Tallman, D.E. & Nicholson, R.V. (1979)
Arsenic species as an indicator of redox condtions in groundwater. *J. Hydro.* **43**, 373-392.

Choi, W.W. & Chen, K.Y. (1979a)
The removal of fluoride from waters by adsorption. *J. Am. Water Works Assoc.* **71**, 562-570.

Choi, W.W. & Chen K.Y. (1979b)
Evaluation of boron removal by adsorption on solids. *Environ. Sci. Technol.* **13**, 189-196.

Chukhlantsev, V.G. (1956)
Russ. J. Inorganic Chem. **1**, 1975. cited in Crecilius et al., 1986.

CMJ [Canadian Mining Journal] (1998)
Alcan gives go-ahead for Alma smelter. *Can. Mining J.*, 31-33.

Cooper, H.P., Paden, W.R., Hall, E.E., Albert, W.B., Rogers, W.B. & Riley, J.A. (1932)
Soils differ markedly in their response to additions of calcium arsenate. *South Carolina Agriculture Experimental Station 45th Annual Report* . 23-27.

Cossa, D & Poulet, S.A. (1978)
Survey of trace metal contents of suspended matter in the St. Lawrence Estuary and Saguenay Fjord. *J. Fish. Res. Board. Can.* **35**, 338-345.

Crane, G. (1998)
The stability of gibbsite in seawater. Unpublished B.Sc. Thesis McGill University .

Crecelius, E.A. (1975)
The geochemical cycle of arsenic in Lake Washington and its relation to other elements. *Limn. Oceanogr.* **20**, 441-450.

Crecelius, E.A., Bloom, N.S., Cowan, C.E. & Jenne, E.A. (1986)
Speciation of Selenium and Arsenic in Natural Waters and Sediments Volume 2: Arsenic Speciation.. Electrical Power Research Institute Report EA-4641. Electrical Power Research Institute: Palo Alto, California.

Cullen, W.R. & Reimer, K.J. (1989)
Arsenic speciation in the environment. *Chem. Rev.* **89**, 713-764

Cundiff, W.H., Shaffer, J.W., McLaughlin, A.E., Breur, R.G., Barham, W.L., Mulloy, J.W., Bellan, P., Hampton, G.B., Elston, W.D., Murphy, J.F. & Todd, J.B. (1985)
Alumina **in** Weiss, L. (ed.) *SME Mineral Processing Handbook Volume 2.* SME/AIMMPE New York. 19-1 - 19-20.

Davis, J.A. & Kent, D.B. (1990)
Surface complexation modeling in aqueous geochemistry **in** Hochella, M.F.; White, A.F. (eds). *Mineral Water Interface Geochemistry* Reviews in Mineralogy 23. Mineralogical Society of America: Washington DC. 178-260.

De Vitre, R., Belzile, N., & Tessier, A. (1991)
Speciation and adsorption of arsenic on diagenetic iron oxyhydroxides. *Limnol. Oceanogr.* **36**, 1480-1485.

Dickson, A.G. (1992)
pH buffers for seawater media based on the total hydrogen ion concentration scale. *Deep Sea Res.* **40**, 107-118.
Dickson, A.G. & Riley, J.P. (1979a)
The estimation of acid dissociation constants in seawater from potentiometric titrations with strong base I The ionic product of water. *Mar. Chem.* **7**, 89-99.
Dickson, A.G. & Riley, J.P. (1979b)
The estimation of acid dissociation constants in seawater from potentiometric titrations with strong base II The dissociation of phosphoric acid. *Mar. Chem.* **7**, 101-109.
Dougan, W.K. & Wilson, A.L. (1974)
The absorptiometric determination of aluminum in water. A comparison of some chromogenic reagents and the developement of an improved method. *Analyst.* **99**, 413-430.
Drainville, G. (1968)
La Fjord du Saguenay I Contribution à l'océanographie. *Naturaliste Canadien.* **95**, 809-855.
Drever, J.I. (1988)
The Geochemistry of Natural Waters. Prentice Hall: Englewood Cliffs. 437 p.
Duchesneau, G. & Riverin, M. (1976)
Etude de la Qualité des effluents du complexe industriel de l'Alcan Ltée, Jonquière, Arvida. Services de protection de l'environnement. Québec, Canada.
Farmer, J.G. & Lovell, M.A. (1986)
Natural enrichment of arsenic in Loch Lomond sediments. *Geochim. Cosmochim. Acta.* **50**, 2059-2067.
Farrah, H., Slavek, J. & Pickering, W.F. (1987)
Fluoride interactions with hydrous alumium oxides and alumina. *Austral. J. Soil Res.* **25**, 55-69.
Fisher Scientific (1990)
Instructions Fluoride Selective Electrode.
Fortin, G.R. & Pelletier, M. (1995)
Synthèse des connaissances sur les aspects physiques et chimiques de l'eau et des sédiments du Saguenay Zonex d'intervention prioritaire 22 et 23.. Enviornment Canada Region du Québec.
Fournier, A. (1994)
LREE mineralization of the St. Honore Carbonatite. M.Sc. Thesis McGill University . .
Frant, M.S. & Ross, J.W. (1966)
Electrode for sensing fluoride ion activity in solution. *Science.* **154**, 1553-1555.
Frant, M.S. & Ross, J.W. (1968)
Use of a total ionic strength adjustment buffer for electrode determination of fluoride in water supplies. *Anal. Chem.* **40**, 1169-1171.
Gagnon, C., Mucci, A. & Pelletier, E. (1995)
Anomalous accumulations of acid volatile sulphides in a coastal marine sediment, Saguenay Fjord Canada. *Geochim. Cosmochim. Acta.* **59**, 2663-2677.
Gendron, L., Biss, R. & Rodrigue, M. (1983)
Underground mining and pyrochlore processing at Niobec Mine, Quebec, Canada. **In** Stuart, H. (ed)*Niobium: Proceedings of The International Symposium* . Metallurgical Society of AIME, New York. 79-97.
Giles, P.L. (1936)
The effect of different colloidal soil materials on the toxicity of calcium arsenate upon the productivity of several important soils of the cotton belt. *J. Agricult. Res.* **52**, 477-491.
Gobeil, C. (1996)
L'arsenic dans les sédiments du Fjord du Saguenay. *Profils Saguenay.* **2:1**, 1-2.
Goldberg, S. (1986a)
Chemical modelling of arsenate adsorption on aluminum and iron oxide minerals. *Soil Sci. Soc. Am. J.* **50**, 1154-1157.
Goldberg, S. (1986b)
Chemical modelling of specific anion adsorption on oxides, clay minerals and soils **in** . *ENVIROSOFT 86.* CML Publications: Ashurs, Southamption, UK. 671.
Goldberg, S., Davis, J.A. & Hem, J.D. (1996)
The surface chemistry of aluminum oxides and hydroxides. **in** Sposito, G. (ed) *The Environmental Chemistry of Aluminum 2nd ed.* CRC Press: Boca Raton. 271-331.

Goldberg, S., Forster, H.S. & Heick, E.L. (1993a)
Temperature effects on boron adsorption by reference materials and soils. *Soil Sci.* **156**, 316-321.
Goldberg, S., Foster, H.S. & Heick, E.L. (1993b)
Boron adsorption mechanisms on oxides, clay minerals, and soils inferred from ionic strength effects. *Soil Sci. Soc. Am. J.* **57**, 704.
Goldberg, S. & Glaubig, R.A. (1988)
Anion sorption on a calcareous, montmorillonitic soil; arsenic. *Soil Sci. Soc. Am. J.* **52**, 1297-1300.
Goldberg, S. & Sposito, G. (1984)
A chemical model of phosphate adsorption by soils. I. Reference oxide minerals. *Soil Sci. Soc. Am. J.* **48**, 772-778.
Grahame, D.C. (1947)
The electrical double layer and the theory of electrocapillarity. *Chem. Rev.* **41**, 441-501.
Gratton, Y. (1995)
Échanges entre le Saguenay et l'Estuaire du Saint-Laurent. *Profil Saguenay.* 1:2, 2-3.
Groupe LGL [Le Groupe LGL] (n.d.)
Unpublished comsultants report.
Guay, G. & Couillard, M. (1980)
Contamination de l'environment par l'usine de chlore-alcali Alcan Arvida. Bureau d'Etude Sur Les Substances Toixiques Report 7; Environnement Québec.
Hao, O.J. & Huang, C.P. (1986)
Adsorption characterstics of fluoride onto hydrous alumina. *J. Environ. Engineer.* **112**, 1054-1069.
Harris, S. (1996)
Adsorption of arsenic and phosphate on oxic sediments of the Saguenay Fjord. Unpublished B.Sc. Thesis McGill University .
Hannson, I. (1973)
A new set of pH-scales and standard buffers for seawater. *Deep Sea Res.* **20**, 479-491.
Hayes, K.F., Papelis, C., & Leckie, J.O. (1988)
Modelling ionic strength effects on anion adsorption at hydrous oxide/solution interfaces. *J. Colloid Interface Sci.* **23**, 187-191.
Helyar, K.R., Munns, D.N. & Burau, R.G. (1976a)
Adsorption of phosphate by gibbsite. I. Effects of neutral chloride salts of calcium, magnesium, sodium, and potassium. *J. Soil Sci.* **27**, 307-314.
Helyar, K.R., Munns, D.N. & Burau, R.G. (1976b)
Adsorption of phosphate by gibbsite II Formation of a surface complex involving divalent cations. *J. Soil Sci.* **27**, 315-323.
Herbelin, A.L. & Westall, J.C. (1994)
FITEQL: A Computer program for the determination of chemical equilibrium constants from experimental data.. Oregon State University Report 94-01. Oregon State University: Corvallis Oregon.
Hingston, F.J. (1981)
A review of anion adsorption. **in** Anderson, M.A.; Rubin, A.J (eds) *Adsorption of inorganics at solid-liquid interfaces* . Ann Arbor Science: Ann Arbor, Michigan. 51-90.
Hingston, F.J., Posner, A.M. & Quirk, J.P. (1971)
Competitive adsorption of negatively charged ligands on oxide surfaces. *Disc. Faraday Soc.* **52**, 334-342.
Hingston, F.J., Posner, A.M. & Quirk, J.P. (1972)
Anion adsorption by goethite and gibbsite. I. The role of the proton in determining adsorption envelopes. *J. Soil Sci.*. **23**, 177-192.
Hohl, H. & Stumm, W. (1976)
Interaction of Pb^{2+} with hydrous α-Al_2O_3. *J. Colloid Interface Sci.* **55**, 281-288.
Honeyman, B.D. & Leckie, J.O. (1986)
Mascroscopic partitioning coefficients for metal ion adsorption: Proton stochiometry at variable pH and adsorption density.**in** Davis, J.A.; Hayes, K.F. (eds) *Geochemical Processes at Mineral Surfaces* . ACS Symposium Series 323, Am. Chem. Soc.: Washington DC 162-190.

Huang, C.P. (1975)
Adsorption of phosphate at the hydrous γ-Al_2O_3-electrolyte interface. *J. Colloid Interface Sci.* **53**, 178-186.

Huang, C.P. & Stumm, W. (1973)
Specific adsorption of cations on hydrous α-Al_2O_3. *J. Colloid Interface Sci.* **22**, 231-259.

James, R.O. & Parks, G.A. (1982)
Characterization of aqueous colloids by their electrical double layer and intrinsic surface chemical properties. *Surface Colloidal Sci.* **12**, 119-216.

Jennane, A. (1992)
Application de la méthode du Plomb-210 dans l'Esuaire et le Golfe du St-Laurent. Taux de sédimentation, flux et modes d'ablation. Unpublished Master's Thesis, Université du Québec à Montréal. 126 p.

Kauranen, P. (1977)
The use of buffers in the determination of fluoride by an ion-selective electrode at low concentrations and in the presence of aluminum. *Anal. Lett.* **10**, 451-465.

Kavanagh, B.V., Posner, A.M. & Quirk, J.P. (1975)
Effects of polymer adsorption on the properties of the electrical double layer. *Faraday Disc. Chem. Soc.* **59**, 242-249.

Kester, D.R., Duedall, I.W., Connor, D.N. & Pytkowicz, R.M. (1967)
Preparation of artifical seawater. *Limnol Oceanogr.* **12**, 176-179.

Kester, D.R. & Pytkowicz, R.M. (1967)
Determination of the apparent dissociation constants of phosphoric acid in seawater. *Limnol. Oceanogr.* **12**, 243-252.

Kinniburgh, D.G. (1986)
General purpose adsorption isotherms. *Environ .Sci. Technol.* **20**, 895-904.

Koritnig, S. (1978)
15-I Phosphorous abudance in natural waters and in the atmosphere.**in** Wedepahl, K.H. (ed) *Handbook of Geochemistry Vol II-2* . Springer-Verlag: New York. p. 15-I-1 – 15-I-12.

Koroleff, F. (1976)
Determination of phosphorus. **in** Grasshoff, K (ed) *Methods of Seawater Analysis*. Verlag Chemie: New York. 117-126.

Krauskopf, K.B. (1979)
Introduction to Geochemistry, 2nd ed. McGraw-Hill: Toronto. 617 p.

Kuo, S. & Lotse, E.G. (1974)
Kinetics of phosphate adsorption and desorption by hematite and gibbsite. *Soil Sci.* **116**, 400-406.

Kyle, J.H., Posner, A.M. & Quirk, J.P. (1975)
Kinetics of isotopic echange of phosphate adsorped on gibbsite. *J. Soil Sci.* **26**, 32-43.

Lantzy, R.J. & Mackenzie, F.T. (1994)
Tentative model of global oceanic cycling behaviour of arsenic **in** Hutchinson, T.C.; Gordon, C.A.; Meema, K.M. (eds.)*Global Perspectives on Lead, Mercury and Cadmium Cycling in the Environment*.. Wiley-Interscience: New York. 95-114.

Lijklema, L. (1980)
Interaction of orthophosphate with iron (III) and aluminum hydroxides. *Environ. Sci. Technol.* **14**, 537-541.

Livesey, N.T. & Huang, P.M. (1981)
Adsorption of arsenate by soils and it relation to selected chemical properties and anions. *Soil Sci.* **131**, 88-94.

Lowenthal, D.H., Pilson, M.E.Q. & Byrne, R.H. (1977)
The determination of the apparent dissociation constants of arsenic acid in seawater. *J. Marine Res.* **35**, 653-669.

Lucotte, M. & d'Anglejan, B. (1988)
Processes controlling phosphate adsorption by iron hydroxides in estuaries. *Chem.Geol.* **67**, 75-83.

Maher, W.A. (1985)
Mode of occurrence and speciation of arsenic in some pelagic and estuarine sdeiments. *Chem. Geol.* **47**, 333-345.

Manning, B.A. & Goldberg, S. (1996)
Modelling competitive adsorption of arsenate with phosphate and molybdate on oxide minerals. *Soil Sci. Soc. Am. J.* **60**, 121-131.
Manning, B.A. & Goldberg, S. (1997)
Adsorption and stability of arsenic(III) at the clay mineral water interface. *Environ Sci. Technol.* **31**, 2005-2011.
Massee, R., Maessen, F.J. & De Goeij, J.J.M. (1981)
Losses of silver, arsenic, cadmium, selenium and zinc traces from distilled water and artifical seawater on various container surfaces. *Anal. Chim. Acta.* **127**, 181-193.
McLaughlin, J.R., Ryden, J.C. & Syers, J.K. (1981)
Sorption of inorganic phosphate by iron- and aluminum-containing components. *J. Soil Sci.* **32**. 365-377.
Millero, F.J. & Sohn, M. (1992)
Chemical Oceanography. CRC Press: Boca Raton. 531 p.
Millero, F.J. & Schreiber, D.R. (1982)
Use of the ion pairing model to estimate activity coefficients of the ionic components of natural waters. *Amer. J. Sci.* **282**, 1508-1540.
MOE [Environment Canada] (1996)
Fact sheet. numbers 43-50,77. Catalog number En153-6/##-1996E. Minister of Supply and Services Canada.
Morse, J.W., Hunt. M., Zullig, J., Mucci, A. & Mendez, T. (1982)
A comparison of techniques for preserving dissolved nutrients in open ocean seawater samples. *Ocean Sci. Engineer.* **7**, 75-106.
Morse, J.W. (1994)
Interactions of trace metals with authigenic sulfide minerals: implications for their bioavailability. *Marine Chem.* **46**, 1-6.
Mucci, A. & Edenborn, H.M. (1992)
Influence of an organic-poor landside deposit on the early diagenesis of iron and maganese in a coastal marine sediment. *Geochim. Cosmochim. Acta.* **56**, 3909-3921.
Mucci, A., Richard, L.F. & Lucotte, M. (1999)
The differential geochemical behaviour of arsenic and phosphorus in the water column and sediments of the Saguenay Fjord Estuary. *Mar. Chem* (submitted)
Muljadi, D., Posner, A.M. & Quirk, J.P. (1966a)
The mechanism of phosphate adsorption by kaolinite, gibbsite and pseudoboehmite. I. The isotherms and the effect of pH on adsorption. *J. Soil Sci.* **17**, 212-229.
Muljadi, D., Posner, A.M. & Quirk, J.P. (1966b)
The mechanism of phosphate adsorption by kaolinite, gibbsite, and pseudoboehmite. III. The effect of temperature on adsorption. *J. Soil Sci.* **17**, 238-247.
Murphy, J. & Riley, L. (1956)
The storage of seawater samples for the determination of dissolved inorganic phosphate. *Anal. Chim. Acta.* **14**, 318-319.
NRCC [National Research Council of Canada Associate Committee On Scientific Criteria For Environmental Quality] (1978)
Effects of arsenic in the Canadian environment. National Research Council Canada Publication 15391. National Research Council of Canada: Ottawa. 349 p.
Okazaki, M., Takamidoh, K. & Yamane, I. (1986)
Adsorption of heavy metal cations on hydrated oxides and oxides of iron and aluminum with different crystallinities. *Soil Sci. Plant Nutrit.*. **32**, 523-533.
Okazaki, M., Sakaidani, K., Saigusa, T. & Sakaida, N. (1989)
Ligand exchange of oxyanions on synthetic hydrated oxides of iron and aluminum. *Soil Sci. Plant Nutrit.* **35**, 337-346.
Onish, H. 1969
33-I. Arsenic abundance in natural waters. in Wedepahl, K.H. ed *Handbook of Geochemistry Vol II-2* . Spring-Verlag: New York 33-I-1 -33-I-16.
Onish, H. & Sandell, E.B. (1955)
Geochemistry of arsenic. *Geochim. Cosmochim. Acta.* **7**, 1-7.

Oscarson, D.W., Huang, P.M., Defosse, C. & Herbillion, A. (1981a)
Oxidative power of Mn(IV) and Fe (III) oxides with respect to As(III) in terrestrial and aquatic environments. *Nature* . **291**, 50-51.

Oscarson, D.W., Huang, P.M. & Liaw, W.K. (1981b)
Role of manganese in the oxidization of arsenite by freshwater lake sediments. *Clay Clay Min.* **29**, 219-225.

Oscarson, D.W., Huang, P.M., Liaw, W.K. & Hammer, U.T. (1983)
Kinetics of oxidization of arsenite by various manganese dioxides. *Soil Sci. Am. J.* **47**, 644-648.

Ouellet, M. (1979)
Geochimie et granulométrie des sédiments superficiels du lac Saint-Jean et de la rivière Saguenay. INRS-Eau -Ministère de l'Environnement du Québec.

Palache, C., Berman, H. & Frondel, C. (1944)
The System of Mineralogy, 7th Edition, Volume 1. Wiley: New York.

Parfitt, R.L., Fraser, A.R., Russell, J.D. & Farmer, V.C. (1977)
Adsorption of hydrous oxides. II. Oxalate, benzoate, and phosphate on gibbsite. *J. Soil Sci.* **26**, 40-47.

Peinemann, N. & Helmy, A.K. (1977)
Sorption of phosphate by hydrous oxides of aluminum and iron. *J. Electroanal. Chem.* **78**, 325-330.

Peterson, M.L. & Carpenter, R. (1986)
Arsenic distributions in porewaters and sediments of Puget Sound, Lake Washington, the Washington coast and Saanich Inlet, B.C. *Geochim Cosmochim Acta.* **50**, 353-369.

Pickering, W.F. (1986)
The effect of hydrolysed aluminum species in fluoride ion determinations. *Talanta.* **33**, 661-664.

Pierce, M.L & Moore, C.B. (1982)
Adsorption of arsenite and arsenate on amorphous iron hydroxide. *Water Res.* **16**, 1247-1253.

Perret, D., Locat, J & Leroueil, S. (1995)
Strength development with burial in fine grained sediments from the Saguenay Fjord, Quebec. *Can. Geotech. J.* **32**, 247-262.

Planas, D. & Healy, F.P. (1978)
Effects of arsenate on growth and phosphorus metabolism of phytoplankton. *J. Phycol.* **14**, 337-341.

Primeau, S. & Goulet, M. (1983)
Résultats d'échantillonnage de l'eau et des sédiments de la baie des Ha! Ha!. ., Ministère de l'Environnement du Québec, Direction générale des inventaires et de la recherche, Service de la qualité des eaux.

Raven, K.P., Jain, A. & Loeppert, R.H. (1998)
Arsenite and arsenate adsorption on ferrihydrate: kinetics, equilibrium and adsorption envelopes. *Environ. Sci. Technol.* **32**, 344-9.

Reedy, C.V.G., Murty, P.S.N., & Sankaranarayanan, V.N. (1968)
An incidence of very high phosphate concentrations in waters around Andaman Islands. *Current Sci. (India).* **37**, 17-18.

Richard, L.F. (1997)
Comparaison des comportements géochimiques du phosphore et de l'arsenic dans la Fjord du Saguenay et l'Estuarie Maritime du St. Laurent. Unpublished Masters Thesis Universite du Québec a Montréal.

Riedel, G.F. (1993)
The annual cycle of arsenic in a temperate estuary. *Estuaries.* **16**, 533-540.

Roberson,C.E. & Hem, J.D. (1969)
Solubility of Aluminum in the Presence of Hydroxide, Fluroide and Sulfate. USGS Water Supply Paper 1827-C. 37 p.

Roy, W.R., Hassett, J.J. & Griffin, R.A. (1986)
Competitive coeffcients for the adsorption of arsenate, molybdate, and phosphate mixtures by soil. *Soil Sci. Soc. Am. J.* **50** 1176-1182

Russell, J.D., Parfitt, R.L., Fraser, A.R. & Farmer, V.C. (1974)
Surface structures of gibbsite goethite and phosphated goethite. *Nature.* **248**, 220-221.

Sadiq, M. (1990)
Arsenic chemistry in marine environments: a comparison between theoretical and field observations. *Marine Chem.* **31**, 285-297.
Sadiq, M. (1992)
Toxic Metal chemistry in Marine Environments. Marcel Dekker: New York.
Schindler, P.W. (1985)
Grenzflächencheime oxidischer Mineralien. *Österreichische Chem. Z.* **86**, 141-146.
Schindler, P.W. & Kamber, H.R. (1968)
Die aciditat von silanolgruppen. *Helvitica Chim. Acta.* **51**, 1781-1786.
Seibert, G.H., Trites, R.W. & Ried, S.J. (1979)
Deepwater exchange processes in the Saguenay Fjord. *J. Fish. Res. B. Can.* **36**, 42-53.
Shaw, A. (1996)
The diagenetic phosphorus cycle in marine environments and the importance of adsorption onto the goethite (α-FeOOH) surface. Unpublished B.Sc. Thesis McGill University . ,
Sholkovitz, E.R. (1978)
The flocculation of dissolved Fe, Mn, Al, Cu, Ni, Co and Cd during estuarine mixing. *Earth Planet. Sci. Lett.*. **41**, 77-86.
Silverberg, N. & El-Sabh, M. (1990)
Chapter 18. The St.Lawrence Estuary: concluding remarks in El-Sabh, M and Silverberg, N. (eds.) *Oceanography of a large-scale estuarine system. The St. Lawrence Estuary*. Springer Verlag: New York.
Sposito, G. (1984)
The surface chemistry of soils. Oxford University Press: New York.
Sposito, G. (1989)
Surface reactions in natural aqueous colloidal systems. *Chimia.* **43**, 169-176.
Stern, O. (1923)
Zur theory der electrolytischen doppelschicht. *Z. Electrochem.* **30**, 508-516.
Stryer, L. (1981)
Biochemistry. W.H. Freeman and Co.: San Francisco 949pp.
Stumm, W., Huang, C.P. & Jenkins, S.R. (1970)
Specific chemical interactions affecting the stability of dispersed systems. *Croat. Chem. Acta.* **42**, 223-244.
Stumm, W., Kummert R. & Sigg. L. (1980)
A ligand exchange model for the adsorption of inorganic and organic ligands at hydrous oxide interfaces. *Croat. Chem. Acta.*
Stumm, W. & Morgan, J.J. (1996)
Aquatic chemistry: Chemical equilbria and rates in natural waters 3rd ed. Wiley-Interscience: New York 1022 pp.
Su, C. & Harsh, J.B. (1994)
Gibbs free energies of formation at 298K for imogolite and gibbsite from solubility measurements. *Geochim. Cosmochim. Acta.* **58**, 1667-1677.
Sullivan, K.A. & Aller, R.C. (1996)
Diagenetic cycling of arsenic in Amazon shelf sediments. *Geochim. Cosmochim. Acta.* **60**, 1465-1477.
Sundby, B. & Loring, D.H. (1978)
Geochemistry of suspended particulate matter in the Saguenay Fjord. *Can. J. Earth Sci.* **15**, 1002-1011.
Thanabalasingam, P. & Pickering, W.F. (1986)
Arsenic sorption by humic acids. *Environ. Poll.: Series B.* **12**, 233-246.
Therrault, J.C. & Lacroix, G. (1975)
Penetration of the deep layer of the Saguenay Fjord by surface waters of the St. Lawrence Estuary. *J. Fish. Res. B. Can.* **32**, 2373-2377.
Tremblay, G.H. & Gobeil, C. (1990)
Dissolved arsenic in the St. Lawrence estuary and the Saguenay Fjord, Canada. *Marine Poll. Bull.* **21**, 465-468.

Turner, D.R., Whitfield, M. & Dickson, A.G. (1981)
The equilibrium speciation of dissolved components in freshwater and seawater at 25°C and 1 atm pressure. *Geochim. Cosmochim. Acta.* **45**, 855-881.

van Riemsdijk, W.H. & Lyklema, J. (1980a)
Reaction of phosphate with gibbsite [$Al(OH)_3$] beyond the adsorption maximum. *J. Colloid Interface Sci.* **76**, 55-66.

van Riemsdijk, W.H. & Lyklema, J. (1980b)
The reaction of phosphate with aluminum hydroxide in relation with phosphate bonding in soils. *Colloids Surf.* **1**, 33-40.

Vieth, J.A. & Sposito, G. (1977)
On the use of the Langmuir equation in the interpretation of "adsorption" phenomena. *Soil Sci. Soc. Am. J.* **41**, 697-702.

Violante, A., Colombo, C. & Buondonno, A. (1991)
Competitive adsorption of phosphate and oxalate by aluminum oxides. *Soil Sci. Soc. Am. J.* **55**, 65-70.

Wagemann, R. (1978)
Some theoretical aspects of stability and solubility of inorganic arsenic in the freshwater environment. *Water Res.* **12**, 139-145.

Warner, T.B. (1969)
Fluoride in seawater: Measurement with lanthanum fluoride electrode. *Science.* **165**, 178-180.

Warner, T.B. (1971a)
Normal fluoride content of seawater. *Deep-Sea Res.* **18**, 1255-1263.

Warner, T.B. (1971b)
Electrode determination of fluoride in ill-characterized natural waters. *Water Res.* **5**, 459-465.

Westall, J. and Hohl, H. (1980)
A comparison of electrostatic models for the oxide/solution interface. *Adv. Colloid Interface Sci.*. **12**, 265-294.

Westall, J.C. (1982)
FITEQL: A computer program for determination of chemical equilibrium constants from experimental data. Oregon State University Report 82-01. Oregon State University: Corvallis, Oregon.

Widerlund, A. & Ingri, J. (1995)
Early diagenesis of arsenic in sediments of the Kalix River estuary, northern Sweden. *Chem.Geol.* **125**, 185-196.

Xu, H., Allard, B. & Grimvall, A. (1988)
Influence of pH and organic substance on the adsorption of As(V) on geological materials. *Water Air Soil Poll.* **40**, 293-305.

Xu, H., Allard, B. & Grimvall, A. (1991)
Effects of acidification and natural organic materials on the mobility of arsenic in the environment. **In** Adriano, D.C (ed.) *Metals in soils, waters, plants and and animals; proceedings of an international conference. Water Air Soil Poll.* **57-58**, 269-278.

Appendicies

Appendix 1.1 Arsenate Adsorption to Gibbsite in Artificial Seawater at 23°C

ID	pH	Final As µM	Ads. µmol/g	ID	pH	Final As µM	Ads. µmol/g
15-07-50-RT	6.80	37.4	2.0	13-07-02-R2	7.61	1.8	0.1
19-07-10-7.4	6.91	9.4	0.5	19-07-50-7.8	7.66	48.0	1.8
15-07-20-RT	6.94	14.6	0.9	13-07-20-R2	7.67	17.6	0.4
11-08-01-RT	6.94	1.1	0.0	16-07-01-RT	7.69	0.9	0.1
15-07-05-RT	6.98	3.3	0.2	13-07-05-R1	7.75	5.0	0.2
15-07-10-RT	6.98	6.1	0.2	11-08-05-RT	7.77	4.8	0.2
15-07-01-RT	7.03	1.1	0.0	07-07-20-RT	7.81	24.9	0.6
15-07-02-RT	7.16	2.0	0.0	10-08-05-RT	7.85	5.4	0.2
16-07-20-RT	7.18	18.5	1.0	19-07-10-8.0	7.85	10.0	0.1
19-07-05-7.2	7.22	4.5	0.5	10-08-01-RT	7.86	1.2	0.1
16-07-05-RT	7.23	5.2	0.2	13-07-02-R1	7.88	2.0	0.1
19-07-05-7.4	7.35	6.3	0.4	13-07-01-R1	7.89	1.0	0.1
16-07-02-RT	7.38	1.9	0.2	05-07-01-RT	7.90	0.9	0.2
19-07-20-7.4	7.40	19.4	0.5	19-07-50-8.2	7.90	49.2	0.9
19-07-50-7.6	7.43	48.2	1.8	07-07-10-RT	7.92	10.5	0.4
19-07-10-7.6	7.44	9.8	0.4	19-07-20-8.2	7.94	19.7	0.4
19-07-50-7.4	7.51	48.0	1.8	13-07-05-R2	7.95	4.4	0.2
11-08-10-RT	7.52	9.7	0.6	07-07-05-RT	7.99	6.2	0.1
11-08-20-RT	7.52	12.2	0.6	19-07-50-8.0	8.03	47.0	0.7
16-07-50-RT	7.52	46.5	1.6	13-07-01-R2	8.04	0.9	0.1
16-07-10-RT	7.53	10.9	0.3	10-08-20-RT	8.14	20.6	0.5
13-07-10-R1	7.53	9.3	0.3	19-07-20-8.4	8.14	19.7	0.4
19-07-20-7.6	7.54	19.0	0.6	10-08-10-RT	8.23	10.3	0.2
13-07-20-R1	7.58	18.2	0.6	10-08-02-RT	8.24	2.2	0.2
11-08-02-RT	7.61	2.0	0.2	05-07-05-RT	8.37	4.8	0.1
13-07-10-R2	7.61	8.6	0.3	19-07-10-8.4	8.43	9.8	0.3
19-07-20-8.0	7.61	19.1	0.8	19-07-50-8.4	8.30	48.7	1.2

Appendix 1.2 Arsenate Adsorption to Gibbsite in Nanopure™ Water at 23° C

ID	pH	Final As µM	Adsorption µmol/g
20-07-05-RT	7.98	3.0	2.1
20-07-10-RT	7.99	7.8	2.2
20-07-20-RT	7.85	17.0	2.2
20-07-50-RT	7.83	47.2	2.3

Appendix 1.3 Phosphate Adsorption to Gibbsite in Artificial Seawater at 23° C

ID	pH	Final P µM	Ads. µmol/g	ID	pH	Final P µM	Ads. µmol/g
17-07-20-RTB	7.26	7.4	1.3	14-07-20-R2	7.75	12.3	0.4
17-07-05-RTB	7.30	1.6	0.4	14-07-20-R1	7.76	13.4	0.5
17-07-05-RTA	7.31	1.5	0.5	08-07-02-RT	7.77	2.1	0.1
17-07-20-RTA	7.34	7.7	1.0	09-07-02-RT	7.77	2.8	0.4
18-07-02-RTB	7.34	4.4	1.1	08-07-20-RT	7.84	20.4	1.1
14-07-10-R1	7.36	6.4	0.5	09-07-20-RT	7.84	20.3	1.0
18-07-02-RTA	7.38	4.5	1.0	08-07-05-RT	7.98	5.4	0.4
14-07-10-R2	7.48	6.0	0.3	09-07-05-RT	7.98	6.3	0.3
14-07-05-R2	7.50	3.1	0.2	08-07-10-RT	8.02	9.9	0.5
18-07-10-RTB	7.53	3.9	0.5	09-07-10-RT	8.02	25.5	1.2
14-07-05-R1	7.54	3.3	0.3	12-07-05-RT	8.37	1.5	0.1
18-07-20-RTB	7.54	8.8	1.4	12-07-10-RT	8.41	1.9	0.1
18-07-20-RTA	7.56	8.8	1.5	12-07-20-RT	8.42	2.5	0.2
17-07-02-RTB	7.64	1.6	0.4	12-07-02-RT	8.50	1.0	0.2
17-07-02-RTA	7.73	1.5	0.4				

Appendix 1.4 Fluoride Adsorption to Gibbsite in Artifical Seawater

ID	pH	As µM	Final F µM	F Ads. µmol/g	ID	pH	As µM	Final F µM	F Ads. µmol/g
05-07-01-RT	7.9	1	54	11	11-08-10-RT	7.5	10	66	2
16-07-01-RT	7.7	1	41	11	19-07-10-8.4	8.4	10	63	3
13-07-01-R2	8.0	1	60	2	19-07-10-7.6	7.4	10	63	6
13-07-01-R1	7.9	1	67	1	19-07-10-8.0	7.9	10	69	1
15-07-01-RT	7.0	1	65	1	10-08-10-RT	8.2	10	60	7
11-08-01-RT	6.9	1	56	10	07-07-10-RT	7.9	10	60	7
10-08-01-RT	7.9	1	52	13	16-07-10-RT	7.5	11	45	9
13-07-02-R2	7.6	2	67	0	11-08-20-RT	7.5	12	60	7
16-07-02-RT	7.4	2	41	11	15-07-20-RT	6.9	15	67	1
11-08-02-RT	7.6	2	64	4	16-07-20-RT	7.2	19	41	11
15-07-02-RT	7.2	2	65	1	19-07-20-7.4	7.4	19	58	8
13-07-02-R1	7.9	2	67	0	19-07-20-7.6	7.5	19	55	12
10-08-02-RT	8.2	2	62	5	13-07-20-R1	7.6	18	43	10
15-07-05-RT	7.0	3	43	10	19-07-20-8.0	7.6	19	58	5
13-07-05-R2	8.0	4	58	2	13-07-20-R2	7.7	18	43	5
19-07-05-7.2	7.2	5	64	3	07-07-20-RT	7.8	25	59	7
05-07-05-RT	8.4	5	62	5	19-07-20-8.2	7.9	20	58	5
11-08-05-RT	7.8	5	52	13	19-07-20-8.4	8.1	20	59	6
13-07-05-R1	7.8	5	60	3	10-08-20-RT	8.1	21	60	7
16-07-05-RT	7.2	5	46	9	15-07-50-RT	6.8	37	65	1
10-08-05-RT	7.8	5	68	0	16-07-50-RT	7.5	46	35	13
15-07-10-RT	7.0	6	54	6	19-07-50-8.0	8.0	47	57	9
07-07-05-RT	8.0	6	65	3	19-07-50-7.8	7.7	48	62	3
19-07-05-7.4	7.4	6	62	5	19-07-50-7.4	7.5	48	62	2
13-07-10-R2	7.6	9	64	1	19-07-50-7.6	7.4	48	65	4
13-07-10-R1	7.5	9	64	2	19-07-50-8.4	8.3	49	56	12
19-07-10-7.4	6.9	9	62	8	19-07-50-8.2	7.9	49	54	4

Appendix 1.5 Arsenate Adsorption to Gibbsite in Artifical Seawater at 4° C

ID	pH	Final As µM	Adsorbtion µM/g
11-08-01-CT	6.89	1.1	0.0
05-07-01-CT	7.50	1.0	0.0
11-08-02-CT	7.50	2.1	0.1
11-08-20-CT	7.56	12.5	0.3
11-08-10-CT	7.61	10.1	0.3
07-07-02-CT	7.73	2.4	0.1
07-07-05-CT	7.79	6.1	0.2
10-08-01-CT	7.79	1.2	0.1
10-08-20-CT	7.81	20.9	0.3
10-08-10-CT	7.84	10.3	0.2
11-08-05-CT	7.87	4.9	0.1
10-08-05-CT	7.89	5.5	0.1
10-08-02-CT	7.90	2.3	0.0
05-07-20-CT	8.24	16.1	0.2

Appendix 1.6 Phosphate Adsorption to Gibbsite in Artificial Seawater at 4°C

ID	pH	Final P µM	Adsorption µmol/g
08-07-05-CT	7.76	5.2	0.6
08-07-20-CT	7.80	20.6	1.0
09-07-20-CT	7.84	20.4	0.9
08-07-10-CT	7.85	10.1	0.3
09-07-02-CT	7.96	2.8	0.4
09-07-10-CT	7.98	25.9	0.9
08-07-02-CT	7.99	2.0	0.2
09-07-05-CT	8.03	6.3	0.3
12-07-10-CT	8.13	1.8	0.2
12-07-05-CT	8.17	1.3	0.2
12-07-20-CT	8.25	2.6	0.2
12-07-02-CT	8.27	1.0	0.2

Appendix 1.7 Adsorption Kinetics of Arsenate to Gibbsite in Artificial Seawater

Initial (μM)	1.24	PH	2.39		5.42		10.16		19.62	
Day	Ads. (μM)	pH	Ads. (μM)	pH	Ads. (μM)	pH	Ads. (μM)	pH	Ads. (μM)	pH
1	0.03	7.67	0.08	7.60	0.14	7.71	0.16	7.61	0.23	7.61
3	0.09	7.74	0.08	7.65	0.21	7.72	0.31	7.80	0.52	7.49
7	0.10	7.89	0.14	7.88	0.22	7.75	0.35	7.53	0.55	7.58

Appendix 1.8 Adsorption Kinetics of Phosphate to Gibbsite in Artifical Seawater

Initial concentration (μM)	2.1		4.1		7.6		14.5	
Day	Ads. (μM)	pH	Ads. (μM)	pH	Ads. (μM)	pH	Ads. (μM)	pH
1	0.2	7.3	0.1	7.5	0.5	7.4	0.5	7.8
3	0.1	7.2	0.1	7.5	0.2	7.4	0.2	7.8
7	0.1	7.2	0.2	7.5	0.1	7.4	0.2	7.6

Appendix 1.9 Adsorption of Arsenate to Gibbsite in Artificial Seawater with Respect to Solid:Solution Ratio

ID	pH	*Solid:Solution* g/L	*Final As* μM	*Adsorption* μmol/g
13-07-01-R1	7.89	2.5	1.0	0.1
13-07-02-R1	7.88	2.5	2.0	0.1
13-07-05-R1	7.75	2.5	5.0	0.2
13-07-10-R1	7.53	2.5	9.3	0.3
13-07-20-R1	7.58	2.5	18.2	0.6
13-07-01-R2	8.04	5	0.9	0.1
13-07-02-R2	7.61	5	1.8	0.1
13-07-05-R2	7.95	5	4.4	0.2
13-07-10-R2	7.61	5	8.6	0.3
13-07-20-R2	7.67	5	17.6	0.4
10-08-01-RT	7.86	1.25	1.2	0.1
10-08-02-RT	7.37	1.25	2.2	0.2
10-08-05-RT	7.85	1.25	5.4	0.2
10-08-10-CT	7.84	1.25	10.3	0.2
10-08-20-RT	8.14	1.25	20.6	0.5

Appendix 1.10 Levels of Dissolved Aluminum in Artificial Seawater

Sample ID	pH	Al ppb
05-01-01-RT	8.14	11
05-03-01-RT	7.90	42
05-01-01-CT	8.18	62
05-07-01-CT	7.16	20
05-14-01-CT	7.66	38
05-01-02-RT	8.00	55
05-14-02-RT	6.91	115
05-01-02-CT	8.43	39
05-03-02-CT	8.18	15
05-01-05-RT	8.23	141
05-14-05-RT	8.31	61
05-01-05-CT	8.23	97
05-07-05-CT	7.96	53
05-01-10-RT	8.17	48
05-03-10-CT	8.20	49
05-01-20-RT	8.12	48
05-01-20-CT	8.21	66
05-03-20-CT	8.23	65
04-00-00-XX	8.03	96
04-03-10-RT	6.18	98
04-03-10-CT	6.34	72
04-28-10-CT	6.22	93
04-03-20-RT	7.22	61
04-03-20-CT	7.97	149
04-28-20-CT	6.29	101